STRUCTURE AND PROPERTIES OF CNT YARNS AND CNT/CNF REINFORCED PAN-BASED CARBON FIBERS

A Dissertation Presented for the
Doctor of Philosophy
Degree
The University of Tennessee, Knoxville

Nitilaksha Phalaxayya Hiremath
December 2016

Copyright 2016 by
Nitilaksha Hiremath

Acknowledgements

It is the supreme art of the teacher to awaken joy in creative expression and knowledge._ Albert Einstein, with this thought I would like to express my sincere and heartfelt gratitude to Dr. Gajanan Bhat for his expert advice and constant guidance all the time I needed. The timely discussions with him has not only helped me to understand and approach a problem but also has influenced me to become a better person.

I also received greatest support from my committee professors, Dr. Jimmy Mays, Dr. Amit Naskar and, Dr. Uday Vaidya, I would like to express my heartfelt gratitude and thank them wholeheartedly. I sincerely thank Dr. Amit Naskar for the valuable discussions on my experimental setup and its modifications.

I would like to extend my sincere thanks to Dr. John Dunlap for training me on FIB, TEM and microtome sample preparations. My gratitude is due to Dr. Maulik Patel for letting me use X-ray diffraction instrument and also on discussions on my data.

I would like to thank Stephen Sheriff, process engineer at UTNRL, for all the help during the wet-spinning setup.

I would like to thank my Auburn friends, Sachin and Seema, Pratheek Hejmady, Naved Siddiqui, Santosh Kulkarni, Harish Rao, Vijay Sheshadri, Sanjay Kulkarni, and Adarsh Jain, for all the encouragement.

I would like to thank my Knoxville friends, Sagar Yadavali, Siddharth Pradhan, Ramesh Alagesan, Maneesha Mohan, Avik Mukherjee, Komal Kooduvalli for making my stay fun filled and encouraging me during tough times.

Finally, I want to thank my nearest and dearest ones, my father, Dr. Phalaxayya R. Hiremath, my mother, Sharada P. Hiremath, my beloved wife Vidya Hiremath, my brothers, Rachayya P. Hiremath and Kshitij P. Hiremath, for all the unconditional love and affection, motivation and encouragement, support, sacrifice, patience and confidence in me.

Abstract

There is continuing effort to enhance the strength and modulus of carbon fibers by various combinations of materials and processing. Carbon fibers are produced from various precursors, and the strength of the CFs are directly related to the type of precursor used to make them. Carbon Nanotubes (CNTs) have received a great deal of attention due to their unique structure and properties. Major focus of this research is on the evaluation of processing, structure and properties of CNT based yarns and composite fibers.

High strength and low cost carbon fibers (CFs) are needed for today's applications. A low cost and low molecular weight textile grade PAN is studied as the precursor polymer with CNT/ carbon nanofibers (CNFs) as the filler material to enhance the strength of the carbon fibers. Efforts by several researchers have shown that incorporation of CNTs into carbon fibers is a challenging task and only a small percent could be introduced successfully. Various concentrations of modified CNTs or CNFs are used as reinforcement and an effort to increase the percentage of CNTs or CNFs in PAN precursor is attempted. The tensile strength of the precursor fibers is 150 MPa for 3.2 wt% CNFs in 12 wt% PAN and 430 MPa for carbonized fibers of the same precursor. Compared to pristine PAN, the reinforcement resulted in 187% increase in strength and 74% increase in modulus.

Commercially available CNT yarns have shown that their tensile properties are much lower than the calculated values. Various characterization techniques such as scanning electron microscopy (SEM), focused ion beam (FIB), transmission electron

microscopy (TEM), tensile testing, and X-ray diffraction (XRD) are used to investigate the morphology of the fibers/yarns. Structural analysis indicated relatively poor packing/ orientation of nanotubes compared to density of CNT and yarn axis, respectively. Possible approaches to further enhance the properties of CNT yarns are investigated. Some of these techniques demonstrated the increase in strength by more than 330 % and modulus by more than 360 %. These observed increases are due to enhanced packing and interaction between the nanotube bundles in the CNT yarn.

Keywords: CNTs, CNT yarns, carbon nanofibers, Wet-spinning setup, PAN precursors, Carbonization

Table of Contents

CHAPTER 1. INTRODUCTION 1

1.1 Background 1

1.1.1 Carbon Fibers and carbon nanotube yarns 1

1.2 Spinning Process 4

1.2.1 Wet Spinning 4

1.2.2 Coagulation Process 6

1.2.3 Melt Spinning 7

1.3 Objective of the Research 7

CHAPTER 2. LITERATURE REVIEW 10

2.1 Introduction 10

2.2 Variants of CFs 12

2.2.1. PAN Based CFs 12

2.2.2. Pitch based CFs 16

2.2.3. Rayon based CFs 19

2.3 Other precursors 19

2.3.1 Graphene based CFs 19

2.3.2 Lignin-based carbon fibers 21

2.4 Carbon Nanotubes (CNT) 25

2.4.1 Introduction to CNT 25

2.4.2 Structure of CNTs 26
2.5 Theory 28
2.6 Synthesis 31
2.7 Carbon Nanotube-based Fibers 39
2.7.1 CNT-based composite fibers 39
2.8 CNTs based CFs 45
CHAPTER 3. EXPERIMENTAL 49
3.1 Materials and methods 49
3.1.1 CNT yarn densification 50
3.1.2 Spinning Solution Preparation 50
3.1.3 Wet Spinning setup 52
3.1.4 Stabilization and Carbonization setup 55
3.2 Characterization techniques 55
3.2.1 Differential scanning calorimetry 55
3.2.2 Thermogravimetric analysis 57
3.2.3 Dynamic mechanical analysis 57
3.2.4 Tensile testing 57
3.2.5 Microscopy 58
3.2.6 X-ray diffraction 59
CHAPTER 4. STRUCTURE AND PROPERTIES OF CNT YARNS 61
4.1 Microstructure analysis 61
4.2 Tensile properties 66
4.3 Effect of Densification on CNT yarn 66

CHAPTER 5. STRUCTURE AND PROPERTIES OF CNFS AND CNTS REINFORCED PRECURSORS 75

5.1 Thermal analysis 75

5.2 Microscopic structure 82

5.3 TEM analysis 85

5.4 Tensile properties 88

5.5 DMA analysis 96

5.6 Tensile properties of hot plate stretched precursors 96

5.7 XRD analysis 100

CHAPTER 6. CHARACTERIZATION OF CARBONIZED FILAMENTS 102

6.1 Microstructure analysis 102

6.2 Tensile properties 103

6.3 XRD analysis 108

CHAPTER 7. CONCLUSIONS AND FUTURE RECOMMENDATIONS 112

7.1 Conclusions 112

7.2 Recommendations for Future work 114

REFERENCES 115

VITA 123

List of Tables

Table 2.1 Advantages and disadvantages of the various synthesis techniques (Szabó, Perri et al. 2010)----------37

Table 2.2 CNT/polymer composites and their tensile strength, elastic modulus, and toughness----------40

Table 3.1 Summary of type of solutions prepared----------51

Table 4.1 Physical properties of CNTYN and CNTYG----------63

Table 4.2 Summary of tensile properties of pristine and infiltrated CNTYN---------69

Table 5.1 Summary of DSC data of PAN fibers with various nanofillers----------77

Table 5.2 Summary of mechanical properties of the precursor fibers----------91

List of Figures

Figure 1.1: SEM images of CNT yarn twisted from the CNT forest on a substrate (Zhang, Atkinson et al. 2004).----------3

Figure 1.2: Plan of experiments----------9

Figure 2.1: A typical SEM image of commercial oxidized PAN fiber (Marcuzzo, Otani et al. 2013) ----------14

Figure 2.2: SEM images of pitch based carbon fibers (Kumar, Anderson et al. 1993)18

Figure 2.3: Conversion of cellulose into carbon fibers----------20

Figure 2.4: A schematic of dry-jet-wet spinning setup----------22

Figure 2.5: A schematic of lignin based carbon fiber production----------24

Figure 2.6: A graphene sheet explaining the formation of different types of carbon nanotubes. a_1 and a_2 are the vectors. Red dots are carbon atoms which inherit metallic behavior and the black dots inherit semiconductor behavior (Harris 2001) ----------29

Figure 2.7: A typical unit cell of armchair type of carbon nanotubes (Harris 2001)---30

Figure 2.8: A typical unit cell of zig-zag type of carbon nanotubes (Harris 2001)-----30

Figure 2.9: Energy vs k-vector along K-Γ-M direction of 2D graphite structure (Ando 2000) ----------32

Figure 2.10: Density of states for a) armchair and b) zig-zag CNTs (Terrones 2003)---33

Figure 2.11: A schematic of arc-discharge tube with a small gap between electrodes--35

Figure 2.12: A schematic of laser ablation technique----------36

Figure 2.13: A schematic of CNTs produced by solar furnace technique----------38

Figure 2.14 A and 2.14 B: Tensile strength and elastic modulus data for Nylon 6-CNT based composite fibers (Gao, Itkis et al. 2005)----------42

Figure 2.15 A and 2.15 B: Tensile strength and elastic modulus data for PVA-CNT based composite fibers from various researchers respectively (Minus, Chae et al. 2009, Young, Blighe et al. 2010)----------46

Figure 3.1: Schematic of CNTY densification setup----------51

Figure 3.2: Schematic of wet spinning setup used to make precursor fibers----------53

Figure 3.3: Schematic of stabilization and carbonization tube furnace used in this work.----------56

Figure 3.4: Schematic of XRD sample mounted on the sample holder----------60

Figure 4.1: SEM images of CNT yarns at low and high magnification. Presence of high void space and lack of orientation of CNTs in the yarn direction is observed----------62

Figure 4.2: FIB milled SEM images of transverse section of CNT yarn and the bottom image shows the longitudinal section of the CNT yarn. It can be observed that there is lot of porosity in the cross section and longitudinal section followed by nonoriented CNTs in the yarn direction (arrows in 4.2E represents CNTs in yarn direction, while CNTs in the middle are perpendicular to yarn direction)----------64

Figure 4.3: Void content analysis of FIB/SEM images of CNTY. 'A' showing lower magnification while 'C' and 'E' showing higher magnification of CNTY. 'B', 'D' and 'F' shows the void percent in the green selected area---------65

Figure 4.4: Strength vs modulus of CNT yarns of three batches----------67

Figure 4.5: Strength and modulus data of CNTYN-pristine and CNTYN infiltrated with DMF, 0.1 wt% PAN and 1 wt% PAN----------69

Figure 4.6: SEM images of CNTYN-pristine tensile tested sample. 'A' and 'B' are lower magnification images while 'C' is the higher magnification image of CNTYN-pristine, respectively----------71

Figure 4.7: SEM images of CNTYN-DMF infiltrated tensile tested sample. 'A' and 'B' are lower magnification images while 'C' is the higher magnification image of CNTYN-DMF infiltrated failed end, respectively----------71

Figure 4.8: SEM images of CNTYN- 0.1 wt% PAN infiltrated tensile tested sample. 'A' and 'B' are lower magnification images while 'C' is the higher magnification image of CNTYN-0.1 wt% PAN of the tearing of CNT ribbon (failed end of tensile tested sample), respectively----------72

Figure 4.9: SEM images of CNTYN- 1 wt% PAN infiltrated tensile tested sample. 'A' and 'B' are lower magnification images while 'C' is the higher magnification image of CNTYN- 1 wt% PAN infiltrated failed end, respectively----------72

Figure 4.10: 'A' TGA data of pristine and infiltrated CNTYN in air and 'B' in nitrogen. 'C' Optical microscopy images of post TGA samples in nitrogen and 'D' in air showing the presence of iron oxide as confirmed by EDS----------73

Figure 5.1: DSC data of PAN fibers with various nanofillers infiltrated PAN fibers--76

Figure 5.2: DSC curves of pristine as-spun, one hour dried and overnight dried PAN fibers----------79

Figure 5.3: TGA data of pristine PAN fibers with 3.2 and 6.4 wt% PAN-g-CNFs in 12 wt% PAN fibers----------80

Figure 5.4: TGA data of PAN fibers (as-spun (red), one hour dried (blue) and overnight dried (green)----------81

Figure 5.5: Effect of low concentration and room temperature coagulation bath-------83

Figure 5.6: SEM images of surface topography and FIB milled cross sections of precursor filaments (A=P0, B= P1, C= P2, D= P4 and E= P5 filaments)--84

Figure 5.7: P1 (3.2 wt% PAN-g-CNF in PAN) filament TEM image----------87

Figure 5.8: P2 (6.4 wt% PAN-g-CNF in PAN) filament TEM image----------87

Figure 5.9: P4 (3.2 wt% PAN-g-CNTs in PAN) filament TEM image----------89

Figure 5.10: P5 (6.4 wt% PAN-g-CNTs in PAN) filament TEM image----------89

Figure 5.11: Tensile strength vs modulus of various precursors----------91

Figure 5.12: SEM images of tensile tested samples showing the failed ends of the filaments. A= P0, B= P1, C= P2, D= P4, E= P5 and F= P3 filament------92

Figure 5.13: Isostrain/isostress calculation of CNFs and CNTs reinforced PAN precursors. ----------95

Figure 5.14: 'A' DMA curves of precursors showing bulk modulus vs temperature and 'B' showing the tan δ vs temperature----------97

Figure 5.15: Schematic of change in hotplate drawn compared to hot water drawn CNFs and CNTs reinforced precursors. ----------98

Figure 5.16: Tensile properties data of precursors (P0′ to P5′) stretched on a hot plate. ----------99

Figure 5.17: Normalized XRD peaks of precursors----------101

Figure 6.1: SEM images of surface topography and FIB milled cross sections of carbon fibers converted from C0 to C5 precursor filaments----------104

Figure 6.2: Tensile properties of carbonized filaments (C0 to C5) ----------105

Figure 6.3: SEM images of tensile tested carbonized filaments. 'A' is failed end of C0, 'B' is failed end of C1, 'C' is failed end of C2, 'D' is failed end of C4, 'E' is failed end of C5----------107

Figure 6.4: Isostrain/isostress calculation of CNFs and CNTs reinforced CFs--------109

Figure 6.5: XRD data of carbonized filaments----------111

List of Abbreviations

PAN	Polyacrylonitrile
CF	Carbon Fiber
CNT	Carbon nanotubes
CNF	Carbon nanofibers
CNTY	Carbon nanotube yarn
DMF	Dimethyl Formamide
GPa	Giga Pascals
MPa	Mega Pascals

CHAPTER 1

INTRODUCTION

1.1 Background

1.1.1 Carbon Fibers and carbon nanotube yarns

Carbon fibers (CFs) are one of the most sought after high performance materials for the unique characteristics they inherit. The CFs are light weight, very strong and stiff materials used in composites application. CFs are mostly used in space applications as they are conductive, light weight, and sustain high temperature by not compromising on structural integrity. The theoretical strength of CF is >1 TPa (terra pascal), however the research on improving the strength properties is a continuing process as the actual strength of currently available CFs is less (12 GPa) **(Chae, Newcomb et al. 2015)**. Strength of the CFs depends on the orientation of the chains in the structure, and values close to that of theoretical strength can be achieved only by orienting the chains parallel to the fiber axis. The precursor fibers, PAN, pitch, rayon etc., are stabilized, carbonized and graphitized for high strength CFs. Most commonly used precursor for high strength carbon fibers is PAN, and the orientation of the chains along the length of the fiber axis and the structural integrity are higher. So to increase the strength of the CFs the precursor fibers should be free from defects such as voids and micro pores, non-uniform diameter distribution, sheath-core structure, low co-monomer percentage etc.

Carbon nanotubes (CNTs) are also used to make carbon yarns (CYs). CNTs are used in various applications from biosensors to electronic devices to heat sinks. In the composite filaments research, CNTs are dispersed in the polymer dope and the filaments are extruded using melt spinning or wet spinning approaches. However due to lack of ordered orientation of the CNTs and limitation to CNTs loading (tendency to agglomerate) in the filaments, theoretical strength is not realized **(Vigolo, Penicaud et al. 2000, Rouse 2005, Coleman, Khan et al. 2006)**. Lately, CNTs yarns are researched as the CNTs possess high strength (20 to 40 GPa). To avoid the use of polymers as fillers, continuous yarns are spun directly from the CNTs forests. While the CNTs are grown using CVD technique, forest height, degree of entanglement and adhesion to the surface (silicon wafer) are all related to drawability. A CNTs web is drawn and twisted to form yarns similar to that in the formation of staple fiber yarns **(Sears, Skourtis et al. 2010)**. A typical SEM picture of web twisted to yarn is shown in figure 1.1 **(Zhang, Atkinson et al. 2004).**

Carbon fiber formation

To achieve high strength CFs the PAN precursor fiber is extensively studied for the processing conditions, structural formation and property development. Achieving precursor fibers with high strength and or less to no defects is dependent on a lot of variables in the spinning process. Available spinning processes are Gel or melt spinning and wet spinning. In the melt spinning, the PAN dope or pitch is pumped through a spinneret into a tower by hot inert gas, the filaments formed are collected below and guided using guide rollers. There is no coagulation bath involved for diffusing the solvent out of the filaments.

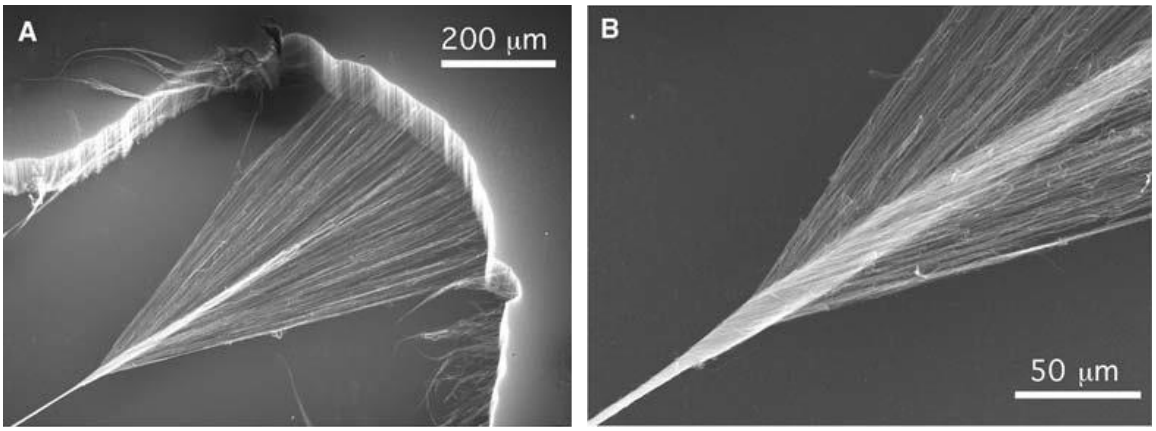


Figure 1.1: SEM images of CNT yarn twisted from the CNT forest on a substrate (Zhang, Atkinson et al. 2004).

Hot inert gases vaporize the solvent as filaments are forming. In the wet spinning process, PAN dope is extruded through a spinneret in to the coagulation bath and solidification takes place by diffusion of solvent in the filament to the coagulation bath while the non-solvent, mostly water, diffuses from the coagulation bath to the filaments. As this process is diffusion controlled, lot of variables are associated. A small variation in the wet spinning is dry-jet wet spinning, where an air-gap is involved between the spinneret and the upper surface of the coagulation bath. The air gap helps to increase the orientation of the chains and hence crystallinity of the final filament.

1.2 Spinning Process

1.2.1 Wet Spinning

The origin of wet spinning of acrylic fibers started in mid-1850's by Chardonnet, where raw cotton was nitrated to form cellulose nitrate dope and further wet spinning was used to make cellulose filaments. In the wet spinning process, the polymer solution is pumped through a spinneret in a coagulation bath containing coagulant, i.e. solvent, and water or other non-solvents. Solvent diffuses out of the polymer solution and the non-solvent diffuses in, resulting in a phase change to a solid polymer plus a liquid (solvent + non-solvent). The concentration of coagulation bath is kept constant by continuous flow of non-solvent in to the coagulation bath.

The polymer concentration of the dope are determined by both physical and practical considerations. As the concentration of the dope increases, the spinning pressure limitation arises. The solubility of the polymer are determined by the strength of the solvent so as to maintain the inhibition to gelation. A high concentration dope can be wet spun in

the lab due to controlled temperature baths, while the same is not the case in an industrial set up. The average molecular weight of the polymers is 100,000- 120,000 g/mol and the spinning dope viscosities are in the range of 500 poise. The spinnerets in the wet spinning consist of large number of capillaries and operate at a very low linear speeds. The polymer concentration is so important that, as the dope gets lighter in concentration, there is a prominent fiber structure change, which may lead to no coagulation due to lack of polymer to form fiber network. Dope could be made up of 100% PAN, however the limitations in processability arise. Hence a co-monomer is added to alter the physical properties. In all of the acrylic fiber processing the wet spun filament are subjected to washing and orientation steps, where the microvoids are collapsed by stretching. These steps are continuous as the filament exits the coagulation bath. Washing process is carried out at close to boiling temperature. The solvent diffuses out at a steady state. Washing is mostly combined with stretching to remove all the residual solvent and collapse the microvoids. In the orientation step the temperature is close to the glass transition temperature and the fiber is stretched from 3 to 12 times. The stretching process orients the fibrillar network formed in the coagulation bath and as a consequence of increased molecular orientation the fiber strength increases. As the fiber exits the orientation step, a finishing is applied to reduce the static charge build up and increase the processability in the future steps, such as yarn formation and fabric formation. In the drying, collapsing and relaxation steps, the drawn filament undergoes collapsing of micro voids and hence the fibrillar network densifies with a simultaneous reduction in diameter. In the relaxation phase the structure under tension relaxes relieving the stress acquired during fiber processing.

1.2.2 Coagulation Process

The coagulation process starts as the polymer in the coagulation bath precipitates out of the solution of solvent and the polymer. The polymer dope pumped through the spinneret holes are collected in the coagulation bath as forming filaments. If the bath is too dilute, the recovery costs of the solvent is higher, whereas if the bath concentration is high then the polymer precipitation does not take place. In the PAN wet spinning, the PAN polymer coagulates in the coagulation bath, initially forming a skin. As the coagulation bath solution diffuses through the center of the filament, a porous gel network forms by separating from the solvent rich phase to polymer rich phase. The porous structure is a gel network with polymer fibrils separated by voids of size 0.3 μm or larger. The diffusion rate of the solvent is dependent on the concentration and temperature of the coagulation bath. Stretching of the filaments is dependent on the rate of coagulation and fiber drawing speed. As the forming filaments are in gel state they can stretched to form oriented network of the polymer matrix and reducing the number of larger voids and uniform distribution of smaller voids. The voids can be reduced down by stretching and drawing in the hot water or on hot rollers. The cross sectional shape and fiber diameter is proportionate with the volumetric transfer rate of the inward diffusion of non-solvent and outward diffusion of the solvent. As the skin of the filament is the one to precipitate out, the volume of solvent in the filament is hindered by diffusion mechanism. If less volume of solvent is present then the fibers are more non-circular in cross section and progresses to become kidney bean shape, whereas, complete removal of solvent leads to circular cross section of the filaments.

1.2.3 Melt Spinning

Melt spinning is carried out by melting the polymer and extruding through a spinneret. As the melting point of the PAN is higher than its decomposition temperature the straight forward melt spinning is not possible. However, a plasticized melt can be extruded as in regular melt spinning. The solvent used for making the dope is vaporized as the filaments form in the melt spinning setup. There is no coagulation bath involved. The hot inert gas around the forming filaments vaporize the solvent thereby consolidating the filaments. For an efficient evaporation of the solvent from the filaments the temperature of the inert gas is maintained above the boiling temperature of the solvent. As the filaments solidify in the spinning vertical column, the solvent is recovered from the inert gas. In melt spinning, the main stages are polymerization, synthesis of spinning solution, melt spinning, and after treatment

1.3 Objective of the Research

The main objective of this research was to investigate novel approaches to enhance the strength and modulus of CNT-based carbon fibers and yarns. Although the CNTs and CNFs have extremely high strength and modulus, the carbon fibers and yarns containing these do not realize their properties to a significant extent. With respect to CNT yarns and CNT reinforced PAN-based carbon fibers, the issues related to high strength and modulus are discussed in terms of the structure of these large scale structures from nanomaterials.

Commercially available CNT yarns claim several advantages, but their physical properties are far below the theoretically possible values based on the properties of CNT. To come up with approaches to improve their properties, it is critical to understand their

structure and properties. This information will help in suggesting pathways to improve the tensile properties of these macrostructures.

Another approach was to study the CNT/CNF reinforced PAN precursors. It is important to design and optimize the conditions for wet spinning PAN + (CNTs or CNFs) fibers followed by converting them to high strength carbon fibers. Textile grade, low molecular weight PAN was used due to the fact that relatively lower viscosity will allow better dispersion of CNT/CNF in the solution, there by allowing higher loading of nanotubes. Also, surface modification of the CNTs, especially to compatibilize with PAN is critical. For that, CNTs and CNFs with surface grafting of short PAN chains are used for dispersing with PAN in the solution. The grafted PAN should not only be compatible with PAN, but will also become part of the carbon fiber developed as the composite precursor fiber, which is further treated to produce carbon fibers. The whole approach is summarized in figure 1.2

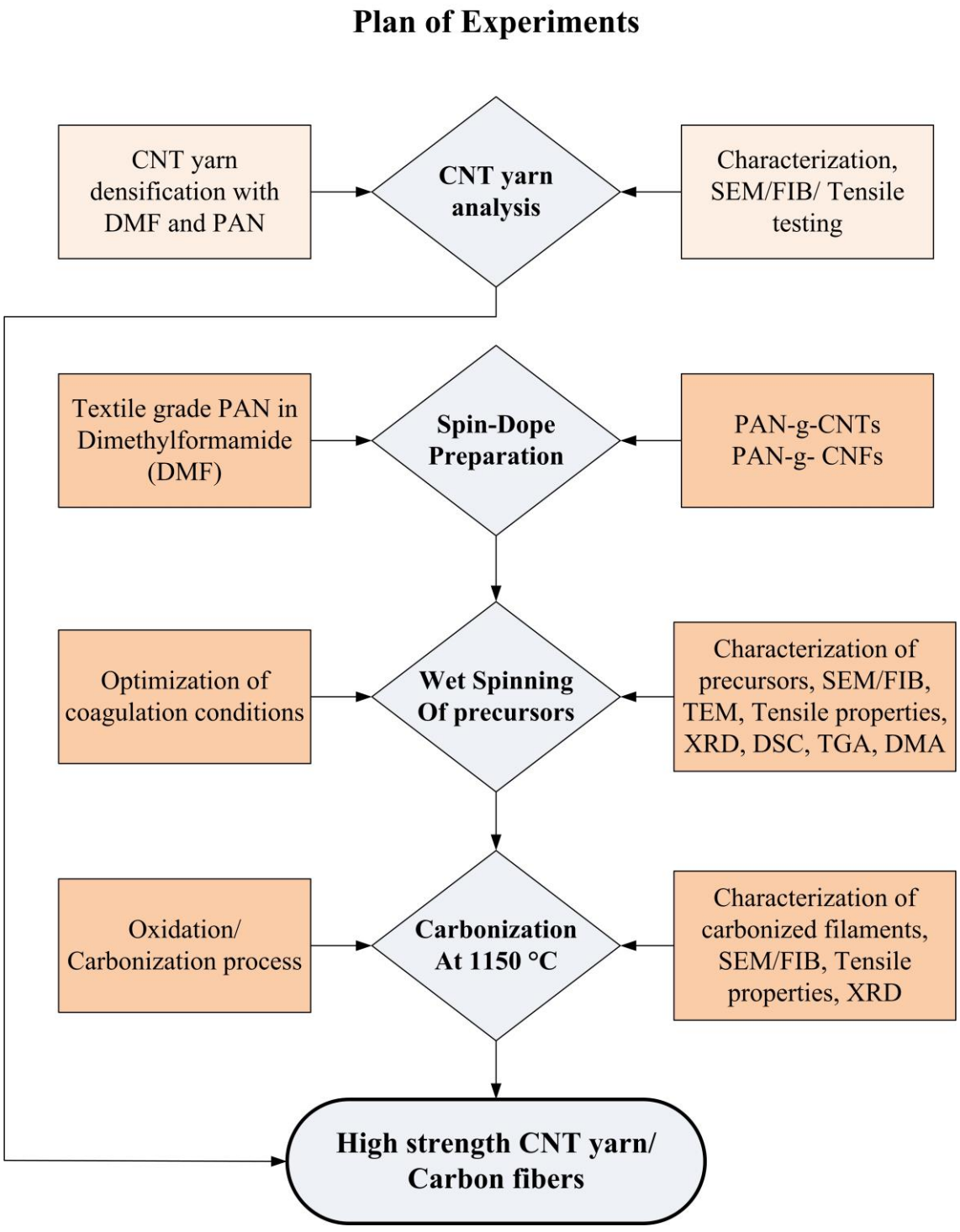


Figure 1.2: Plan of experiments

CHAPTER 2

LITERATURE REVIEW

2.1 Introduction

Carbon's exceptional capacity to form bonds, both to a wide range of other atoms and to other carbon atoms, makes it the most studied element for advanced scientific research. Ordered arrangements of covalently bonded carbon atoms produce various (nano) structures such as graphene, nanotubes, fullerenes, and diamond. Bonded arrangements of carbon atoms in one dimension, produce ultra-high strength fibers, commonly known as carbon fibers (CF). Commercially, CFs are produced from various precursors, polyacrylonitrile (PAN), pitch and rayon; however, other precursors such as carbon nanotubes (CNTs), graphene, lignin, cellulose, polyethylene, etc. are also being studied. PAN-based fibers are produced by spinning a filament, and processing it through stabilization, carbonization and graphitization processes, all under tension. Industrially accepted spinning techniques include wet spinning, dry spinning, dry-jet wet spinning, and melt spinning **(Liu and Kumar 2012)**. Pitch fibers are made from molten aromatic plastics or natural sources such as petroleum products. Pitch fibers also undergo stabilization, carbonization, and graphitization. Rayon is one of the first commercially used precursors for CF. Rayon is a regenerated cellulose fiber and is mixed with a suitable solvent to make it spinnable. Following the spinning process, the rayon fibers undergo stabilization and carbonization to form CFs.

Lately, there has been increasing interest in using CNTs. CNTs exist in different forms, multi-walled carbon nanotubes (MWCNTs) and single-walled carbon nanotubes (SWCNTs) (chiral, armchair and zigzag) **(Harris 2001)**. CNT-based CFs are reported to have higher strength than CFs derived from other precursors. Recently production of graphene-based CFs with good properties has been demonstrated. Theoretically, the highest tensile strength (> 1TPa) can be achieved by graphene-based CFs **(O'connell 2006)**. To increase the strength of the CFs, intra-fiber interactions must be improved by surface modification. Commonly practiced surface treatments are oxidation (gas-phase, liquid phase and catalytic), plasma treatment, washing, and sizing **(Liu and Kumar 2012)**. However, high strength, low cost fabrication, and large scale production of CFs cannot be achieved at the present time due to limitations, such as lack of inexpensive precursors, optimized synthesis techniques, marketability, etc.

Diameter of the CFs are mostly in the range of 5 to 10 μm. Thousands of such strands of CFs are assembled to form a tow or yarn, and such yarns are used for various applications. CF, being a thin long filament, contains more than 90 wt. % of carbon and exhibits outstanding properties. High tensile strength (2 ~ 7 GPa), high compressive strength (up to 3 GPa), high elastic modulus (200 ~ 900 GPa), low thermal expansion, and high electrical and thermal conductivity are some of the prominent properties of CFs. Because of these outstanding properties, CFs are used in composite materials in the airline and automotive industries, in sporting goods, in wind turbine blades, etc. (Liu and Kumar 2012). In addition, as the CF density is lower than that of steel and it has higher specific strength than steel, virtually products of any shape that exhibit excellent structural properties can be fabricated. The first application of CFs, made by pyrolyzing cellulosic

fibers, was in incandescent lamp filament, by Edison in the 1870s. In order to use CFs in commercial applications, it is critical to characterize them thoroughly so that the desired working standards (such as, for electrical or mechanical applications etc.) are ensured with the use of CFs alone or in the composite structure. In the following sections, variants of CFs from different precursors, other new precursors that are being researched, CNTs and CNT-based CFs, CNTs based composite polymer fibers, applications of CFs and CNTs, current trends, and future prospects are discussed.

2.2 Variants of CFs

Commercially available carbon fibers vary in processing, structure and properties based on the precursors such as PAN, pitch and rayon. Finding new precursors has been of continuing interest to the community and recent materials, such as graphene, lignin, poly (p-phenylene vinylene), etc., and low cost CF are important. A brief overview on processing techniques and characterization of CFs from various precursors is presented in the following sections.

2.2.1. PAN Based CFs

PAN is the most important precursor in the CF industry, and it contains about ~ 68 wt. % carbon. The high melting temperature of PAN is due to the presence of the polar nitrile groups, which promote strong intermolecular interactions. Because PAN degrades below its melting temperature, it is mostly processed by solution spinning techniques. Acidic co-monomers are added to reduce the stabilization temperature and glass transition temperature, resulting in heat release and advancing stabilization reactions **(Godshall,**

Rangarajan et al. 2003, Paiva, Kotasthane et al. 2003, Naskar, Walker et al. 2005). Manufacturing CFs involves several steps including polymer synthesis, fiber spinning followed by stabilization, carbonization and graphitization. The tensile properties of the resultant CFs may be enhanced by careful optimization of the processing conditions. The cross section of a PAN-based CF is as shown in figure 2.1, which shows a microstructure with very high level of order and orientation **(Marcuzzo, Otani et al. 2013)**. Currently the gel-spinning technique is most widely employed for the production of precursor fibers as it provides a high draw ratio of up to 51 for PAN fibers **(Yamane, Sawai et al. 1997, Sawai, Kanamoto et al. 1998, Sawai, Yamane et al. 1999, Sawai, Kanamoto et al. 2004, Chae, Minus et al. 2006)**. The stabilization process is carried out under exothermic conditions and released heat should be carefully dissipated out of the forming fibers. Various physical and chemical changes such as shrinkage of the fiber in the axial direction, cyclization, aromatization structure evolutions are observed **(Deurbergue and Oberlin 1991, Dalton, Heatley et al. 1999, Bajaj, Sreekumar et al. 2001, Wu, Lu et al. 2005, Shokuhfar, Sedghi et al. 2006, Yu, Wang et al. 2006, Catta Preta, Sakata et al. 2007, Rahaman, Ismail et al. 2007, Hou, Sun et al. 2009)**. Differential scanning calorimetry (DSC) is used to monitor the kinetics of the exothermic reactions during the stabilization process. A single broad exothermic peak is often observed, even though various reactions occur such as cyclization, oxidation, dehydrogenation and cross linking can occur during the stabilization process **(Devasia, Nair et al. 2003, Zhang, Liu et al. 2004, Hou, Liu et al. 2006, Yu, Wang et al. 2010)**.

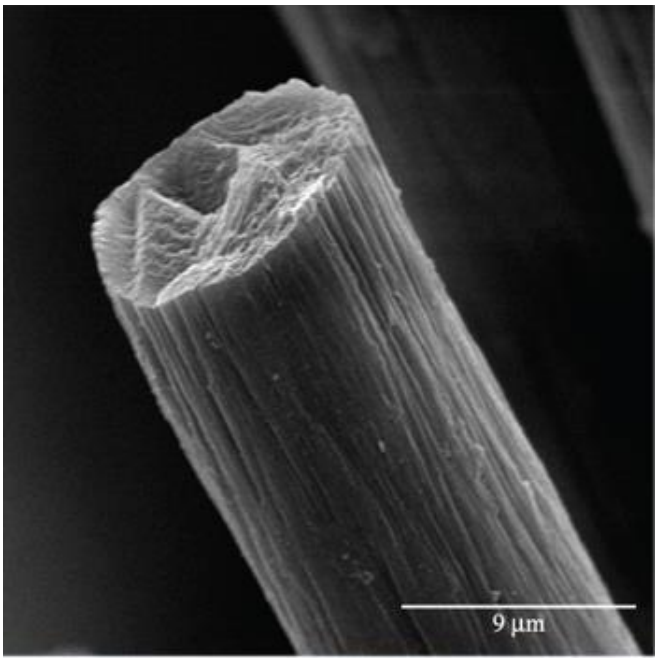


Figure 2.1: A typical SEM image of commercial oxidized PAN fiber **(Marcuzzo, Otani et al. 2013).**

As PAN stabilization is a slow process, it is common to pretreat the PAN fibers by exposure to high energy radiations such as UV, electron beam and γ- rays to trigger partial cyclization before stabilization in air. This can lead to a reduction in stabilization reaction activation energy and the reaction time. In oxidative stabilization, oxygen diffusion controls the reaction. A skin-core morphology is observed in oxidative stabilization, as the skin contains higher oxygen content than the core, resulting in weaker surface influencing crack formation and propagation **(Lv, Ge et al. 2009, Tan and Wan 2011, Yuan, Wang et al. 2011)**. To prevent the skin-core morphology a stabilization reaction inhibitor is coated on the PAN fibers to reduce the surface oxidation rate. Boric acid coated PAN fibers are found to retard the rate of oxidative stabilization reaction on the surface, balancing the stabilization reaction throughout the fiber cross section **(Ge, Liu et al. 2009, Wu, Lu et al. 2011)**.

Chemical and physical structural changes during stabilization are studied using various characterization techniques such, as X-Ray Diffraction (XRD), DSC, FTIR, etc. **(Liu and Kumar 2012)**. The other way of improving the performance of CFs is by reinforcing PAN fiber with CNTs. The CNTs improve the orientation of PAN fibers and hence the strength of the PAN based CFs **(Liu and Kumar 2012)**. For example, inclusion of 5 wt. % SWNT in dry-jet wet spun fibers increased tensile strength from 0.24 to 0.34 GPa, tensile modulus from 7.8 to 13.6 GPa, PAN crystal size from 3.7 to 5 nm and Herman's orientation factor from 0.52 to 0.62 **(Sreekumar, Liu et al. 2004, Coleman, Khan et al. 2006, Moniruzzaman and Winey 2006)**. After heat treating PAN- and mesophase pitch- (MPP) based CFs in the range of 1300 – 2700 °C mechanical properties such as Young's modulus increase for both. However, the tensile strength of PAN-based

CFs decreases after reaching a maximum, while that of MPP-based CFs continues to increase with heat treatment temperature. After heat treatment at 2700 °C the tensile strength of MPP-based CFs exceeds that of PAN-based CFs. Evolution of structure of CFs at various temperatures leads to rearrangement of layers of graphene resulting in differences in the mechanical properties. Physical entanglements and covalent crosslinking of graphene ribbons contribute to a higher shear stress, however, it also generates voids and cracks due to extensive transformation from a turbostratic to ordered structure along with removal of nitrogen. For MPP-based CFs radial texturing with ordered and parallel arrangement of graphene layers in the cross-section helps to bond to adjacent layers leading to fewer voids and cracks **(Qin, Lu et al. 2012)**.

PAN fibers form a rigid ladder structure by intramolecular cyclization when heated and stretched in a steam bath in the presence of nitrogen. Due to this preferred orientation and crystallite dimensions the resultant mechanical properties are enhanced as compared with those of untreated CFs. Mechanical properties of CFs are also enhanced by boron doping and heating the CF at 2500 °C. Increase in boron content in the fiber increases the tensile strength and modulus by 16% and 26%, respectively, as compared to untreated CFs. Boron diffuses substitutionally and interstitially, which helps remove structural defects and relax the distortions in the CF structure to enhance its mechanical properties (Qin, Lu et al. 2012, Qin, Lu et al. 2012).

2.2.2. Pitch based CFs

Pitch is produced either from natural sources such as petroleum or coal or by pyrolyzing synthetic polymers. The molecular weight of pitch is in the range of 600 ~ 1000

g/mol, and it contains aromatic groups. The major cost of pitch-based CFs is due to the purification steps involved. The diameter of pitch-based CF range between 10 ~ 12 µm. MPP contains an anisotropic phase which corresponds to the high degree of molecular alignment along the fiber axis. The MPP-based fibers have higher tensile modulus as compared to PAN-based CFs, however the compressive strength is lower. The tensile strength and modulus of pitch based CF are ~ 3 GPa and 960 GPa, respectively. The cross sections of pitch-based CFs are shown in figure 2.2 **(Kumar, Anderson et al. 1993)**. A highly developed sheet-like morphology (A-1, A-2 and B) and extended sheets along the fiber axis make them highly oriented strong fibers. Pitch-based CFs also require optimization of pitch type, fiber spinning, thermal treatment, surface and structural modifications **(Dauche, Barnes et al. 1998, Yang, Lee et al. 1999, Watanabe, Korai et al. 2000, Mora, Blanco et al. 2002, Park, Kim et al. 2003, Park, Kim et al. 2004, Diez, Alvarez et al. 2012)**. Pitch has isotropic and anisotropic regions. These regions correspond to the smaller and larger micro-domains in the resultant CFs, respectively. By controlling the structure of isotropic and anisotropic phases, the mechanical properties of the resultant CFs can be manipulated. Pitch-based CFs can also be reinforced with CNTs, **(Andrews, Jacques et al. 1999).** Adding 5% SWNT into isotropic pitch-based CF increased the tensile strength and modulus from 0.47 to 0.83 GPa and 34 to 77 GPa, respectively. However the tensile strength and modulus of CNT reinforced mesophase pitch-based CFs were moderately reduced in comparison to that of isotropic pitch-based CFs **(Cho, Lee et al. 2003, Kim, Im et al. 2007)**.

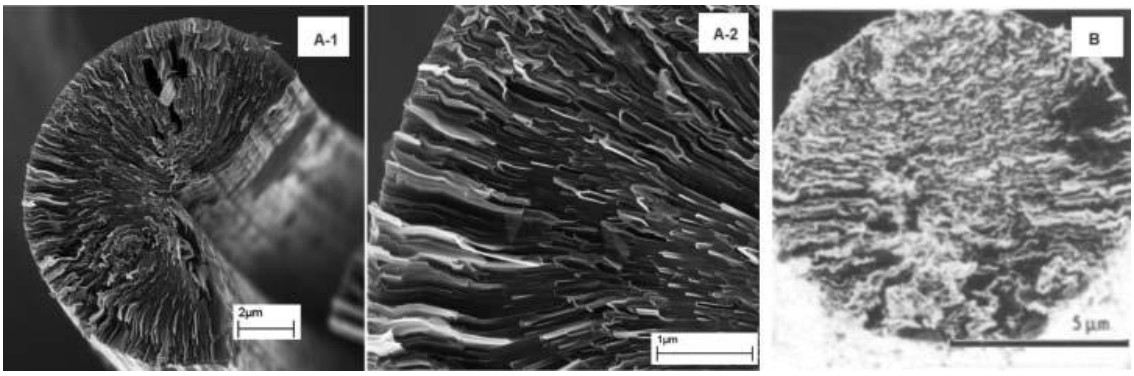


Figure 2.2: SEM images of pitch based carbon fibers **(Kumar, Anderson et al. 1993).**

2.2.3. Rayon based CFs

Rayon is a regenerated cellulose fiber. Derived primarily from wood pulp, rayon is made soluble chemically and filaments of cellulose fibers are produced by wet spinning. Cellulose fibers, first used by Thomas Edison in his famous electric bulb design experiment, by pyrolyzing it to a carbon filament that conducted electricity, are also proven precursors for CF synthesis **(Dumanlı and Windle 2012)**. The reactions involving the conversion of cellulose to CF are as shown in figure 2.3. First, oxidative reactions take place in stages 1 and 2. Carbonization of cellulose is the process of formation of graphitic layers from 300 to 900 °C as shown in Stages 3 and 4. Once the graphitic layers are formed, following graphitization at a high enough temperature (900 to 3000 °C), CF with more than 99% carbon content can be achieved. The Young's modulus also increases as the process is carried out in tension. The reported tensile strength and modulus of rayon-based CFs are about 580 MPa and 59 GPa, respectively **(Dumanlı and Windle 2012)**.

2.3 Other precursors

2.3.1 Graphene based CFs

There has been a recent surge in research on synthesis of graphene-based fibers. The impetus behind choosing graphene as the raw material for CF synthesis is that large mesogenic graphitic structures that are solution spun at room temperature could be ideal building blocks for making high-performance CFs in an economical process **(Kosynkin, Higginbotham et al. 2009)**. Graphene layers form liquid crystals in superacid, and this finding has led to solution-spun mesogenic graphitic structure fibers **(Ericson, Fan et al. 2004, Behabtu, Young et al. 2013)**.

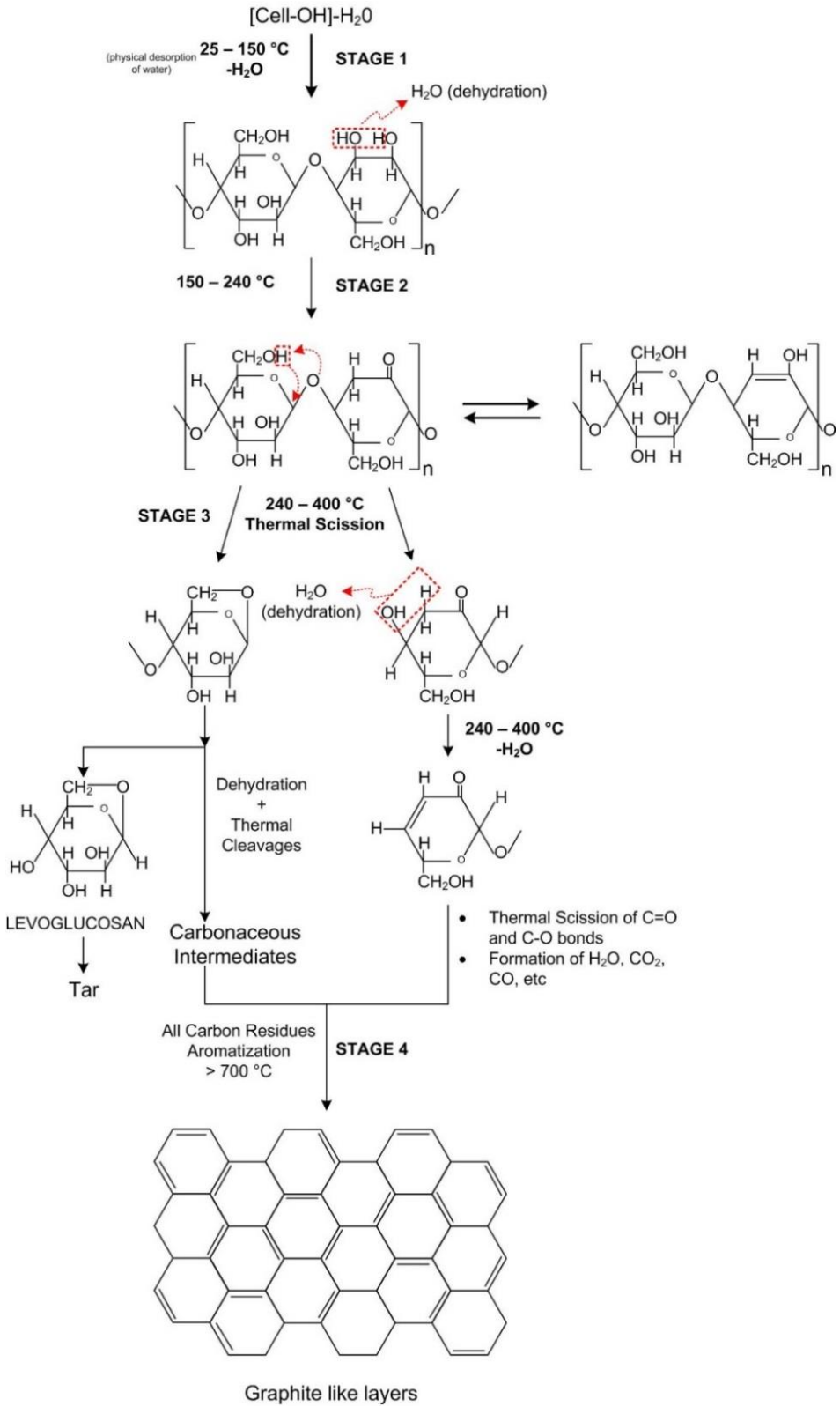


Figure 2.3: Conversion of cellulose into carbon fibers.

The graphene is oxidized to prevent agglomeration, and the graphene oxide nanoribbons (GONR) are usually obtained by oxidative unzipping of multiwalled CNTs **(Higginbotham, Kosynkin et al. 2010)**. These GONRs can be directly spun by choosing the right solvent for dispersion and selecting an appropriate coagulation bath. The GONRs are chemically reduced and spun into fibers followed by annealing. Annealing helps eliminate residual stresses that are generated during the spinning process. The spinning method practiced is wet spinning where the GONRs are dispersed in a solvent such as chlorosulfonic acid, generally found in manufacturing sulfonamide antibacterial and pesticides, to form anisotropic liquid crystal phases. The dispersed GONRs are then passed through a spinneret under pressure using a piston. The fibers are collected in a coagulation bath as shown in figure 2.4. The air gap in the fiber drawing process controls the drawability and tensile properties. The most commonly used coagulation bath solvent is diethyl ether. As the GONRs are constructed with preformed graphene layers, the stabilization process may not be necessary. Both the GONR and chemically reduced GONRs are soluble in chlorosulfonic acid making it a preferred solvent for CF manufacture. The typical tensile strength and Young's modulus values for graphene based fibers (8 wt. % with 12 cm air gap) after thermally annealing at 1050 °C were ~ 378 MPa and ~36 GPa, respectively **(Xiang, Behabtu et al. 2013)**.

2.3.2 Lignin-based carbon fibers

Lignin-based CFs were first produced in 1965 by melt-spinning and dry spinning **(Otani 1969)**. The CFs were about 20 to 30 μm in diameter and exhibited tensile strength of about 0.785 GPa.

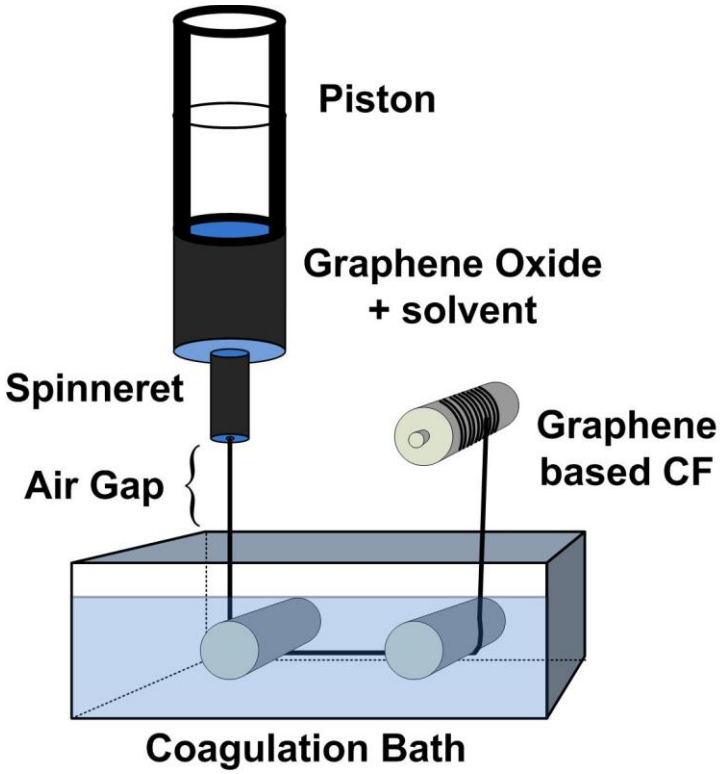


Figure 2.4: A schematic of dry-jet-wet spinning setup.

Since lignin is a very inexpensive precursor, low cost CFs could be produced on a large scale meeting the demand of the market for low cost CFs. The preferred method of manufacturing of CF from lignin is by preparing lignin to be melt spinnable into a fiber in an inert atmosphere. The resulting fiber is then thermally stabilized in an oxidative atmosphere, followed by carbonization. The glass transition temperature T_g of the lignin fiber should be above the processing temperature allowing for crosslinking of lignin fibers to increase strength. To make lignin melt spinnable the process should be designed such that the softening temperature should be low so the liquid flows under low shear. So in a narrow range of temperatures CF precursors may be made from lignin. The greatest advantages of lignin over pitch or PAN are that it is very inexpensive, renewable and can be thermally stabilized at much higher rates than PAN. Typical manufacturing of lignin based CFs is as shown in figure 2.5. In a new technique for developing low cost CFs, lignin is copolymerized with acrylonitrile in dimethyl-sulfoxide (DMSO) by radical copolymerization **(Maradur, Kim et al. 2012)**. Following wet spinning, the resulting fibers are further thermally stabilized at 105 °C for an hour in air and at 280 °C for an hour in nitrogen. Carbonization is carried out under tension (7.86 Pa) at 800 °C in a nitrogen atmosphere. The highest tensile strength and modulus reported are 1.7 GPa and 176 GPa, respectively **(Baker and Rials 2013)**.

Many scientists are trying to find new precursor materials for making low cost CFs. According to Baker's **(Baker and Rials 2013)** review, 51% of the cost of production of CFs is due to the precursor material. Hence, finding an inexpensive precursor which can yield high strength CFs could lead to a billion dollar business. Synthesis and carbonization of triethylammonium- based poly (p-phenylenevinylene) (PPV) has led to a new precursor

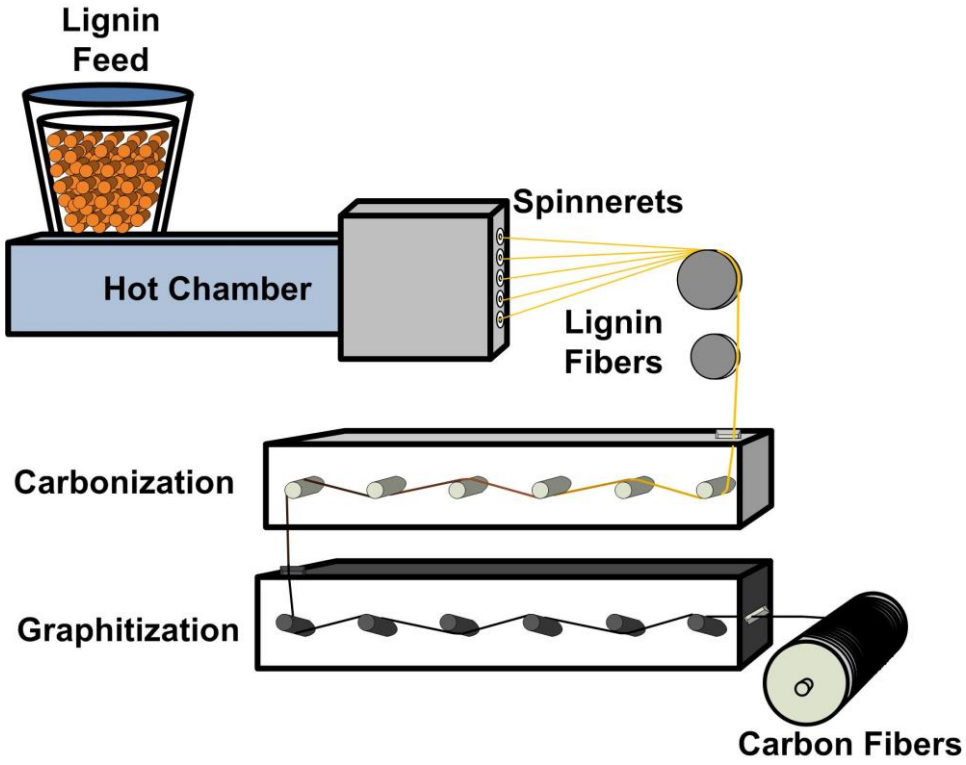


Figure 2.5: A schematic of lignin based carbon fiber production.

material. Unsubstituted PPV is hard to process so the synthesis of a DMSO soluble ammonium-based PPV precursor solves that problem (Buchmeiser, Unold et al. 2013). Also, most of the polymers with carbon backbones contain a high concentration of carbon which could be used as precursor materials for conversion to CFs. Aromatic polyimides have been used as precursors for carbon nanofiber preparation, and various other carbon materials such as membranes, foams, nanofibers, etc., (Inagaki, Ohta et al. 2013). The advantages of using polyimides as precursors are availability of a wide range of chemical structures, a high yield after carbonization, and a simple procedure for carbonization and graphitization steps. Polyacetylene fibers have also been investigated as precursors. Modified polyacetylene fibers are melt spun, thermally stabilized, and carbonized at 1000 °C, resulting in tensile strength and modulus of 2.3 GPa and 386 GPa, respectively (Krutchen 1974). Another example is polyethylene (PE), an inexpensive synthetic polymer. PE fibers are oxidized, sulfonated using sulfuric acid, followed by carbonization at 1200 °C. The resulting CFs result in carbon yield of 75% and a tensile strength of 2.5 GPa and a modulus of 139 GPa **(Horikiri, Iseki et al. 1978)**. Recently, partially biobased PAN-lignin blends have been studied as potential CF precursors (Seydibeyoğlu 2012). Lignin alone has a tensile strength of 3 – 5 GPa, therefore when lignin is mixed with PAN it improves the overall strength of the blend, **(Seydibeyoğlu et al)**.

2.4 Carbon Nanotubes (CNT)

2.4.1 Introduction to CNT

In this section, a brief overview on the discovery, structure, theory, and synthesis of CNTs is presented. Though it is important to understand the precise structure of CNT,

it is not easy to conceive, as there are many theories related to its explanations **(Harris 2001)**. Readers are requested to refer to the references for a deeper understanding on the physics of CNTs.

Smalley and Kroto, in 1985, started their work to identify the products of vaporization of graphite, as their motive was to understand the processes that occur on stars. They used high energy lasers to vaporize graphite in a helium atmosphere and found that the soot contained C_{60}, a carbon nano sphere or the famous "buckminsterfullerene". In similar experiments, Krätschmer and Huffman in 1990, were able to find 90% C_{60} and 10% C_{70}. In 1991, Iijima, in the NEC laboratories in Japan, discovered CNTs which are cylindrical in nature with closed ends. CNTs "archetypal" zig-zag and armchair structures could be understood by bisecting along the three-fold axes and five-fold axis, respectively; figures 2.7 and 2.8. Chirality comes into picture depending on the angle of rotation along the axis of the nanotube. To understand the chirality of the structure of the nanotube, we have to open up the nanotube to form a layer of carbon atoms, a graphene sheet. CNTs are of interest to many researchers from various fields such as physics (electronic, magnetic and thermal properties, etc.), chemists (bonding, nano-test-tubes, etc.), and materials scientists (mechanical properties such as strength, modulus, elasticity, etc.) **(Harris 2001)**.

2.4.2 Structure of CNTs

To understand the structure of nanotubes, it is hard to implement the rules of crystallography even though the structure of CNT is crystalline in nature. Certain biological structures come close to that of CNT, however the factors governing these cylindrical biological structures are insufficient for CNT structure analysis. Many scientists have

introduced different methods to explain the nature of formation of the nanotube. Theoretical structure analysis has helped understand the electronic and vibrational properties of CNTs. Experimental studies, using high resolution electron microscopy, have helped further understand and affirm the structure of CNTs **(Harris 2001, O'connell 2006)**.

The two possible symmetric structures of nanotubes are armchair and zig-zag. In reality, the hexagons on the CNTs arrange helically along the CNT axis. The degree of helical arrangement or chirality is given by θ. To understand the structure in terms of vector, *C*, which joins two equivalent points on the graphene layer as shown in figure 2.6, vectors a_1 and a_2. A cylinder is formed when the graphene sheet is rolled such that the two end points of the vector are superimposed. From figure 2.6, integer (n, m) represents a tubule structure. Therefore vector *C* could be expressed as

$$\boldsymbol{C = na_1 + ma_2}$$

where a_1 and a_2 are of length 0.246 nm as the C–C bond length is 0.142 nm. Furthermore, it is explicit that for n = m, armchair tubes (with $\theta = 30°$) could be formed and for m = 0, zig-zag tubes (with $\theta = 0°$) could be formed. For these tubes the diameter *d* could be calculated by the expression **(Harris 2001, O'connell 2006**),

$$\boldsymbol{d = \frac{0.246\sqrt{(n^2 + nm + m^2)}}{\pi}}$$

and the angle of chirality could be expressed by θ

$$\boldsymbol{\theta = sin^{-1}\frac{\sqrt{3m}}{2\sqrt{n^2 + nm + m^2}}}$$

A unit CNT has the form translation of cylinder. In **Figures 2.7** and **2.8**, unit cells

of armchair and zig-zag are shown. In the armchair type structure the width of the unit cell is same as vector a, while for zig-zag it is √3a. The length of the unit cell depends on the diameter of the CNT. Furthermore, for chiral structures lower symmetry results. The number of carbon atoms in the unit cell can be calculated by the expression

$$\boldsymbol{N = 2\ (n^2 + nm + m^2)d_H}\ \text{if}\ n - m \neq 3xd_H$$

and

$$\boldsymbol{N = 2\ (n^2 + nm + m^2)\ 3d_H}\ \text{if}\ n - m = 3xd_H$$

where d_H is highest common factor of n and m and x is some integer.

2.5 Theory

Since CNTs have diameters smaller than 10 nm, these structures exhibit quantum mechanical behavior. Many scientists have investigated the physics of CNTs structures and have claimed that CNTs possess metal- and semiconductor-like natures. Certain structures with a precise diameter (all armchair structures and n, m multiples of 3) exhibit metal-like character and others behave as semiconductors. As the CNTs are highly anisotropic, electron mobility along the basal planes is high while mobility perpendicular to the planes is low **(Harris 2001, O'connell 2006)**. Wallace, in 1947, calculated band structures for conduction only in planes, while ignoring conduction between the planes. The expression is as follows,

$$\boldsymbol{E_{2D}(k_x, k_y) = \pm\gamma_0\sqrt{\left\{1 + 4cos\left(\frac{\sqrt{(3)}}{2}k_x a\right)cos\left(\frac{k_y a}{2}\right) + 4cos^2\left(\frac{k_y a}{2}\right)\right\}}}$$

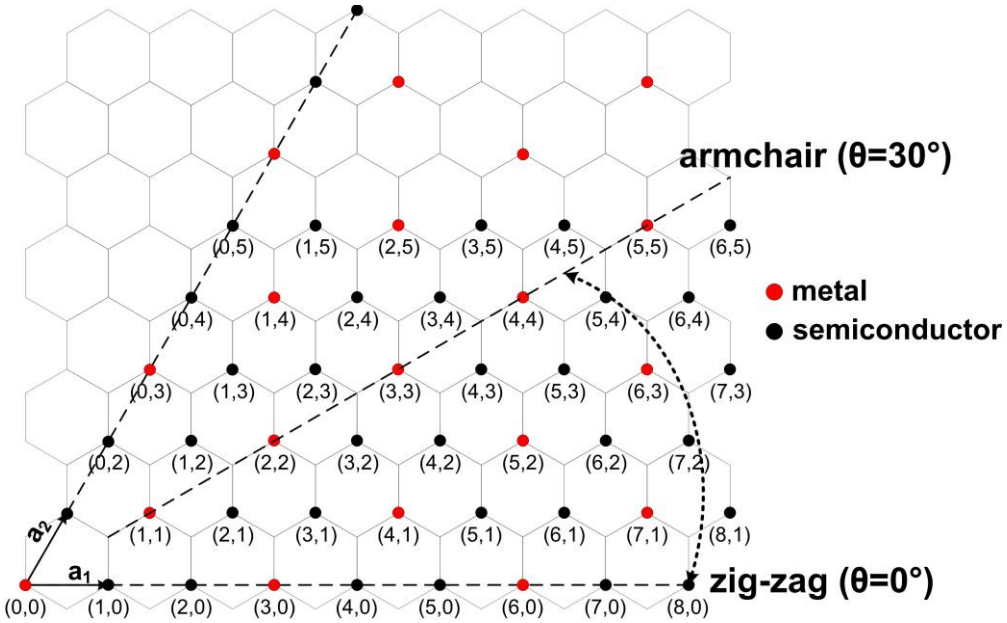


Figure 2.6: A graphene sheet explaining the formation of different types of carbon nanotubes. a_1 and a_2 are the vectors. Red dots are carbon atoms which inherit metallic behavior and the black dots inherit semiconductor behavior **(Harris 2001).**

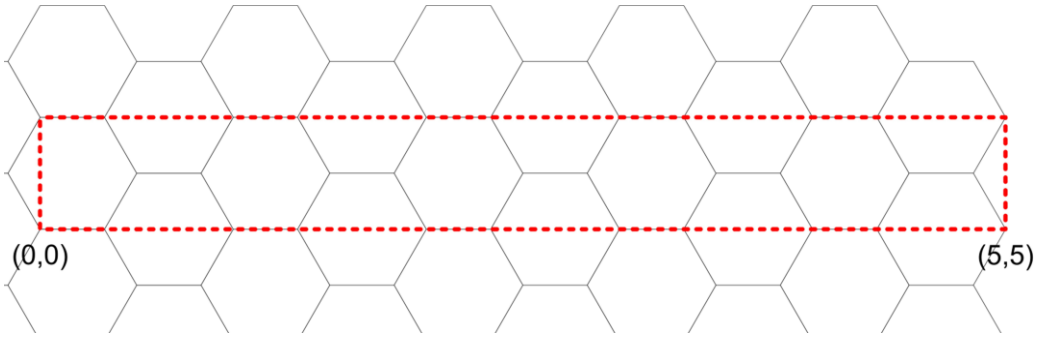


Figure 2.7: A typical unit cell of armchair type of carbon nanotubes **(Harris 2001).**

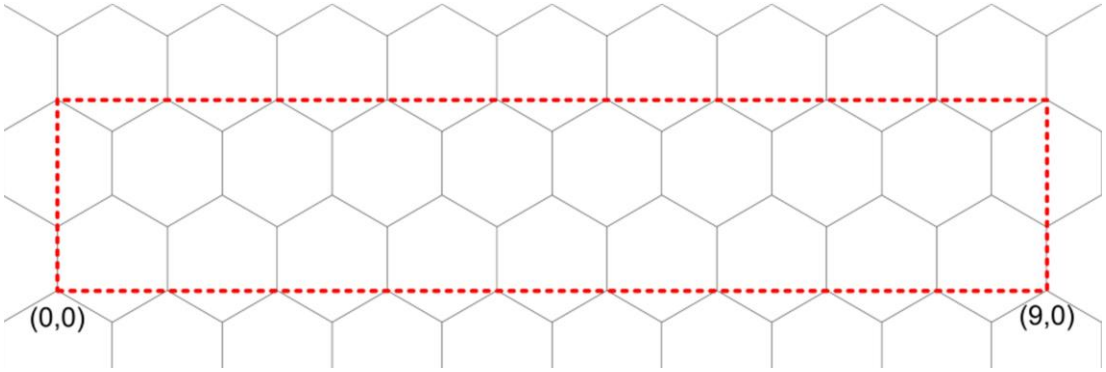


Figure 2.8: A typical unit cell of zig-zag type of carbon nanotubes **(Harris 2001).**

where γ_0, nearest-neighbor transfer integral and a = 0.246nm, in-plane lattice constant. The above expression is for 2D graphite structure with 2 atoms in the unit cell. This yields four valence bands (three σ bands and one π band). figure 2.9 shows the E vs k data for the 2D graphite structure along K−Γ−M **(Ando 2000)**. figure 2.10 shows the density of states for armchair and zig-zag CNT structures **(Terrones 2003)**.

2.6 Synthesis

To achieve the amazing properties of ideal CNTs, it is critical that the CNTs should be fabricated to 100% purity. In reality, however, this is extremely difficult. Various other carbon materials such as amorphous carbon, other carbon nanoparticles, etc., act as impurities. Some of the synthesis techniques used to fabricate high purity CNTs are briefly discussed herein followed by a summary of the synthesis techniques.

Arc discharge

A low voltage (12 to 25V), high current (50 to 120 amps) power supply on graphite electrodes (5 to 20 mm in dia) placed 1 mm apart in the presence of He or Ar gas (100 to 1000 torr) produces CNTs with typical yields ranging from 30 to 90%, as shown in figure 2.11. In the arc discharge method variations are made in the procedure to tune the properties of the CNTs. By mixing different gases, Ar and He, the properties can be varied, for example a higher Ar : He ratio produces smaller diameter CNTs **(O'connell 2006)**. This process is inexpensive and yields high purity CNTs with varying length. It is a batch process.

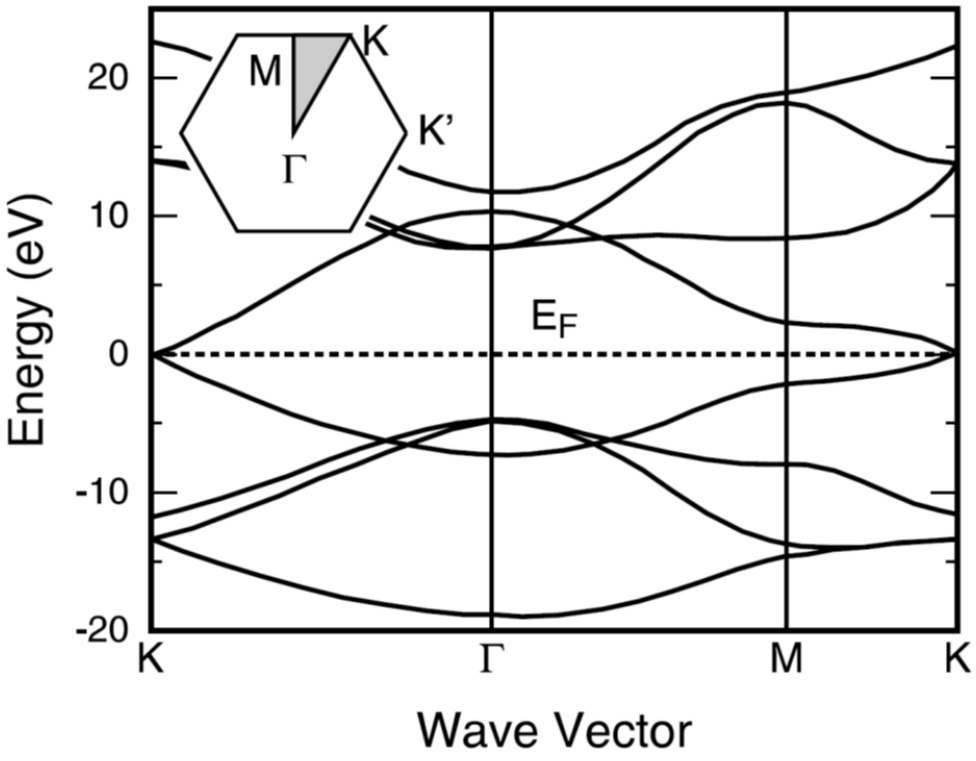


Figure 2.9: Energy vs k-vector along K-Γ-M direction of 2D graphite structure **(Ando 2000).**

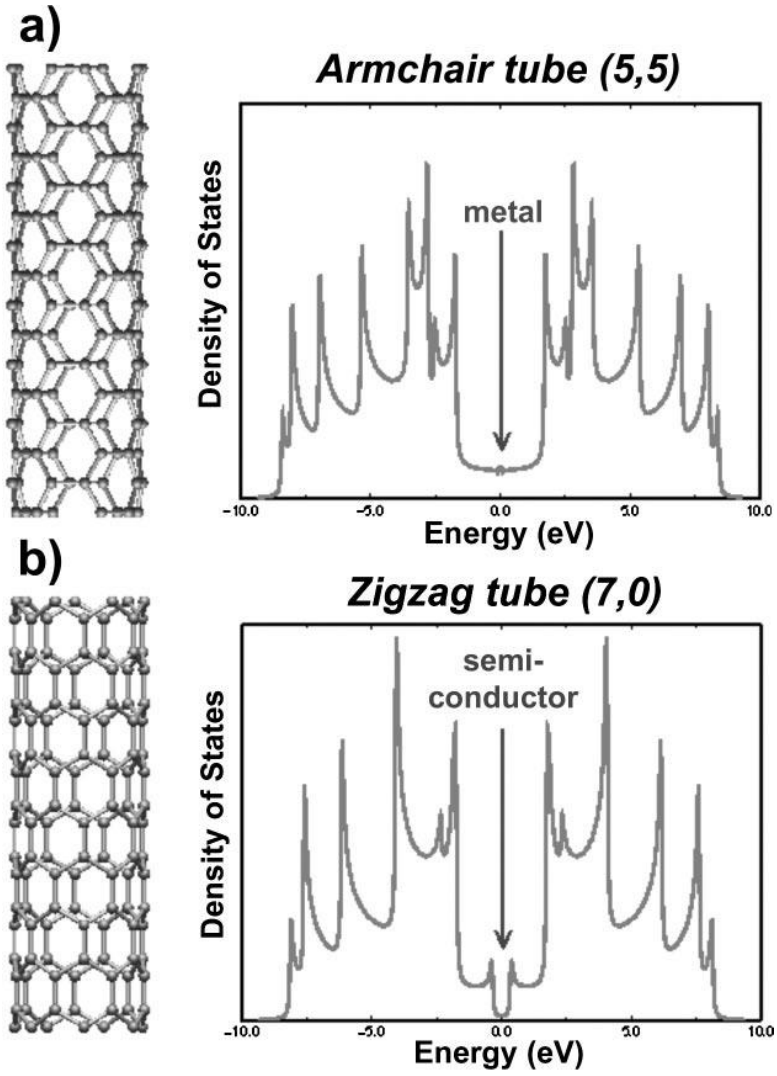


Figure 2.10: Density of states for a) armchair and b) zig-zag CNTs **(Terrones 2003).**

Laser ablation technique

A cobalt/nickel with graphite composite target is evaporated by pulsed or continuous laser by placing the electrode in a quartz tube, at 1200 °C, in an inert atmosphere of He or Ar, at 500 torr, with a typical yield of about 70%. A metal impregnated graphite target produces SWNTs and pure graphite target produces MWNTs and fullerenes. A schematic of a laser ablation technique is shown in **Figure 2.12**. The CNTs are deposited on the cold finger **(O'connell 2006)**. This is a batch process and yields high purity CNTs with a good diameter control. A very expensive process.

Chemical Vapor Deposition (CVD)

Gaseous carbon feedstock, such as methane, is passed over metal nanoparticles at temperatures ranging from 550 to 1200 °C, where the feedstock reacts with the nanoparticles to produce SWCNTs. This method provides higher purity of CNTs (99%) in bulk quantities. Other types of CVD include hot filament, water assisted, oxygen assisted, microwave plasma, radio frequency, thermal, plasma enhanced etc. **(O'connell 2006)**. Some of the recent advancements in CNTs synthesis involve finding new precursors, for example coal, and new processing methods, such as the solar furnace, as shown in figure 2.13. Coal is much less expensive than graphite and high purity hydrocarbon gas sources. Even though CNTs can be produced from both arc-discharge and thermal plasma jet with coal as precursor, large scale production is not currently possible **(Moothi, Iyuke et al. 2012)**. However, CVD can be used to synthesize CNTs in large quantities by optimizing the experimental conditions.

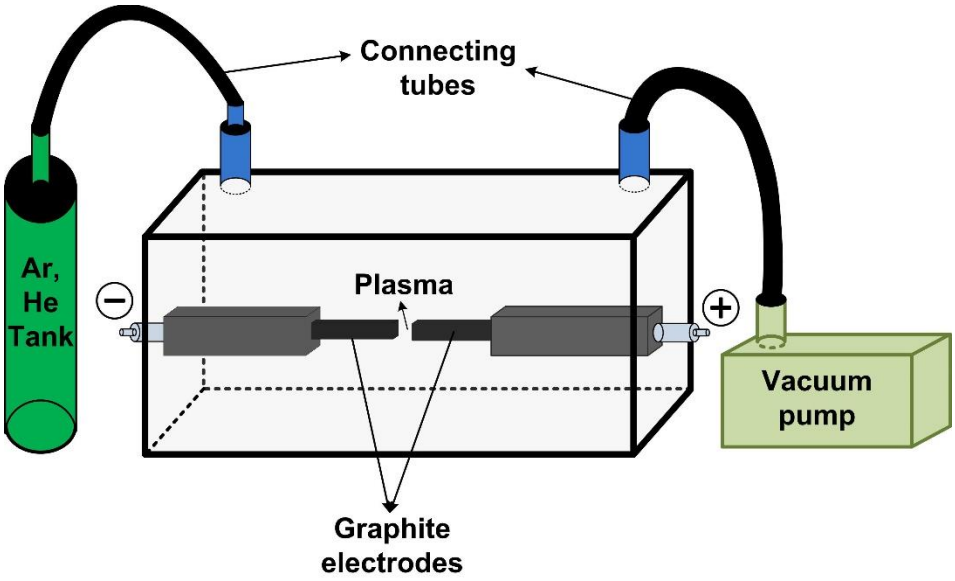


Figure 2.11: A schematic of arc-discharge tube with a small gap between electrodes.

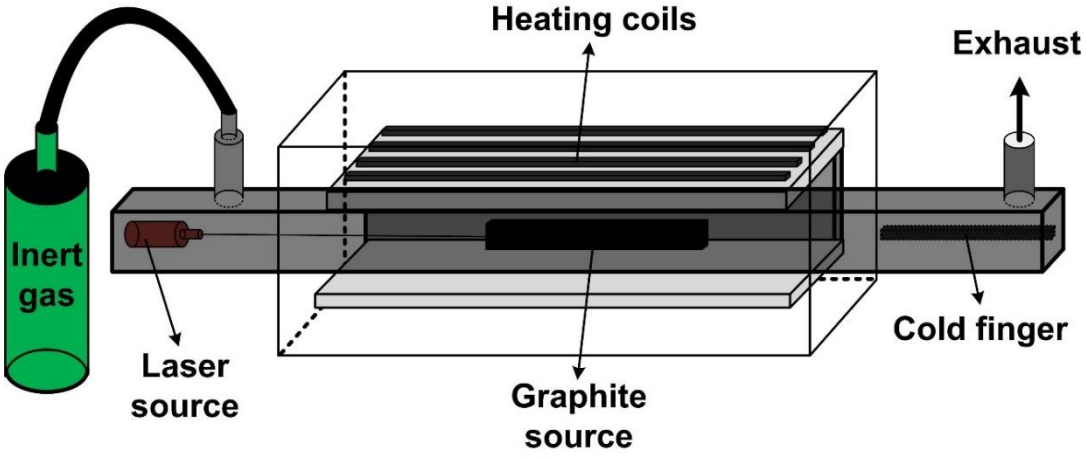


Figure 2.12: A schematic of laser ablation technique.

Solar Furnace

In the solar furnace method the graphite source with a metal catalyst is placed in a graphite crucible. A highly directed solar beam hits the source creating a temperature of about 3000 °K, triggering evaporation of carbon and resulting in soot settling on the walls of the graphite tube. This soot on the walls of the graphite tube contains CNTs and other forms of carbon nanostructures such as fullerenes. A schematic is as shown in figure 2.13. The dia of the CNTs produced by this method is in the range of 1.2 to 1.5 nm, with high purity comparable to those of CNTs produced by the laser ablation technique **(Laplaze, Bernier et al. 1998, Flamant, Ferriere et al. 1999)**. However the lengths of the tubes are random and it is a very slow process with a yield of upto 60%. Table 2.1 summarizes the advantages and disadvantages of various CNT synthesis techniques.

Table 2.1: Advantages and disadvantages of the various synthesis techniques **(Szabó, Perri et al. 2010)**.

Methods	Typical Yield	Advantages	Disadvantages
Arc Discharge	30 - 90%	Simple process, inexpensive, high yield and high purity, dia = 1 to 20 nm	Shorter tubes with random length, batch process
Laser Ablation	~ 70%	High purity, good diameter control	Cost of the equipment is high, batch process
Chemical vapor deposition	~ 95%	High purity, long tubes, easy processing, continuous process, dia = 0.8 to 2 nm	High defects present
Solar furnace	~ 60%	dia= 1.2 to 1.6 nm	Very slow process and random length tubes.

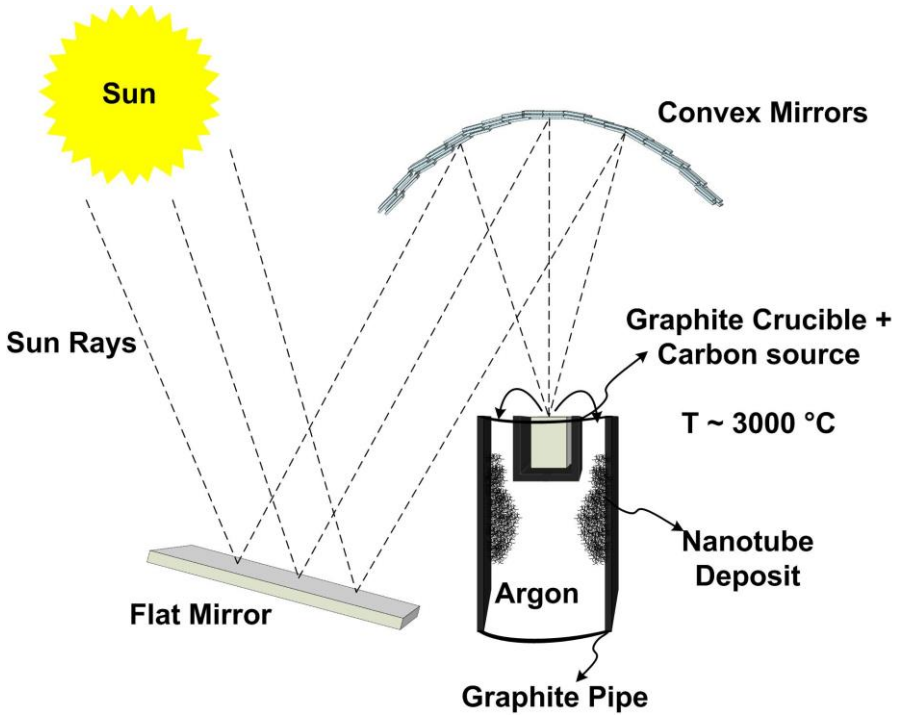


Figure 2.13: A schematic of CNTs produced by solar furnace technique.

2.7 Carbon Nanotube-based Fibers

2.7.1 CNT-based composite fibers

The high performance fiber industry has changed the face of the textile market, because of the properties that high performance fibers exhibit. To make composite fibers many researchers have studied new processes and materials that deliver high strength. A polymer matrix with CNTs has proven to increase the strength and modulus considerably, however the results have fallen far short of the theoretical values. **Table 2.2** summarizes the strength and modulus of various compositions of composite fibers derived using CNTs as fillers **(Song, Zhang et al. 2013)**. From the table we can see that for carbonized PAN with 1 wt. % SWNT, the tensile strength and modulus increased by 60% and 49%, respectively. For Nylon 6, from addition of 1.5 wt. % of SWNT, the tensile strength and modulus have increased by ~ 66% and 172% respectively. Similarly for PAN with 1 wt. % SWNT, the tensile strength and modulus have increased by ~18% and ~30% respectively. About a 4-fold increase in strength and about a 6-fold increase in modulus are reported by Meng, Zhang et al. in the case of PVA + 10 wt%. SWNT. A more than 35-fold increase in strength and more than 55-fold increase in modulus, in the case of UHMWPE + 5 wt%. MWNT, has been reported by Ruan, Gao et al. A brief overview on various composite fibers, mentioned in Table 2.2 are summarized below. Figure 2.14 (A, B, C, and D) are pictorial representation of the difference between the tensile strength and elastic modulus of various composite fibers discussed in table 2.2.

Nylon-CNT composite fiber

The CNT- polycaprolactam sonicated suspension was heated and mechanically stirred to 250 °C with 6-aminocaproic acid addition. Following the mixture formation, the

Table 2.2: CNT/polymer composites and their tensile strength, elastic modulus, and toughness.

Composite fiber (CNT wt.% + polymer)	Tensile Strength (GPa)	Elastic modulus (GPa)	Toughness	References
Carbonized PAN	2.0 ± 0.4	302 ± 32	N/A	**(Chae, Minus et al. 2007, Chae, Choi et al. 2009)**
Carbonized PAN + 1 wt% SWNT	3.2 ± 0.4	450 ± 49	N/A	
Nylon 6	0.045	0.44	N/A	**(Gao, Itkis et al. 2005)**
Nylon 6 + 0.1 wt% SWNT	0.086	0.54	N/A	
Nylon 6 + 0.2 wt% SWNT	0.093	0.66	N/A	
Nylon 6 + 0.5 wt% SWNT	0.083	0.84	N/A	
Nylon 6 + 1.0 wt% SWNT	0.083	1.15	N/A	
Nylon 6 + 1.5 wt% SWNT	0.075	1.2	N/A	
Polyacrylonitrile (PAN)	0.9 ± 0.18	22.1 ± 1.2	35 ± 9 MPa	**(Chae, Minus et al. 2006)**
PAN + 0.5 wt% SWNT	1.06 ± 0.14	25.5 ± 0.8	41 ± 8 MPa	
PAN + 1 wt% SWNT	1.07 ± 0.14	28.7 ± 2.7	39 ± 8 MPa	
Poly(p-phenylenebenzobisoxazole) (PBO)	2.6 ± 0.3	138 ± 20	N/A	**(Kumar, Dang et al. 2002)**
PBO + > 10wt% SWNT	4.2 ± 0.5	167 ± 15	N/A	
Polypropylene (PP)	0.71	6.3	7.93 dN/tex	**(Kearns and Shambaugh 2002)**
PP + 0.5 wt% SWNT	0.84	9.3	9.37 dN/tex	
PP + 1 wt% SWNT	1.03	9.8	11.5 dN/tex	
Poly(vinyl alcohol) (PVA) + >60 wt% SWNT	0.15	9 to 15	N/A	**(Vigolo, Penicaud et al. 2000, Dalton, Collins et al. 2003)**
PVA + 60 wt% SWNT	1.8	80	570 $J.g^{-1}$	
PVA (commercial fiber)	1.6	40	N/A	**(Razal, Coleman et al. 2007)**
PVA + >60 wt% SWNT	1.8	78	120 ± 152 $J.g^{-1}$	

Table 2.2: (Continued)

Composite fiber (CNT wt.% + polymer)	Tensile Strength (GPa)	Elastic modulus (GPa)	Toughness	References
PVA + 60 wt% SWNT	0.3	40	600 $J.g^{-1}$	**(Dalton, Collins et al. 2004)**
PVA	1.2 ± 0.3	21.8 ± 3.0	55.8 ± 12.3 $J.g^{-1}$	**(Meng, Zhang et al. 2013)**
PVA + 10 wt% SWNT	2.5 ±0.1	36.3 ± 1.3	101.4 ± 11.4 Jg^{-1}	
PVA + 10 wt% SWNT	4.4 ± 0.5	119.1 ± 8.6	171.6 ± 30.4	
PVA	~0.4	~13	N/A	**(Wang, Ciselli et al. 2007)**
PVA + 1 wt% SWNT	~1.2	~17.5	N/A	
PVA	1 ± 0.1	45 ± 7	22 ± 4 $J.g^{-1}$	**(Minus, Chae et al. 2009)**
PVA	1.6 ± 0.1	48 ± 3	40 ± 6 $J.g^{-1}$	
PVA + 1 wt% SWNT	1.4 ± 0.1	60 ± 6	29 ± 6 J.g-1	
PVA + 1 wt% SWNT	2.6 ± 0.2	71 ± 6	59 ± 7 $J.g^{-1}$	
PVA + 2-31 wt% SWNT	~2.9	~244	N/A	**(Young, Blighe et al. 2010)**
Ultra- high molecular weight polyethylene (UHMWPE)	0.11 ± 0.002	2.42 ± 0.4	361.8 ± 22.9 MPa	**(Ruan, Gao et al. 2006)**
UHMWPE	3.51 ± 0.13	122.6 ± 1.9	76.7 ± 7.5 MPa	
UHMWPE + 5 wt% MWNT	0.13 ± 0.004	2.62 ± 0.32	593.2 ± 114.5 MPa	
UHMWPE + 5 wt% MWNT	4.17 ± 0.04	136.8 ± 3.8	110.6 ± 10.5 MPa	

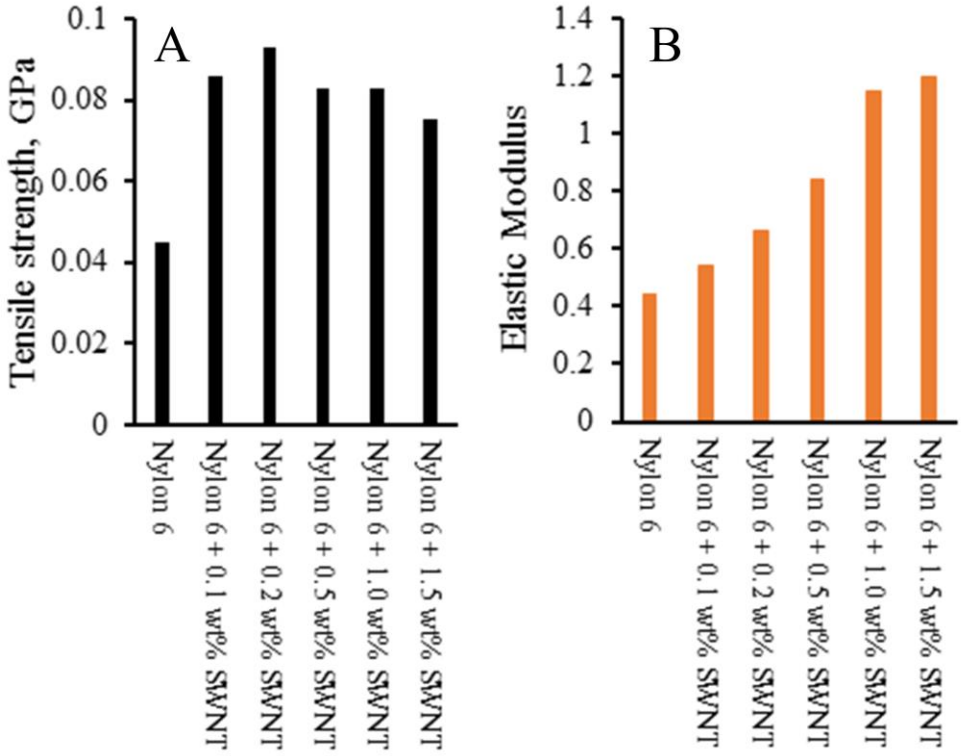


Figure 2.14 A and 2.14 B: Tensile strength and elastic modulus data for Nylon 6-CNT based composite fibers **(Gao, Itkis et al. 2005)**.

product was poured in water and the hard polymer was precipitated. The polymer was broken into small pieces was heated to 250 °C and extruded using a spinneret by pressurized nitrogen gas. The fibers were then characterized with various mechanical tests. The incorporation of 1.5 wt % SWNTs into nylon 6 increased the tensile modulus and tensile strength about three and two times, respectively. These improvements in strength and modulus data are compared in figures 2.14A and 2.14 B.

PBO-CNTs

High pressure carbon monoxide nanotubes (SWNTs) were added to the PBO polymerization solution in the ratio of 90 : 10 :: PBO : SWNT and 95:05. The fibers were spun using dry-jet wet spinning process using a piston driven setup. The fibers were collected in the distilled water coagulation bath maintained at room temperature. The air gap was maintained at 10cm from the spinneret to coagulation bath. The fibers with 10% SWNT in PBO increased the tensile strength to 50% of the PBO fibers and increased the creep resistance.

PP-CNTs

The SWNTs were dispersed in decalin by sonication and the PP pellets were added to the solvent mixture. The PP-SWNTs mixture, in the form of coarse powder was extruded with a spinneret of 1.22 mm diameter and the fiber was further drawn. Though the PP-SWNT composite fibers were of not enough strength compared to other composite fibers, 1 wt% loading of nanotubes, the fiber tensile strength increased by 40% and the modulus increased by 55%.

By incorporating CNTs dispersed in sodium dodecyl sulfate, a surfactant, by sonication, the solution was injected in a co-flowing system of a polymer solution. The

resulting CNT ribbon was taken out and dried and characterized with mechanical properties. The strength of the ribbon was 10 times higher than high quality bucky paper. Also knotting the fibers revealed that the fiber can be curved through 360° in few micrometers, which demonstrates the flexibility and high torsion resistance of those fibers.

PVA-CNTs

In Razal's, Dalton's and Meng's research; the PVA-CNTs composite fibers were extruded in different spinning mechanism. Razal's group used coagulation-spinning method, which involved dispersion of SWNT injected into a PVA solution flowing in a glass tube. In Dalton's group, the aqueous dispersion of nanotubes was spun in a rotating coagulation bath of aqueous PVA solution. In Meng's group, shear-flow gel spinning method was used, in which the methanol was stirred to provide shearing as the PVA-SWNT solution was injected to form fiber. The spun fiber were subsequently drawn on hot plates at 90 °C and 160 °C. Hence there were variations in the tensile strengths of the PVA-CNTs composite fibers.

In Wang's research group, the SWNTs were dispersed in DMSO, and PVA solution was mixed to form the PVA-SWNT composite mixture. The mixture was spun by solid-state spinning with a draw ratio of 5. The tape drawn from the composite (PVA-SWNT) was 200% stronger than the PVA tape of same length. Hence, addition of 1 wt% SWNTs increased the strength drastically. However in Minus's group, the PVA-SWNT composite fiber was extruded by gel spinning method. The tensile properties of the composite fibers were higher than that of the composite fibers from Wang's group. This could be due to spinning method, the solution preparation techniques involved and the fiber diameter, purity of CNTs and interfacial binding between the polymer and the CNTs, etc. In Young's

group, the PVA-CNT composite fiber was extruded using coagulation spinning. The diameter of the fiber was in the range of 1~ 15 μm, the mean modulus was about 244 GPa and strength about 2.9 GPa. This high strength was attributed to the distribution of the CNTs in the polymer matrix and binding. Higher the concentration of the CNTs in the matrix higher the load bearing interaction. The increasing trend in strength and modulus observed with addition of CNT in PVA fibers are showed in figures 2.15A and 2.15B respectively. Some of the authors **(Vigolo, Penicaud et al. 2000, Dalton, Collins et al. 2004, Razal, Coleman et al. 2007)** claim to have carbon nanotubes as high as 60 wt% in the PVA based composite fibers, however, the percentage calculated from the procedure in the respective papers does not exceed 8 wt% of CNTs. From several studies it is well known that incorporating higher concentrations of CNT especially above 5 wt% is extremely difficult and one cannot believe that the authors produced PVA samples with 60 wt% CNT loading.

UHMWPE-CNTs

In Ruan's group, multiwalled CNTs were used as reinforcement in the polymer matrix. 5 wt% MWCNTs were reinforced in gel-spun ultra-high molecular weight polyethylene (UHMWPE) resulting in a yield strength of 4.2 GPa and strain at break of 5%. By reinforcement of CNTs in UHMWPE there was an increase of 18.8% in tensile strength and 15.4% in ductility. In addition, a 44.2% increase in energy to fracture was observed.

2.8 CNTs based CFs

CNT-based CFs are produced by various approaches, such as aqueous dispersion, dispersion in strong acids, drawing from CNT forests, drawing from CVD reactor in the

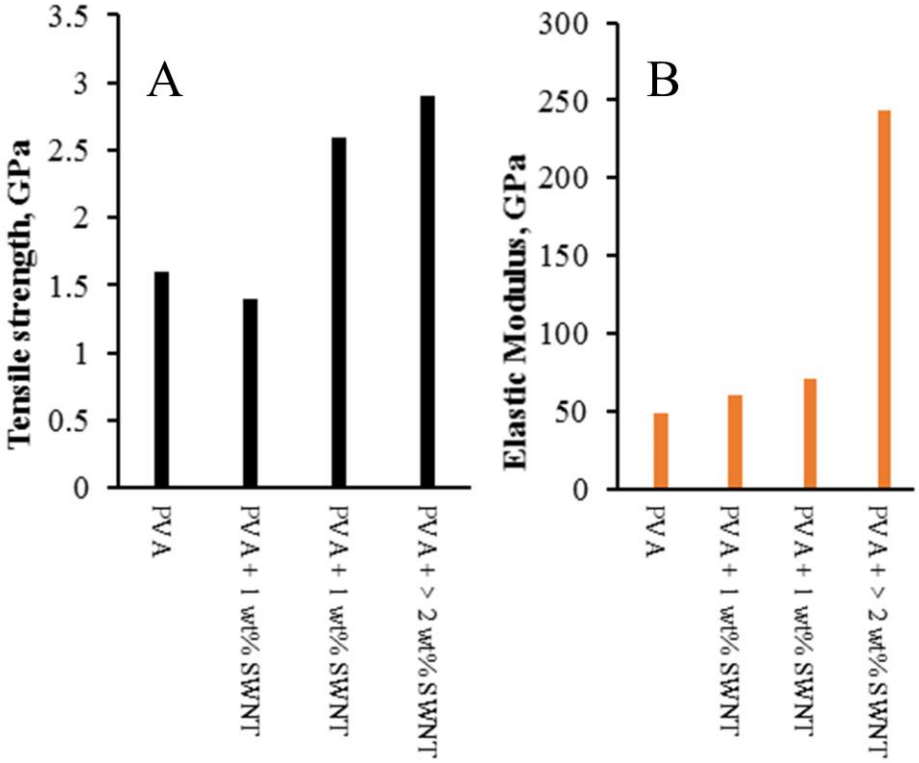


Figure 2.15 A and 2.15 B: Tensile strength and elastic modulus data for PVA-CNT based composite fibers from various researchers respectively **(Minus, Chae et al. 2009, Young, Blighe et al. 2010)**

form of aerogel, etc. They are relatively ductile when compared to PAN- or pitch-based CFs because the knot efficiency of the CNT-based CF is ~ 1 while PAN- or pitch-based CFs cannot be knotted **(Liu and Kumar 2012)**. The tensile strength and modulus of CFs are higher for CNT fiber spun from CNTs forests and from CVD reactors. However, stretching the CFs aligns the CNTs and improves the mechanical properties by increasing the interaction between CNTs. Longer CNTs do help to improve the performance, chemical modification, gamma-ray induced crosslinking, and heat treatment, etc., on the CNTs surface, which further enhance inter-nanotube interaction, resulting in increasing in strength. However, the compressive strength achieved was low **(Liu and Kumar 2012)**. When synthesizing CNTs by various processes discussed in section 2.4.4, if there is a possibility to isolate the pure CNTs, so that the quality of the CF produced using such nanotubes would yield higher strength and modulus. However during the preparation of CNTs there are various other structures generated, such as fullerenes, amorphous carbon agglomerates, and these structures are the weak points or defects in CNT-based CFs **(Harris 2001)**

Furthermore, the CNTs that are produced with highest purity must also be dispersed well in the medium of interest. Generally the CNTs are dispersed in suitable polymers and melt drawn to high draw ratios. Increasing the draw ratio helps align the CNTs in the polymer matrix and hence increases the strength of the CFs. CNTs can also be grafted into the CFs, such as PAN- or pitch-based, to increase the alignment of the polymer matrix or to act as the load bearing structures in the CF matrix **(Song, Li et al. 2012)**. Carbon nanofibers produced by the pyrolysis of cellulose contain no skin-core morphology, resulting in high tensile modulus of 60 and 100 GPa,

when carbonized at 1500 and 2200 °C, respectively **(Deng, Young et al. 2013)**. By producing high purity and continuous nanotubes the inter-nanotube interaction can be increased resulting in high strength carbon fibers. In an attempt to make the CNTs long, in 2009, a research group from Peking University, China, led by Qunqing Li, grew ultra-long single wall carbon nanotubes using an improved CVD technique. Using ethanol or methane as the feed and Fe-Mo monodispersed catalyst, super aligned ultra-long CNT was grown for a length of 18.5cm **(Wang, Li et al. 2009)**. Homogeneous temperature spatially during the growth process is the key for constant electrical characteristics. However, improving the mechanical properties of the CNTs along the length is also equally important for high strength materials applications. In 2013, Yingying Zhang from Tsinghua University, China, reported that 550 mm long CNTs were fabricated using a floating CVD process and catalyst activation/deactivation probability. Following optimized processing parameters half-meter long CNTs fabricated exhibited a tensile stress of up to 120 GPa **(Zhang, Zhang et al. 2013)**.

CHAPTER 3

EXPERIMENTAL

3.1 Materials and methods

Materials used, sample preparation and characterization methods used in this research are covered in this chapter. The experimental setup for the wet spinning of PAN, with or without carbon nanotubes (CNTs) or carbon nanofibers (CNFs), and carbonization of the precursor fibers was developed. A brief overview of the preparation of the dope for wet spinning is discussed, followed by process for wet spinning and the process of converting the precursor into carbon fibers. The precursor and carbonized samples are further characterized using various techniques, such as, scanning electron microscopy (SEM), focused ion beam (FIB), transmission electron microscopy (TEM), Tensile testing (for mechanical properties evaluation), thermogravimetric analysis (TGA) and X-ray diffraction.

CNT yarns were obtained from Nanocomp Technologies, Inc., Merrimack, NH and General Nano, Cincinnati, OH. These are indicated as CNTYN and CNTYG in most of the discussion. These yarns are synthesized in a CVD reactor where CNTs grown on a substrate are spun and twisted to make a CNT yarns. CNF were obtained from Applied Sciences Inc., Cedarville, OH. Also, a textile grade PAN was used as the polymer and was obtained from Carbon fiber technology facility at Oak Ridge National Laboratory (ORNL), Oak Ridge, TN. Dimethylformamide (DMF) was purchased from Fisher Scientific Co.

3.1.1 CNT yarn densification

CNTYN samples were used to study the effect of densification on the mechanical properties of the yarn. Four samples were studied with one as the control. Three of the four samples were densified with DMF (solvent), 0.1 wt% PAN and 1 wt% PAN, respectively. The schematic of the densification setup is as shown in figure 3.1. W1 is greater than W2 and the sample is held in the solution using spectra fibers along the pulley. A constant load W2 was suspended, as shown in the figure, to maintain the sample under tension. The samples were kept in solvent/solution for two hours under specified tension. After that the samples were dried in the fume hood at room temperature overnight at a constant load of 500 g. Furthermore, due to ribbon like nature of the yarn the diameter was calculated based on the circumference of the yarn.

3.1.2 Spinning Solution Preparation

For extruding the filaments using wet spinning approach, the spin-dope was prepared by dissolving the PAN in DMF. For optimizing the conditions of spinning, various concentrations of PAN (6, 9, 12, 13, 14, 15, 16, 18, and 21 wt %) were prepared. After trying wet-spinning the successful spinnable dope concentrations were determined to be 12, 13, 14 wt% PAN for the lab scale wet spinning set-up. 12 wt% PAN suited well as the viscosity was lower than that of 14 wt% PAN and dispersion of the CNTs or CNFs was easier.

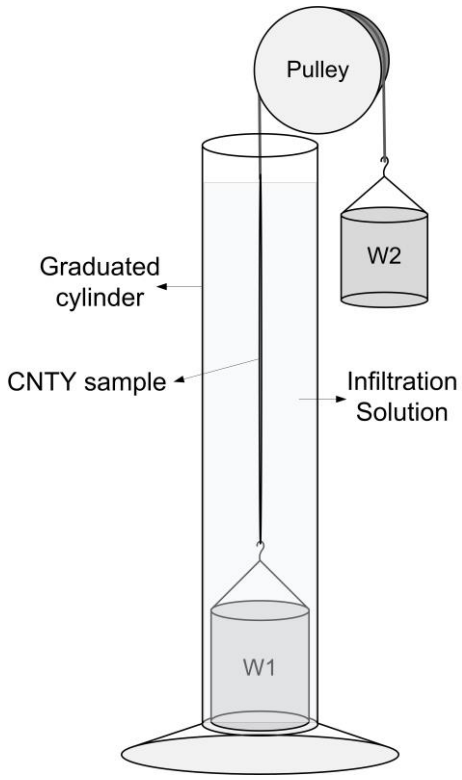


Figure 3.1: Schematic of CNTY densification setup.

Table 3.1: Summary of type of solutions prepared.

12 wt% PAN dissolved in DMF	P0
3.2 wt % PAN-g-CNTs in 12 wt% PAN	P1
6.4 wt % PAN-g-CNTs in 12 wt % PAN	P2
3.2 wt % PAN-g-(CNT+CNF) in 12 wt % PAN	P3
3.2 wt % PAN-g-CNFs in 12 wt % PAN	P4
6.4 wt % PAN-g-CNFs in 12 wt % PAN	P5

Cross-linked engineered CNTs and CNFs were prepared in the chemistry department (Dr. Mays group). CNTs were crosslinked with 30% PAN (70% CNT + 30% PAN) while CNFs were crosslinked with 20% PAN (80% CNFs + 20% PAN). So the resulting PAN-g-CNTs contained 70% CNTs and PAN-g-CNFs contained 80% CNFs. A series of dispersion experiments were conducted wherein 0.2, 0.4, 0.8, 1.6, 3.2, 6.4 and 12.8 wt % of PAN-g-CNFs were added to 12 wt% PAN to see the optimal concentration that could be wet-spun. As the goal was to increase the nanofiller concentration in PAN, 3.2 and 6.4 wt% of PAN concentrations were better in terms of maintaining dispersion with no large agglomerates in the solution and avoiding any clogging of the spinneret needle. Accordingly, a total of five solutions and one control (12 wt% PAN) solution were prepared, as shown in Table 3.1, (P0 to P5) at room temperature, filtered, degassed and stored in 60 ml glass bottles, for wet-spinning.

3.1.3 Wet Spinning setup

Following dope preparation, the PAN + CNTs or CNFs filaments were extruded using the simple wet spinning line put together in our laboratory. Schematic of the wet spinning set up is as shown in figure 3.2. The first coagulation bath was 122 cm × 15.24 cm × 15.24 cm in dimensions and two smaller baths of 60.96 cm × 15.24 cm × 15.24 cm were fabricated using stainless steel sheets. The wet spinning setup consisted of a long first coagulation bath with higher concentration of DMF in water (65%) followed by a second coagulation bath with 30% DMF concentration in water. A hot water bath (90 °C) was used for washing as well as drawing. Most of the filament stretching was carried out in the hot water bath. A winder at the end of the hot water bath was used to collect the continuous

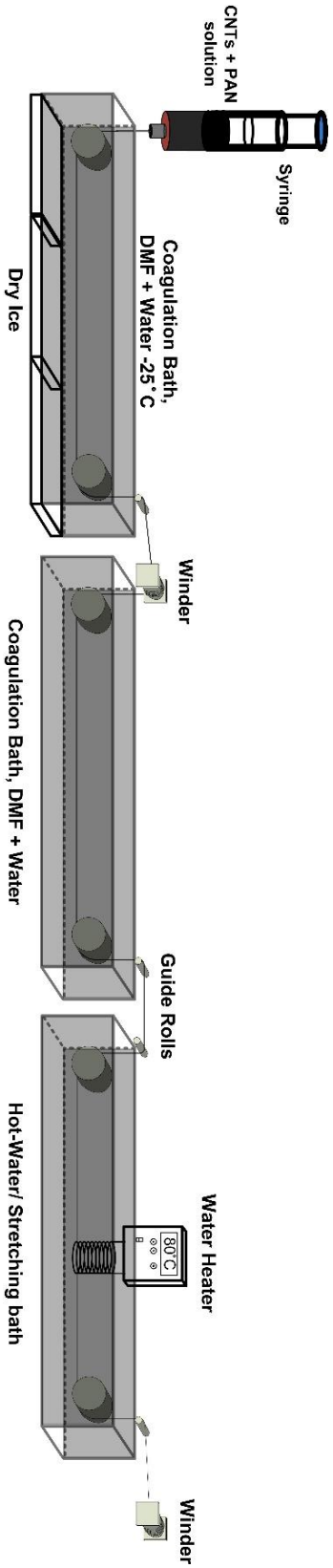


Figure 3.2: Schematic of wet spinning setup used to make precursor fibers.

filament on a spool. Thirty gauge, 160 µm inner diameter flat tip needles, obtained from CML supply Inc., Lexington KY, were used as spinneret attached to a 3 or 5 ml syringes, obtained from Becton, Dickinson and Company, Franklin lakes, NJ. A high torque low speed screw driven pump, bought from New Era Pump Systems, Inc., Farmingdale, NY, was used to push the spin dope from syringe through needle. The set-up was also coupled with two take-up rollers, one after the first coagulation bath and the other after the hot water stretching bath. The first coagulation bath was maintained below 0 °C using dry-ice. Second coagulation bath was kept at room temperature and the hot water bath was maintained at 90 °C. Single filament extruded from the needle in the first coagulation bath was collected on the first take-up roller at a draw ratio of 1 to 1.2 while the draw ratio at the last take-up roller for winding was maintained at 6 to 6.43. The total draw ratio was about 6 to 7.7.

The diameter of the filament at the first take-up roller was about $\approx 82 \pm 3$ µm whereas the diameter after final hot water stretching was about $\approx 30 \pm 7$ µm. The reduction in diameter of the filament at the first take-up roller, is because the filament experiences drag and the hydrodynamic force is smaller than the tension on the filament as per the mathematical model of wet spinning by **(Ockendon and Terrill 1993)**. Furthermore, the precursors were hand stretched on a hot plate set at 120 °C. As the filaments were stretched, the diameter reduction enhanced the orientation of the polymer chains and the nanofillers. After hot plate stretching the precursors were further characterized for strength and microscopic structure of the filaments.

3.1.4 Stabilization and Carbonization setup

Different filaments formed in the wet spinning line were subjected to oxidative stabilization, at 230 °C (1.5 hours) and 245 °C (one hour) while carbonization was carried out at 1100 to 1150 °C in nitrogen atmosphere. The temperature and time breakdown for stabilization and carbonization is as follows, 40 (5min) – 230 (45 min) – 230 (1 hour 30 min) – 245 (10min) – 245 (1 hour) – 500 (40 min) – 700 (40 min) – 900 (40 min) – 1150 (40 min). Schematic of the lab scale stabilization and carbonization set-up is shown in figure 3.3. The tube furnace used in this work was made by Applied test systems Inc. Stabilization of the filaments were carried out at 100 ml/min air flow in the tube furnace followed by 100 ml/min nitrogen flow for carbonization. The filaments were subjected to a tension of 1-1.5 MPa/1000 filaments, throughout the heat treatment process. As the temperature increased from 900 to 1100 °C, the tension on the filaments increased to 5 MPa/1000 filaments (30g/1000 filaments). All the precursor filaments, P0 to P5, were converted to carbon fibers, C0 to C5.

3.2 Characterization techniques

3.2.1 Differential scanning calorimetry

A Mettler 840 differential scanning calorimeter (DSC) was used to determine the temperatures of cyclization and the enthalpies of exothermic reactions of the fiber samples. Diffusion mechanism of DMF from PAN was also investigated using DSC. About 2.7 to 10 mg samples were weighed and mounted in the 40 µL aluminum pans covered with lid.

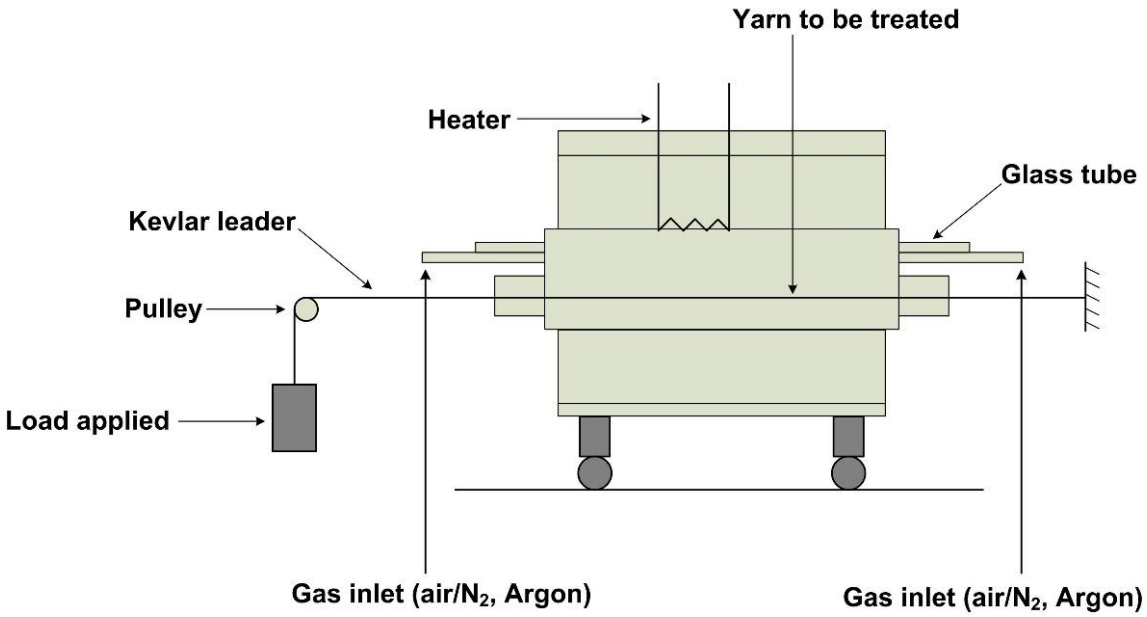


Figure 3.3: Schematic of stabilization and carbonization tube furnace used in this work.

A couple of holes were punctured on the lid so that the sample would be in the purge gas atmosphere. The samples were scanned from 25 °C till 320 °C at a heating rate of 5 °C /min.

3.2.2 Thermogravimetric analysis

Thermogravimetric analysis (TGA) was conducted on various samples using the Mettler 840 TGA. The purge and reactive gas used was nitrogen and the heating rate was 10 °C /min. The temperature range was from room temperature to 1000 °C.

3.2.3 Dynamic mechanical analysis

Dynamic mechanical analysis (DMA) was conducted, using DMA RSA3 TA instrument at ORNL, on precursor samples. 10 filaments of each sample were mounted on 1.25 cm gauge length card templates. The template was inserted into grips and tightened with screws. Precursor filaments from P0 to P5 were tested at 10 HZ and from – 50 °C to 180 °C at a heating rate of 5 °C /min. Strain on the sample was set at 0.5%

3.2.4 Tensile testing

MTS single filament tensile tester, at ORNL, was used to determine the mechanical properties of the precursor fibers and carbonized filaments. A 2N load cell was used and 25 mm gauge length was adopted for the sample preparation. An extension rate of 1 mm/min was set for the precursor fibers and 0.2 mm/min for the carbonized filaments. Single filament was mounted on a 25 mm gauge length card paper template using super glue. After overnight drying, average of ten diameter measurements were taken optically

for each sample. After mounting the template with the filament on the tensile tester, the samples were tested. Later, the broken ends were observed under SEM to examine the failure behavior.

3.2.5 Microscopy

SEM, FIB and TEM.

The SEM and the focused ion beam (FIB) instrument used in this work was Auriga 200 at the University of Tennessee, microscopy center. The samples were mounted on aluminum stubs using a carbon tape. Gold was sputtered on the surface to avoid any charge development in the SEM. FIB uses gallium ions to mill or cut through the material in an evacuated chamber. The sample preparation for FIB is similar to SEM, however, platinum was deposited on the surface before milling with a finer probe current. Larger probe current (8 nA) was used to mill the sample transversely, while a finer probe (100 pA) was used to polish the sample.

SEM/FIB pictures of CNT yarns were analyzed using ImageJ software from national institute of health (NIH). Diameter of the CNT yarns, diameter of the CNTs and twist angle were measured from the SEM pictures of the surface of the yarns using the software. The void % was also measured using the software by shading the area with no nanotubes with red color; the fraction of shaded area represented in percentage is reported as the void or unoccupied area.

Zeiss Libra 200 MC TEM was used to analyze the CNTs or CNFs distribution and orientation in the PAN matrix. Precursor samples were prepared by embedding the filaments in epoxy. After curing the epoxy overnight at 100 °C in an oven, the epoxy

containing samples were mounted on a vice and cut using a microtome blade to make the sample in the epoxy perpendicular to the face of the cut. For final sectioning, Leica microtome instrument was used to slice. A diamond knife was mounted on the instrument to slice the samples in to 100 nm thick sections. The sliced sections were embedded on a copper grid electrostatically, and used for TEM analysis.

3.2.6 X-ray diffraction

X-Ray diffraction (XRD) study was carried out on the precursors and carbonized filaments on Empyrean XRD instrument from Panalytical, Westborough, MA, USA. The XRD instrument uses a copper source to generate X-rays of wavelength of 1.54 Å at 40 kV and at 40 mA current. The fiber samples were cut to one inch and mounted on a single crystal silicon disc, which is transparent to the X-rays, and further placed in the sample holder. The filaments were arranged to keep them straight and were mounted equatorial to XRD beam direction as shown in the figure 3.4. Each sample was exposed to X-rays for one hour to reduce noise in the data. XRD of the samples revealed the information of angle at which the peaks were observed and also the presence of CNF's/CNTs. XRD of commercial CF, commercial grade PAN fibers and CNT yarn was also carried out to compare with the precursors and carbonized sample prepared in the lab.

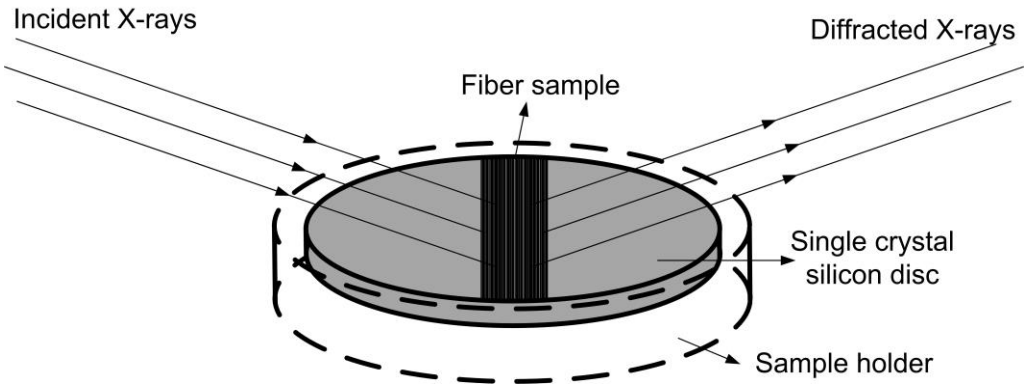


Figure 3.4: Schematic of XRD sample mounted on the sample holder.

CHAPTER 4

STRUCTURE AND PROPERTIES OF CNT YARNS

4.1 Microstructure analysis

SEM/FIB imaging

In figure 4.1, the SEM images of CNT yarns at low and high magnifications show the void content and poor orientation of the CNTs along the yarn direction. The SEM images 'A' and 'B' are CNTYN, 'C' and 'D' are CNTYG. The orientation of CNTs along the yarn direction for CNTYN (A, B) is higher than for the CNTYG (C, D). In figure 4.2, FIB milled images show the void space in the cross section and also show poor orientation of CNTs in the longitudinal section (E). FIB images 'A' and 'B' are for CNTYN, 'C' and 'D' are from CNTYG. In terms of void content based on the transverse section, CNTYN (A, B) are better than the CNTYG (C, D). In table 4.1, physical properties of the CNT yarns from both the sources are summarized. It can be noted that diameter, void % and twist angle of the CNTYG are larger than CNTYN, which reflects in its relatively poorer mechanical properties. From the FIB milled SEM images of CNT yarn, the cross section is clearly resolved (figure 4.3) and shows that the yarn is comprised of loosely packed nanotubes, each about 20 nm in diameter. The contact area between individual tubes and bundles is poor by large empty spaces in the yarn. High porosity results in poor load transfer between bundles and therefore the strength of CNTY is low as compared to the properties of CNTs.

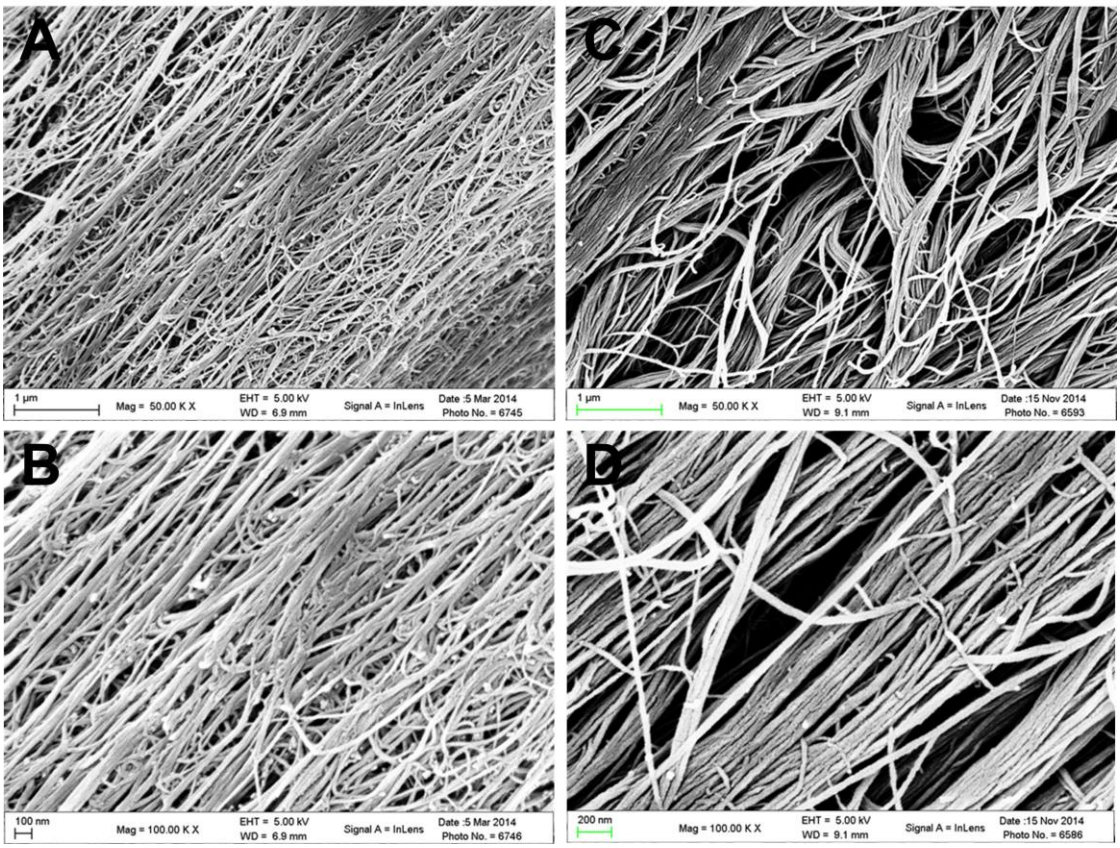


Figure 4.1: SEM images of CNT yarns at low and high magnification. Presence of high void space and lack of orientation of CNTs in the yarn direction is observed.

The degree of porosity or void percent was calculated as shown in figure 4.3 (B, D, and F). The fraction of area covered with red color to the total area in the green boundary was measured. The data that summarize the differences in structure of two different yarns are shown in Table 4.1. In addition to higher void content, higher twist angle observed indicates the relatively lower orientation of bundles with respect to the yarn axis. Whereas some twist is required to hold the nanotube bundles together, too much of twist will reduce the orientation of the bundles. If the twist is too low, then there is not enough cohesion between the bundles. Also, twisting process can help enhancing the packing of bundles, when done properly. That is why an optimum amount of twist, especially as low as possible as to get enhanced packing with minimum disorientation of bundles is important to achieve higher tenacity in the yarns The presence of high void content in the structure shows the importance of densification of the yarn to enhance the strength and modulus of the CNTY. Densification of the CNT yarn with polymers such as PAN, could increase the packing as well. Solvent densification alone also improves packing and strength by increasing the load transfer between CNT bundles **(Jung, Kim et al. 2015)**.

Table 4.1: Physical properties of CNTYN and CNTYG.

Physical property	CNTYN	CNTYG
Dia of yarn (µm)	53.7 ± 0.9	64.7 ± 2.4
Stress (MPa)	267.4 ± 20.7	219.6 ± 18.9
Modulus (GPa)	10.4 ± 1	5.8 ± 2
Strain %	9.5 ± 1.03	3.9 ± 0.76
Dia of CNTs (nm)	40.0 ± 28.9	33.8 ± 13.6
Apparent Void %	41.2 ± 6.7	53.7 ± 9.4
Twist angle (θ°)	9.7 ± 0.98	15.1 ± 2.81

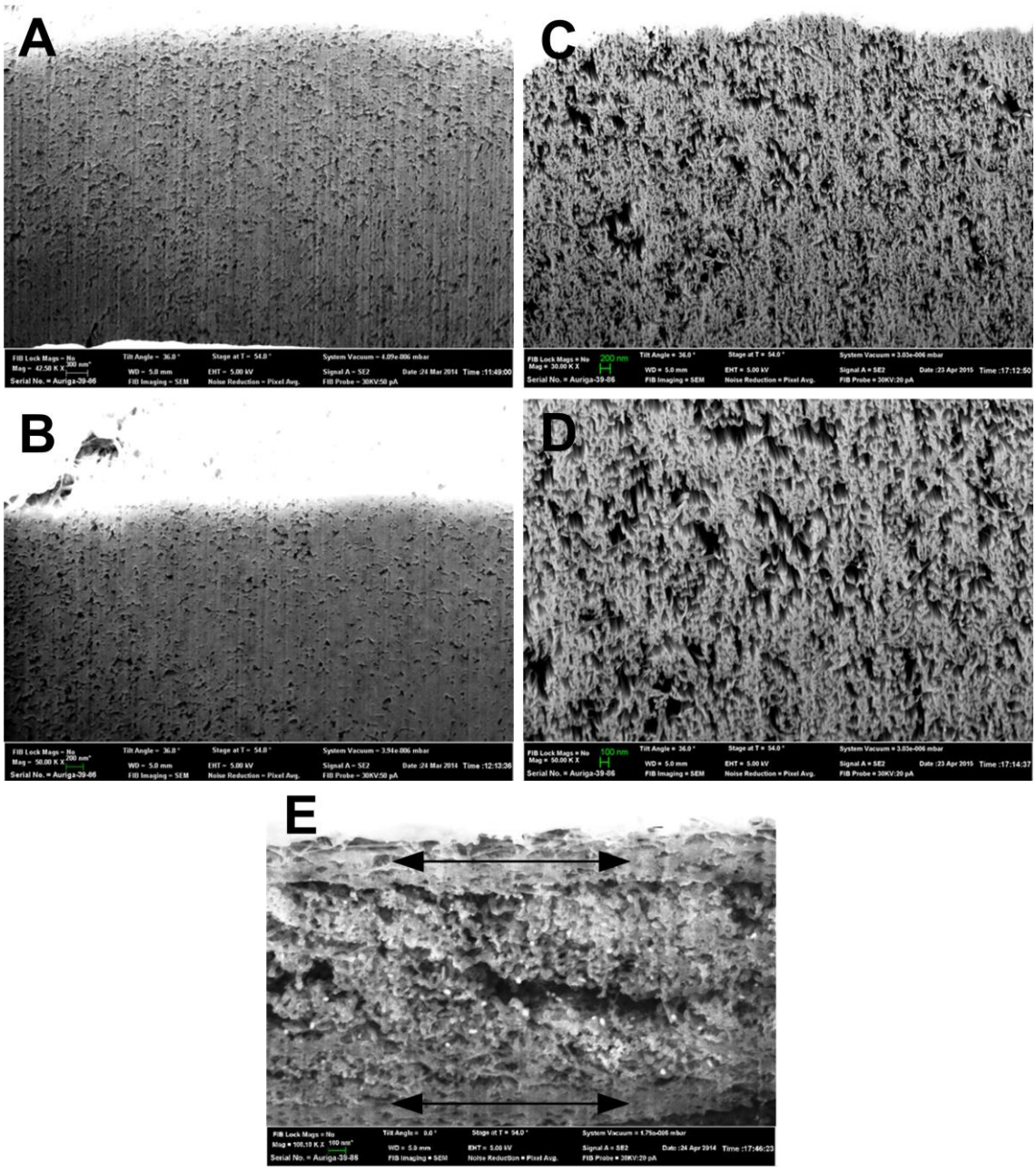


Figure 4.2: FIB milled SEM images of transverse section of CNT yarn and the bottom image shows the longitudinal section of the CNT yarn. It can be observed that there is lot of porosity in the cross section and longitudinal section followed by nonoriented CNTs in the yarn direction (arrows in 4.2E represents CNTs in yarn direction, while CNTs in the middle are perpendicular to yarn direction).

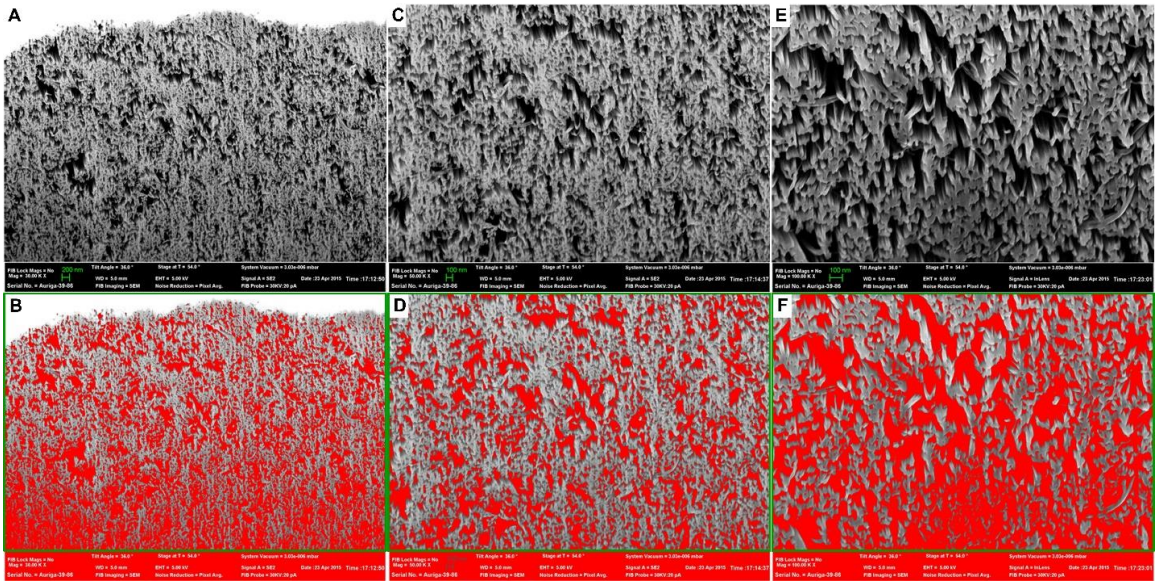


Figure 4.3: Void content analysis of FIB/SEM images of CNTY. ‘A’ showing lower magnification while ‘C’ and ‘E’ showing higher magnification of CNTY. ‘B’, ‘D’ and ‘F’ shows the void percent in the green selected area.

4.2 Tensile properties

The tensile testing data of CNTYN and CNTYG are shown in figure 4.4. There is a large variation in the strength and modulus between the samples. This variation could be due to the quality of CNTs used, twist angle, possible inconsistency in the growth conditions of CNTs and void content in the CNT yarns. From Table 4.1, the diameter, void % and twist angle are smaller for CNTYN and hence the strength and modulus values are higher than that of CNTYG. Furthermore, as the twist angle increases, the orientation of the nanotubes along the yarn direction decreases and hence lowers the tensile strength and modulus of the yarn. Increase in void content concentrates the stress on fewer nanotubes that are aligned which affects total strength of the yarn. FIB pictures in figure 4.2 show CNTYN is more tightly packed than the CNTYG (24% void). Denser packing means better interaction between nanotubes, and it helps to distribute the stress among the nanotubes and increase the overall strength of the yarn. The diameter and void % also show the number of nanotubes present in the yarn contributing to the total strength of the yarn. Based on all the results, it is evident that the lower strength and modulus realization in CNT yarns is due to poor packing and orientation of the nanotubes. Any feasible approach that will help improve packing and orientation of nanotubes should lead to further improvement in tensile properties.

4.3 Effect of Densification on CNT yarn

From the tensile testing data and the physical properties of the CNTYN and CNTYG, it is evident that densification of the CNT yarn is required. CNTYN yarn samples were studied for densification using three different approaches.

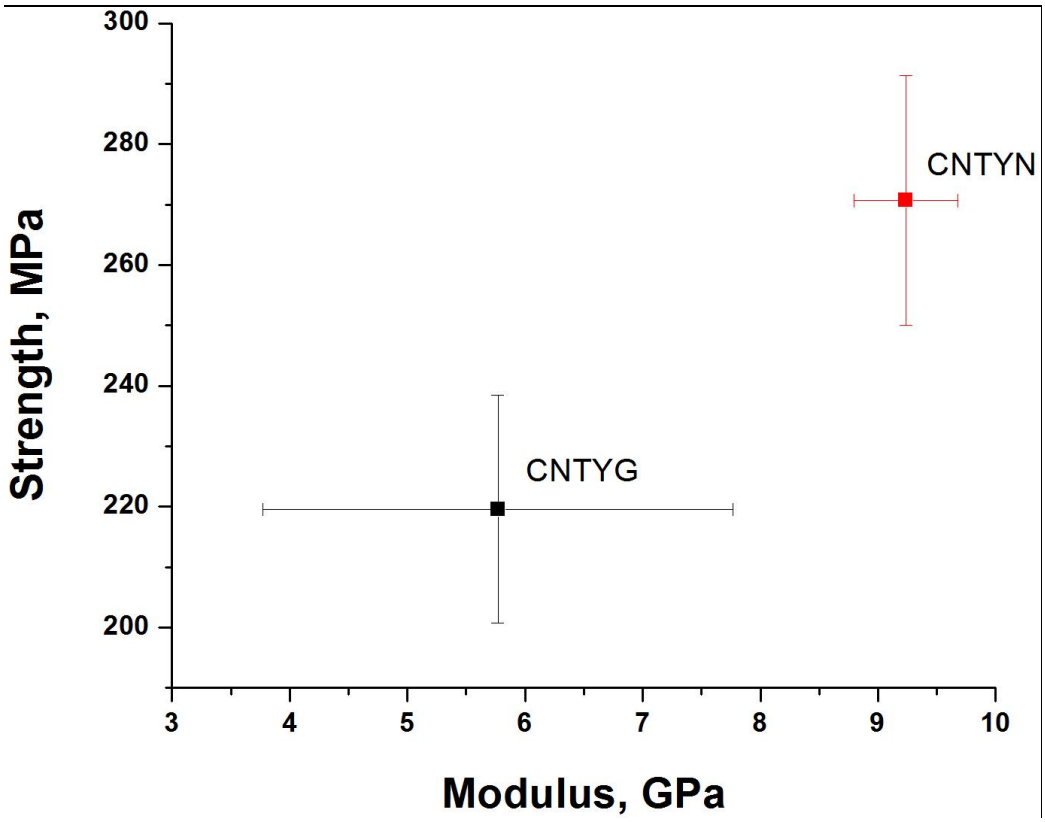


Figure 4.4: Strength vs modulus of CNT yarns of three batches.

CNTYN-1 was used as control sample, CNTYN-2, 3 and 4 were infiltrated with DMF, 0.1 wt% PAN and 1 wt% PAN respectively as described in section 3.1.1. Figure 4.5 shows the tensile properties of CNTYN-pristine, DMF, 0.1 wt% PAN and 1 wt% PAN infiltrated samples. From the infiltration work the strength and modulus of CNTYN has increased compared to pristine sample. DMF (solvent) densification has increased the strength and modulus by 293.5% and 306.7%, respectively, compared to that of pristine yarn. 0.1 wt% PAN infiltration has increased the strength and modulus by 321.6% and 363.4% respectively, compared to pristine while 1 wt% PAN increased strength and modulus by 140.3% and 150.1% compared to pristine. Table 4.2 shows the tensile properties of pristine and infiltrated CNTYN samples. Strength and modulus of the samples infiltrated with DMF or PAN are higher than that of pristine yarn as the CNTs were closely packed and load transfer increased. It should be noted that the diameter of the pristine sample is much larger than infiltrated samples. This change in diameter is not solely because of infiltration under constant load. The CNTYN contained a lot of variation in diameter when received and linear density could not be used for tensile test because each sample had larger variation of diameter in itself. Average of 10 diameter measurements for 25mm gauge length was taken for the tensile test, and average of eight specimens are reported for tensile properties of each sample type. SEM images of CNTYN-pristine (figure 4.6), clearly show that the CNTs are more tightly packed and the yarn is ribbon like with variation in diameter along the length. It is also evident that CNTs are tightly packed than the previous sample, figure 4.1 (A and B), however there is still lack of orientation of CNTs.

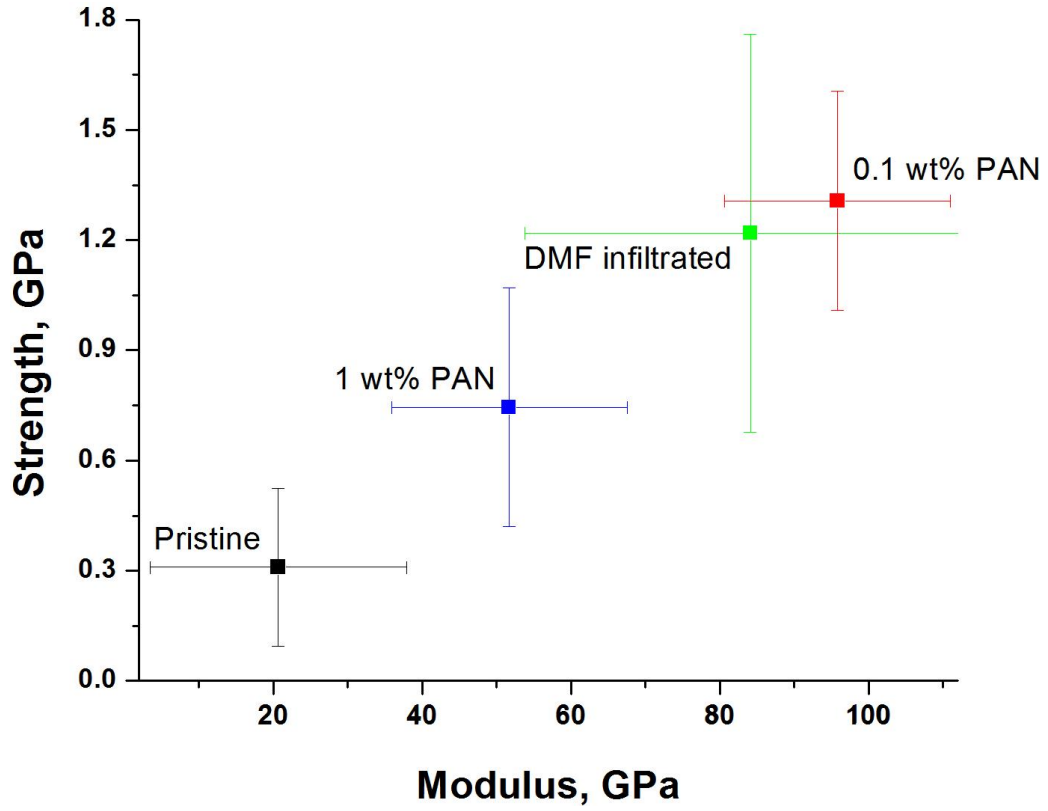


Figure 4.5: Strength and modulus data of CNTYN-pristine and CNTYN infiltrated with DMF, 0.1 wt% PAN and 1 wt% PAN.

Table 4.2: Summary of tensile properties of pristine and infiltrated CNTYN samples.

	Dia (µm)	**Std**	**Modulus, GPa**	**Std**	**Strength, GPa**	**Std**	**Load applied (g)**
CNTYN-P (control)	367.1	173.6	20.68	17.23	0.31	0.214	0
CNTYN-DMF	162.15	27.13	84.12	30.33	1.22	0.541	650
CNTYN-0.1% PAN	160.21	14.84	95.84	15.17	1.30	0.298	750
CNTYN-1% PAN	200	20.35	51.72	15.85	0.74	0.324	750

Tensile tested samples show a semi-ductile or brittle fracture (no shearing or tearing observed) with very small stretching of the yarn. Tensile strength and modulus of pristine CNTYN are lower, as shown in figure 4.5. SEM images of DMF infiltrated CNTYN (figure 4.7), indicate that the CNT bundles are torn off of the CNTYN during tensile testing. DMF infiltration assisted consolidation in tension has improved the orientation of nanotube bundles along the yarn direction with improved packing, and hence enhanced the strength and modulus, as seen in the tensile properties data (figure 4.5). SEM images of CNTYN infiltrated with 0.1 wt% PAN (figure 4.8) show the PAN polymer binding to the surface of the yarn. There is no evidence of PAN inside the yarn structure, however due to enhancement in tensile properties one can concur that the infiltration of PAN has increased the packing and also orientation of the CNTs. From the SEM images of CNTYN infiltrated with 1 wt% PAN (figure 4.9), it is evident that the PAN adsorption on the surface is much higher and densification has also increased. However, the increase in strength and modulus of the sample is relatively smaller than that of DMF or 0.1 wt% PAN infiltrated samples. This relatively lower increase in strength and modulus should be attributed to the fact that PAN chains are not infiltrating the structure and do not contribute to improved inter-CNT bonding, but only improve packing of CNTs. Also, most of the PAN is deposited on the surface of the CNT yarns as the DMF evaporates after infiltration treatment.

TGA analysis

TGA analysis was conducted on the pristine and infiltrated CNTYN in nitrogen and in air. The graphs are as shown in the figure 4.10, 'A' shows the TGA data in nitrogen and 'B' in air. From the figure it is evident that the weight loss in nitrogen is 20 to 28% for

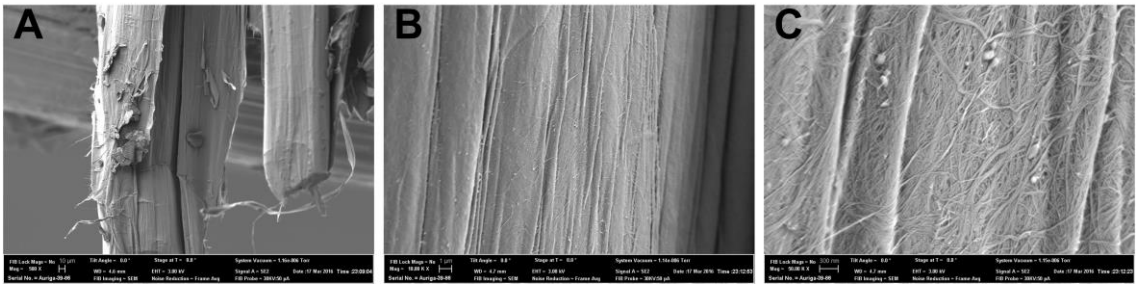


Figure 4.6: SEM images of CNTYN-pristine tensile tested sample. ‘A’ and ‘B’ are lower magnification images while ‘C’ is the higher magnification image of CNTYN-pristine, respectively.



Figure 4.7: SEM images of CNTYN-DMF infiltrated tensile tested sample. ‘A’ and ‘B’ are lower magnification images while ‘C’ is the higher magnification image of CNTYN-DMF infiltrated failed end, respectively.

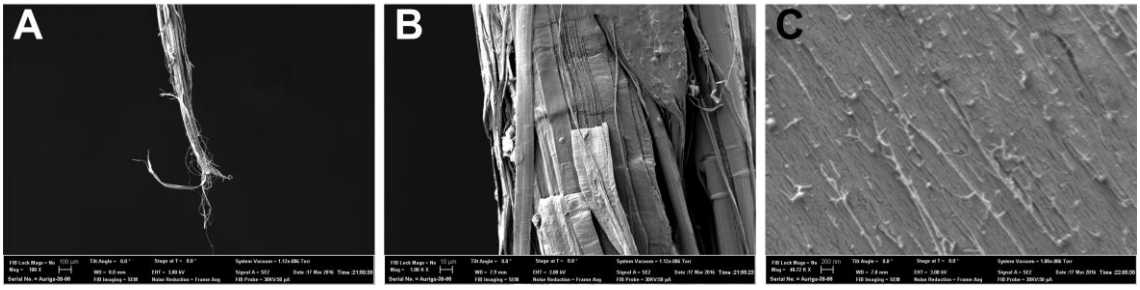


Figure 4.8: SEM images of CNTYN- 0.1 wt% PAN infiltrated tensile tested sample. 'A' and 'B' are lower magnification images while 'C' is the higher magnification image of CNTYN-0.1 wt% PAN of the tearing of CNT ribbon (failed end of tensile tested sample), respectively.

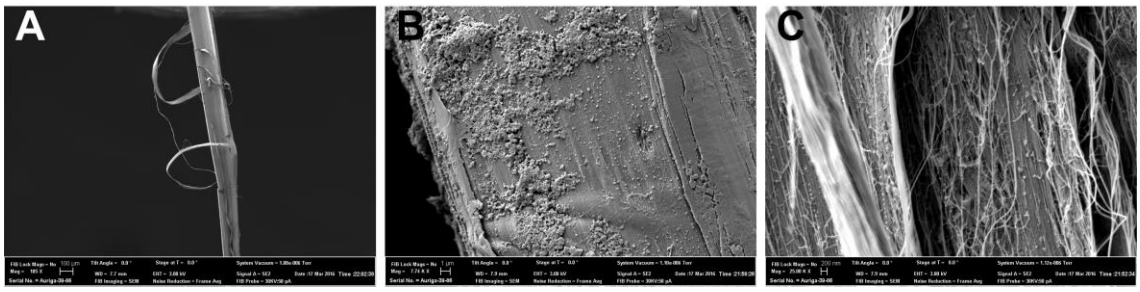


Figure 4.9: SEM images of CNTYN- 1 wt% PAN infiltrated tensile tested sample. 'A' and 'B' are lower magnification images while 'C' is the higher magnification image of CNTYN- 1 wt% PAN infiltrated failed end, respectively

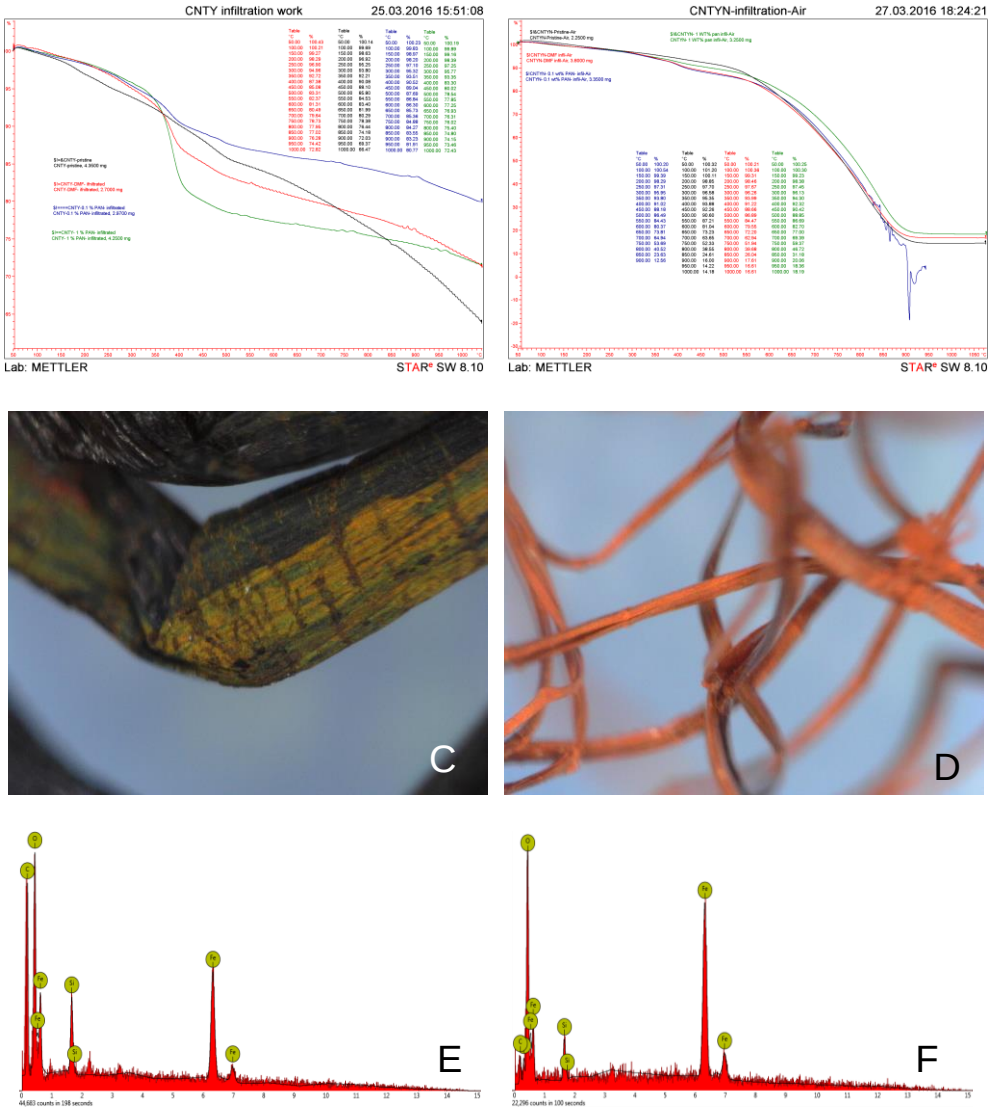


Figure 4.10: 'A' TGA data of pristine and infiltrated CNTYN in air and 'B' in nitrogen. 'C' optical microscopy images of post TGA samples in nitrogen and 'D' in air showing the presence of iron oxide as confirmed by EDS 'E' (in nitrogen) and 'F' (in air).

infiltrated CNTYN and 34% for pristine while the weight loss in air is more than 86% for pristine and 84 to 88% for infiltrated CNTYN. The weight loss also confirms that the CNTYN was not only made of CNTs alone but also embedded in a polymer which resulted in increasing the toughness of the final yarn. Optical microscopy was conducted on the post TGA samples in nitrogen and in air. From the images it is clear that the iron catalyst used in the synthesis of CNTs oxidized when exposed to high temperatures and in oxidative atmosphere. CNTYN in air shows red to orange color while the samples run in nitrogen show yellowish-orange color which is the oxide of Fe element. Further validation from EDS showed the presence of iron and oxygen in the post TGA samples as shown in 4.10 'E'.

CHAPTER 5

STRUCTURE AND PROPERTIES OF CNFS AND CNTS REINFORCED PRECURSORS

5.1 Thermal analysis

Differential scanning calorimetry (DSC)

DSC was used to study the reaction temperatures and the extent of the exothermic reactions of the PAN, PAN + CNTs or CNFs fibers, as well as diffusion nature of DMF during wet spinning. From figure 5.1 and the data shown in Table 5.1, it is evident that the exothermic reactions start from 235 to 262 °C for various precursor fibers based on the DSC scans done at 10 °C per minute. Whereas these temperature differences are good for comparison, based on the heating conditions, actual transition temperatures vary. However, the differences in transition temperatures for various samples should show a similar trend. For pristine PAN fibers (C0), the exothermic reaction starts at 287 °C; for C1 at 262 °C, C2 at 251 °C, C4 at 236 °C, and C5 at 248 °C. Due to the influence of nanofillers (CNTs or CNFs), the width of the exothermic curve is wider hence there is no significant localized heating as compared to the pristine PAN. These differences are observed more in the presence of air, and in nitrogen atmosphere the observed shift is negligible. The observed shift of the exotherms to lower temperatures and due to the combination of faster diffusion kinetics and the activity of modified CNTs/CNFs in their ability to catalyze cyclization and

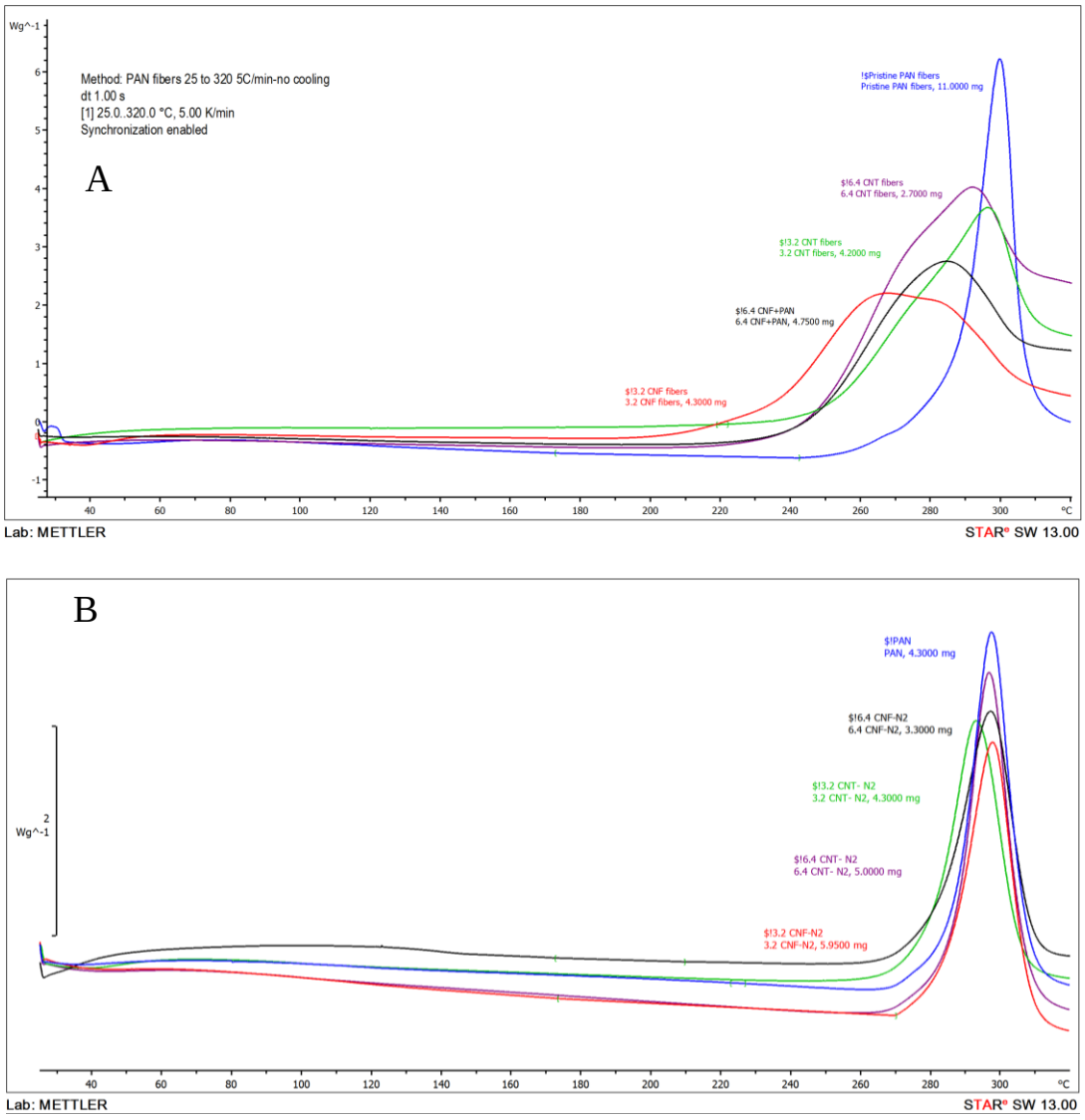


Figure 5.1: DSC data of PAN fibers with various nanofillers infiltrated PAN fibers.

Table 5.1: (A): Summary of DSC data of PAN fibers with various nanofillers (in air)

Sample	Enthalpy (Jg^{-1})	Onset (°C)	Endset (°C)
Pristine PAN	964.2	288	306
3.2 CNT fibers	763.8	262	308
6.4 CNT fibers	872.0	251	307
3.2 CNF fibers	973.1	236	305
6.4 CNF fibers	827.8	248	306

(B): Summary of DSC data of PAN fibers with various nanofillers (in nitrogen)

Sample	Enthalpy (Jg^{-1})	Onset (°C)	Endset (°C)
Pristine PAN	595.7	286	307
3.2 CNT fibers	517.8	280	306
6.4 CNT fibers	578.6	285	307
3.2 CNF fibers	523.1	283	308
6.4 CNF fibers	508.1	281	308

aromatization reactions. These need to be explored further. However, because of the nanofillers, the diffusion kinetics in the fibers have changed when compared to pristine PAN fibers. Furthermore, this change could also be due to variation of fiber diameters.

To understand the effect of residual DMF due to spinning conditions and its implications on the timing of post-processing on PAN fibers, DSC scans were done for some samples immediately after spinning, after one hour dry time and, overnight dried. In figure 5.2, DSC curves of as-spun, one hour dried, and overnight dried PAN fibers are shown. The wet-spinning flow rate of these fibers was set at 1.5 ml/hr and extruded at draw ratio of 0.9 to 1. The as-spun fibers showed an endotherm corresponding to evaporation of DMF and moisture. For all the samples, exothermic peak starts at a temperature > 220 °C due to the fact that the heating rate is very high. The enthalpy values are slightly different and are within the experimental error considering small differences in composition and microstructure.

Thermogravimetric analysis

TGA was used to investigate the weight loss of PAN and PAN + CNFs fibers, in as-spun, one hour dried, overnight dried, and hot water stretched PAN fibers. From figure 5.3, the weight loss of CNFs reinforced PAN fibers is lower than that of pristine PAN fibers. The differences between the TGA scans show the residual amount of carbon for CNFs wt %, which match closely with the concentration of CNFs in PAN (P1 and P2 filaments). From figure 5.4, the weight loss as a function of temperature is measured for pristine as-spun, one hour dried and overnight dried PAN fibers. From this data the as-spun fibers show higher weight loss, as there is evaporation of DMF present in the fibers and

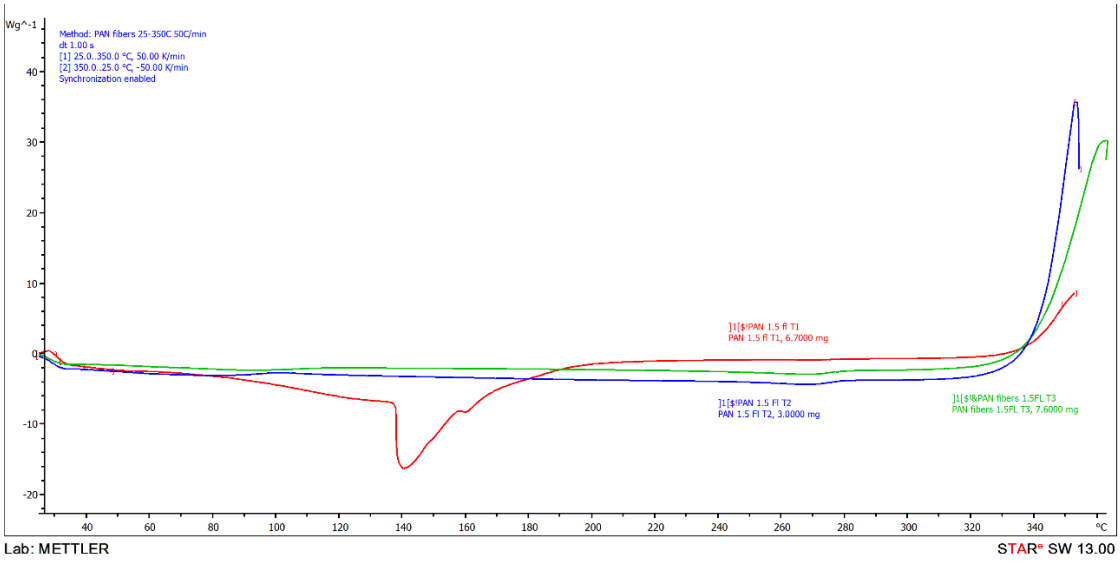


Figure 5.2: DSC curves of pristine as-spun, one hour dried and overnight dried PAN fibers.

.

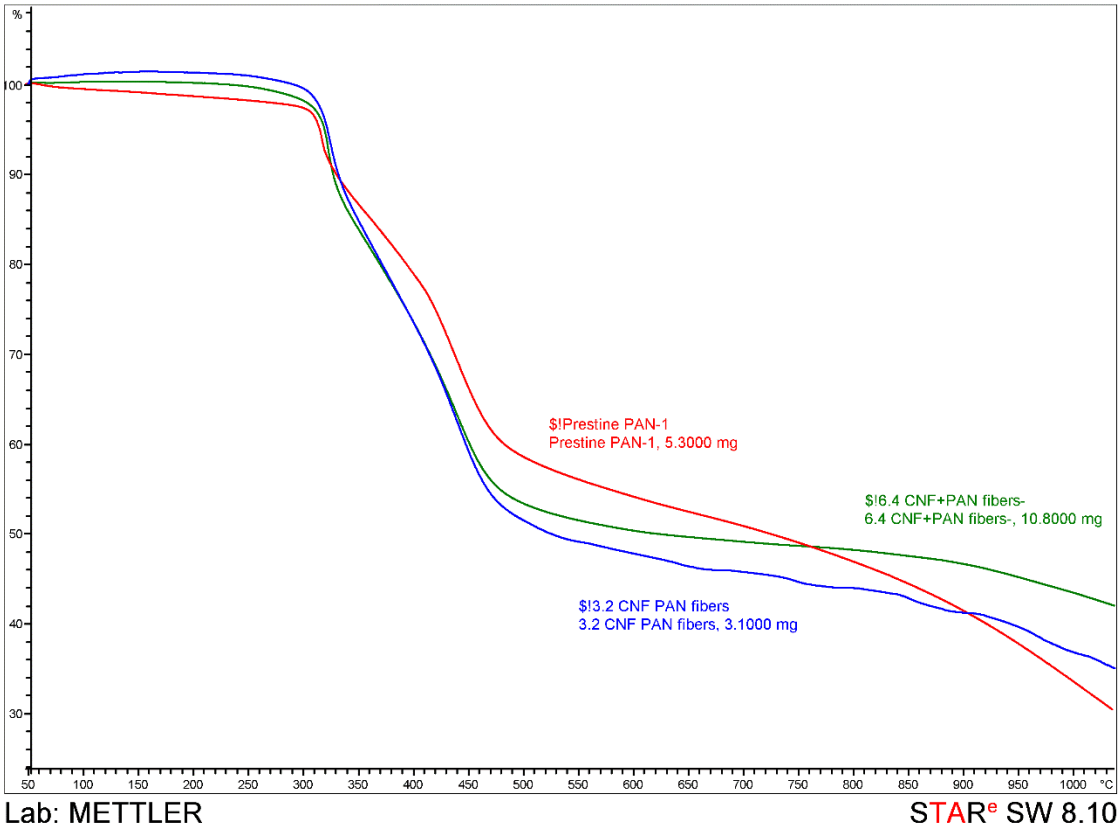


Figure 5.3: TGA data of pristine PAN fibers with 3.2 and 6.4 wt% PAN-g-CNFs in 12 wt% PAN fibers.

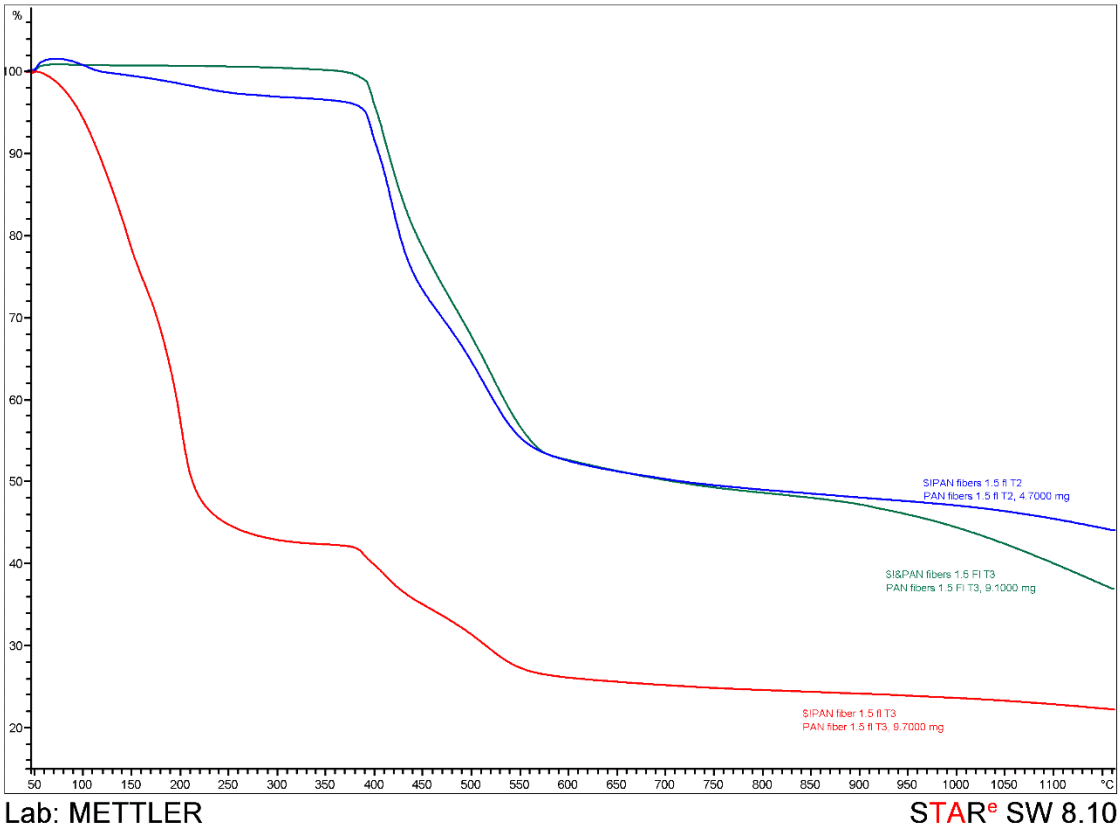


Figure 5.4: TGA data of PAN fibers (as-spun (red), one hour dried (blue) and overnight dried (green)

one hour dried shows relatively lower weight loss as most of the DMF evaporated in an hour. Similarly overnight dried fiber does not show any weight loss in the corresponding temperature range due to the fact that all of the DMF/water being evaporated. TGA results are consistent with the observations in DSC.

5.2 Microscopic structure

SEM/FIB

SEM/FIB images are as shown in figures 5.5 and 5.6 (A, A′ to E, E′). Figure 5.5 shows the cross section of PAN fiber when extruded in a low concentration (20% DMF in water) coagulation bath at room temperature. The voids that are formed are large (> 20 μm) and the strength of the fiber is poor. Due to inefficient coagulation the PAN chains are loosely packed (as seen in higher magnification image). Figure 5.6 shows the SEM images of surface topography and FIB milled cross sections of the precursor filaments (P0 to P5) with draw ratio = 6.4. In figure 5.6, A, A′ and A′′ are surface topography and FIB milled cross section images of P0. From the cross section it is evident that there are no large voids present and coagulation of the filament is uniform. B, B′ and B′′ are surface topography and FIB milled cross section images of P1 filaments. From the cross section image uniform distribution of CNFs is evident and that there are no visible voids present showing uniform coagulation process during wet spinning. C, C′ and C′′ are surface topography and FIB milled cross section images of P2 filaments. Higher density of CNFs are present and the uniform distribution shows no agglomeration. Absence of visible voids show optimized coagulation conditions. No agglomeration, parallel orientation of the CNFs and absence of voids should also reflect in the enhancement of tensile properties. D, D′ and D′′ are surface

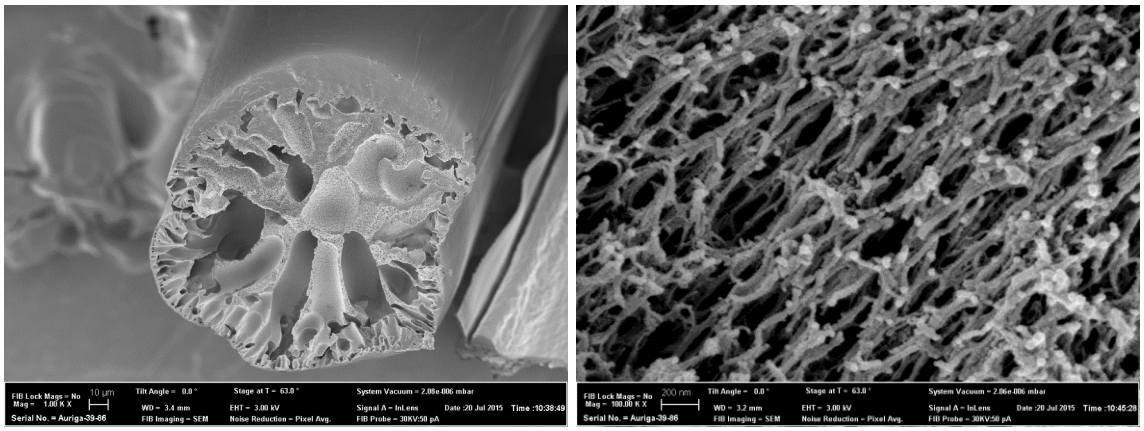


Figure 5.5: Effect of low concentration and room temperature coagulation bath.

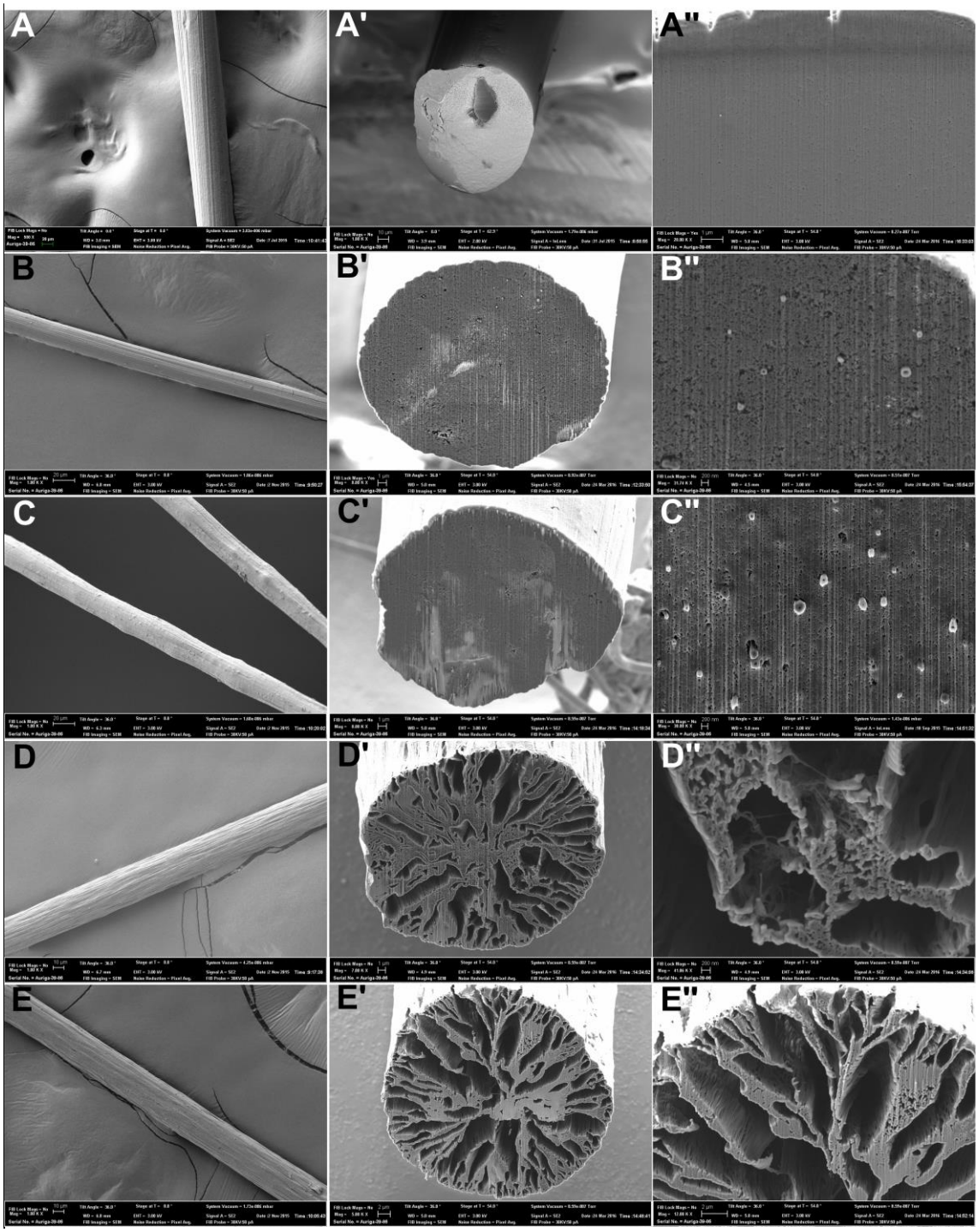


Figure 5.6: SEM images of surface topography and FIB milled cross sections of precursor filaments (A=P0, B= P1, C= P2, D= P4 and E= P5 filaments).

topography and FIB milled cross section images of P4 filaments. The void content in the filament is high leading to inefficient coagulation conditions. Furthermore, the CNTs are agglomerated and not uniformly distributed as seen in D′′. The formation of voids in the filament is probably due to rapid coagulation i.e. fast diffusion of DMF from the filament to the coagulation bath and water from the coagulation bath to the filament. This quick change in concentration has caused sudden phase change and also could have attributed to pushing the CNT agglomerates towards the periphery of the filaments. E, E′ and E′′ are surface topography and FIB milled cross section images of P5 filaments. Presence of large voids show that the drawing of the filament was insufficient, and these voids would cause stress concentrations in the filament which results in poor tensile properties. Another important observation to be made is that the CNT agglomerates are present in the void space.

5.3 TEM analysis

TEM analysis was conducted on the precursor samples to study the sub-micron level structure, especially the distribution of the nanofillers and binding with PAN matrix. In figure 5.7, P1 filament cross section image is shown. Low magnification image shows the distribution of CNFs in the PAN matrix. Higher magnification images show the binding with the matrix with no void or pore formation. White hole in the low magnification image is due to popping of CNF from the spot while slicing with diamond knife in microtome instrument. From higher magnification image we can also notice the walls of the CNFs. Most of the CNFs are cut along transverse direction, however few CNFs were observed that were partly along the surface of the sliced TEM sample. This also shows that there are

CNFs which are not parallel to the filament direction. From figure 5.8, it is evident that CNFs are fairly uniformly distributed. However, due to shearing of CNFs during sample preparation, the walls of the CNFs are also seen. Another confirmation to the formation of "void" due to popping of CNFs from their spot is evident. The marks or streaks on the images are due to the diamond blade during sample preparation. Uniform distribution of CNFs in PAN matrix can be due to high quality CNFs (graphitized up to 2900 °C) and the PAN grafting on the CNFs are done by e-beam irradiation technique. Furthermore, while preparation of the CNF in PAN solution, it was noted that the CNF agglomerates that were forming when kept dry in the bottle were completely broken down during shear mixing in PAN + DMF. Filtration of this solution led to uniformly distributed CNFs in PAN. As explained in chapter three, higher concentration (> 6.4 wt% PAN-g-CNF) of CNF in PAN led to larger agglomerates and clogging of spinneret (needle) during wet spinning. 6.4 wt% PAN-g-CNF in PAN is the best concentration for wet spinning as there is less to no clogging of spinneret in this particular lab scale wet spinning setup. As we can observe from figure 5.9, the PAN-g-CNTs have formed large agglomerates in PAN matrix. Furthermore, the TEM image also shows large void content in the PAN matrix and CNTs are along the surface of the filament. Higher magnification image shows that the CNTs are not oriented along the filament direction and lacks uniform distribution and is the major effect of the cause of poor strength and modulus. Because of non-oriented CNTs and presence of void in the cross section, it also shows that the diffusion of DMF from the filament to the coagulation bath was not uniform but rapid and has also caused the formation of larger voids that did not coalesce enough to form solid core with only CNT agglomerates.

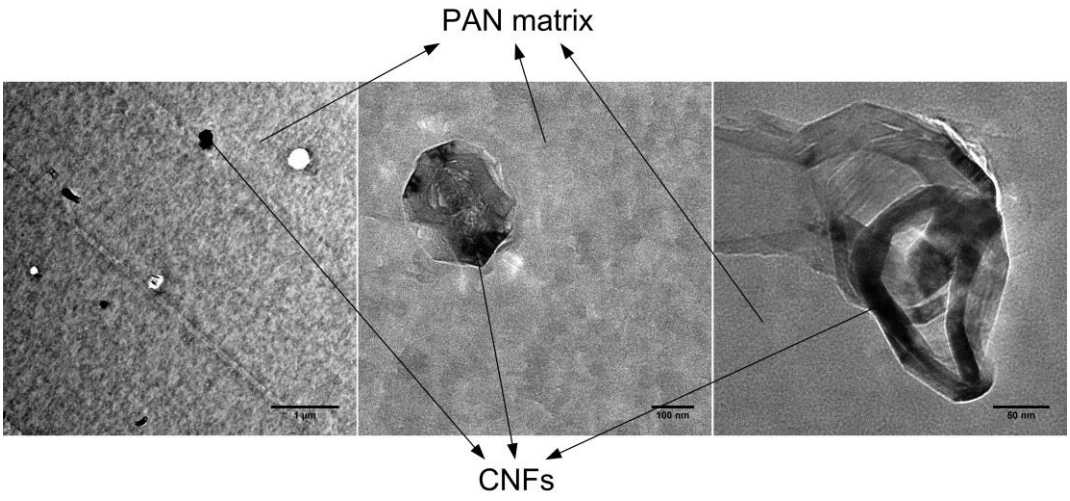


Figure 5.7: P1 (3.2 wt% PAN-g-CNF in PAN) filament TEM image.

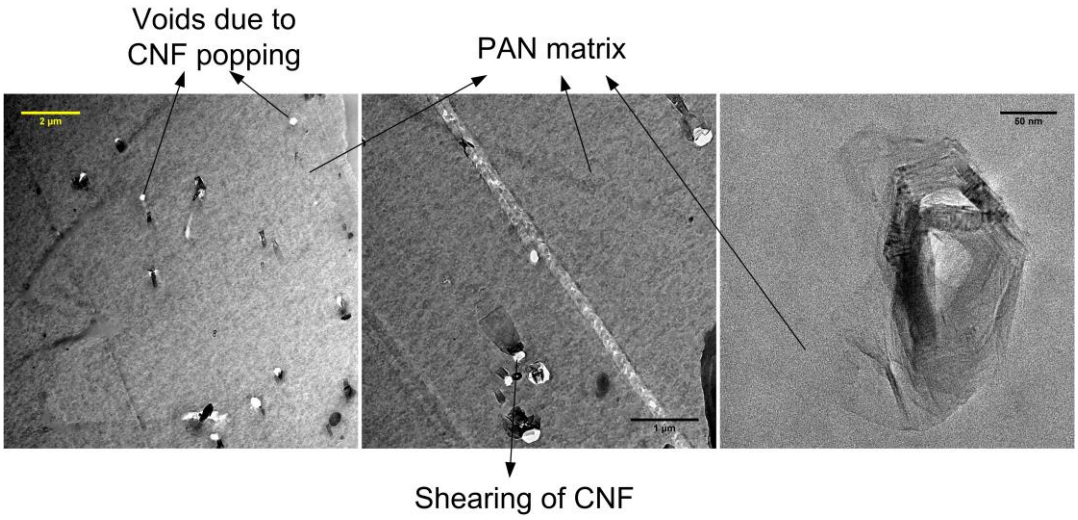


Figure 5.8: P2 (6.4 wt% PAN-g-CNF in PAN) filament TEM image.

Furthermore, the reason for agglomeration of CNTs could be due to the PAN grafting process. PAN grafting on CNTs were carried out in a glass flask in the presence of DMF. DMF being a polar solvent, the CNTs agglomerates were strongly bound to one another electrostatically and could not be broken down to individual CNT during solution preparation with PAN. Furthermore, longer PAN grafting could also be the reason (for entanglement of PAN molecules). The strength of PAN-g-CNTs in PAN filaments are much lower than the PAN-g-CNFs in PAN filaments (i.e. P1 and P2 vs P4 and P5) because of the quality of the CNTs. From the EDS data of the CNTs, it was found that the nanotubes contained iron catalyst which was not removed from the CNTs. This affects the final tensile properties of the precursors because the impurity lowers the strength of the CNT itself. In figure 5.10, we can observe that CNTs have agglomerated largely towards the surface of the filament and there is void around the CNTs. CNTs might be affecting the diffusion process of the solvent and hence they are also surrounded by void. The CNTs are not oriented and they are along the plane of TEM section. Such agglomeration and generation of void content in the filament acts as stress concentrating factors and leads to poor strength of the filaments as can be seen from the tensile properties data summarized in figure 5.11 and table 5.2.

5.4 Tensile properties

Figure 5.11 shows the tensile strength and modulus of all the precursor fibers, and Table 5.2 shows the summary of the mechanical properties of these fibers. Compared to the strength and modulus of PAN fiber, the values of CNT reinforced fibers are slightly lower and those of CNF reinforced fibers are significantly higher than that of pure PAN.

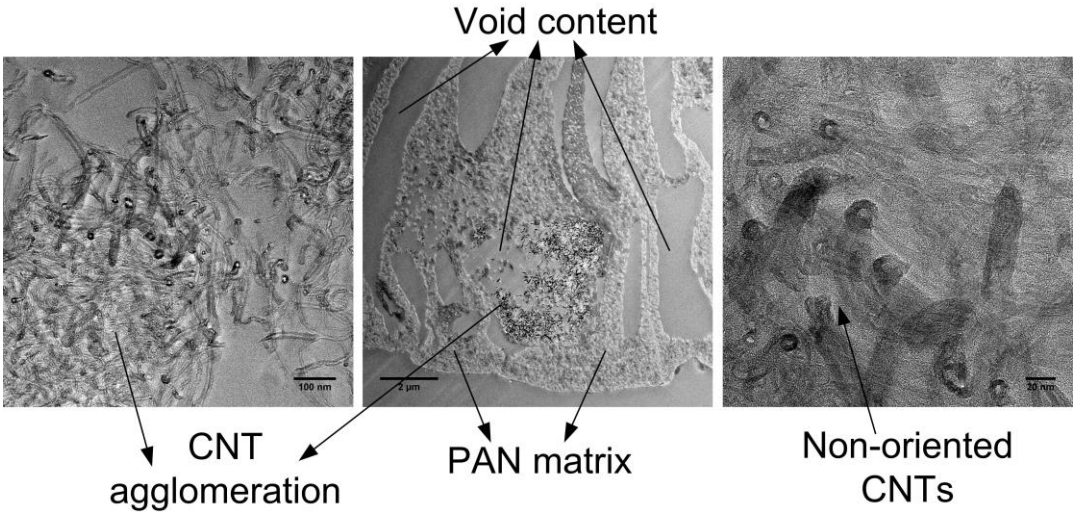


Figure 5.9: P4 (3.2 wt% PAN-g-CNTs in PAN) filament TEM image.

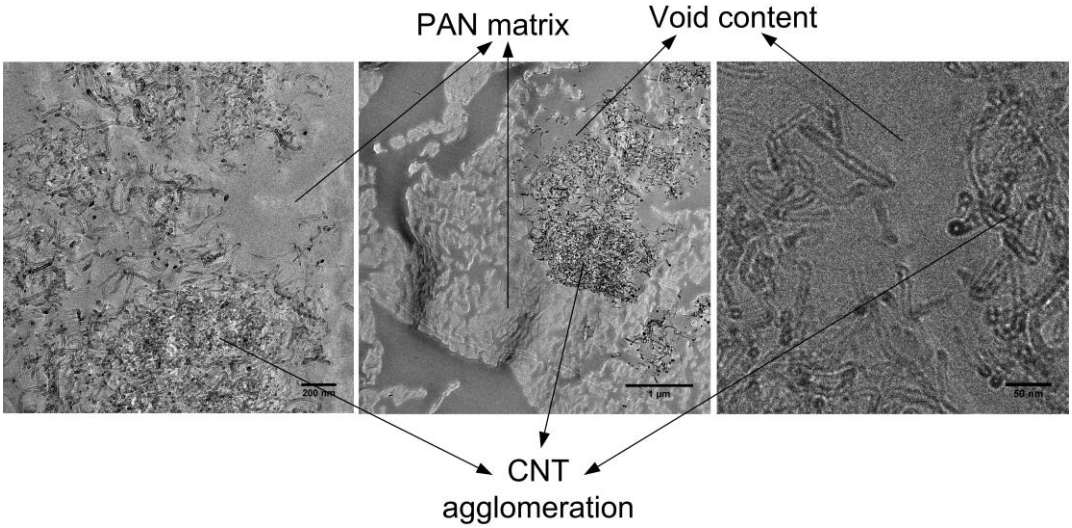


Figure 5.10: P5 (6.4 wt% PAN-g-CNTs in PAN) filament TEM image.

It is to be noted that CNT reinforced fibers had much larger diameter because of the difficulty in processing. With larger diameter the probability of defects increases and failure is likely to occur at lower stress values. Also, uniformity of CNT distribution has not been verified and any nonuniform distribution or agglomerations act as stress concentrating factors lowering the tenacity values. From the SEM/FIB images we can see that there is high void content in the CNTs infiltrated PAN i.e. P4 and P5 filaments. These voids do not contribute to distribution of load and lead to concentrates of stress on a small portion of the fiber and results in poor mechanical properties. For CNFs infiltrated PAN i.e. P1 and P2 filaments, the void content is very low to nil and hence the strength and modulus of the fibers is much higher than that of PAN. As P3 was an experimental one, we can observe that the strength is comparable to PAN precursor filament, this is because of the addition of CNFs with CNTs. Though CNT agglomerates hinder the strength properties, CNFs (because of uniform distribution) lead to enhanced strength close to that of pristine PAN. SEM images of tensile tested specimens are shown in figure 5.12. 'A' is the SEM image of tensile tested P0 filament specimen. It is evident that, though there are few 50 nm sized voids in the FIB image of P0 filament, the specimen experienced brittle facture. This shows that additional drawing may be required to consolidate the filament further to reduce the voids. 'B' and 'C' show the SEM images of tensile tested ends of P1 and P2 filaments, respectively. From the images we can see that the CNFs are protruding out of the failed ends showing the reinforced failure mode which is not brittle in nature. However, further stretching on hot plate would result in compaction and enhanced load transfer between the PAN matrix and CNFs. D' and 'E' show the failed ends of P4 and P5 filaments, respectively.

Table 5.2: Summary of mechanical properties of the precursor fibers.

Sample	Dia (µm)	Std	Strength, MPa	Std	Modulus, GPa	Std
3.2 CNT	36.56	1.86	47.57	06.89	2.0685	0.6895
6.4 CNT	37.38	3.45	46.88	12.41	2.0685	0.6895
3.2 CNF	22.95	0.93	157.2	40.67	4.8265	1.3790
6.4 CNF	27.14	1.73	103.4	15.17	3.4475	0.6895
PAN	84.00	1.90	54.60	23.44	2.7580	0.6895
3.2 CNF+CNT	36.31	4.13	55.15	20.68	2.7580	0.6895

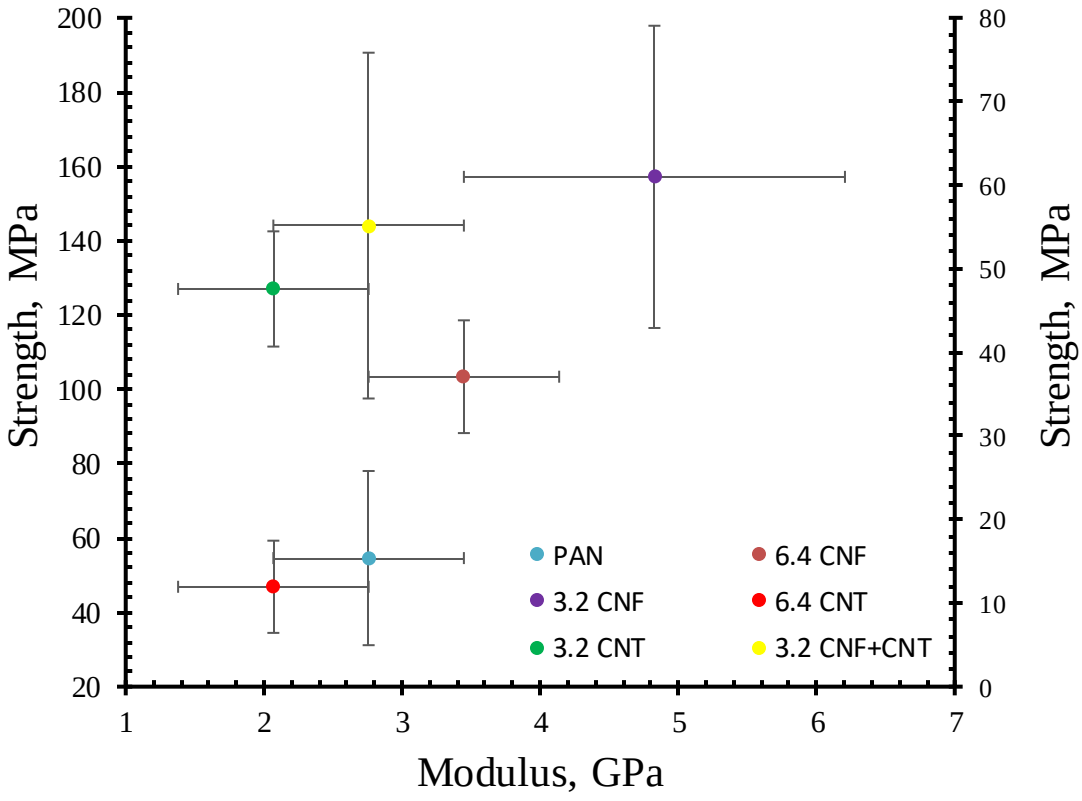


Figure 5.11: Tensile strength vs modulus of various precursors.

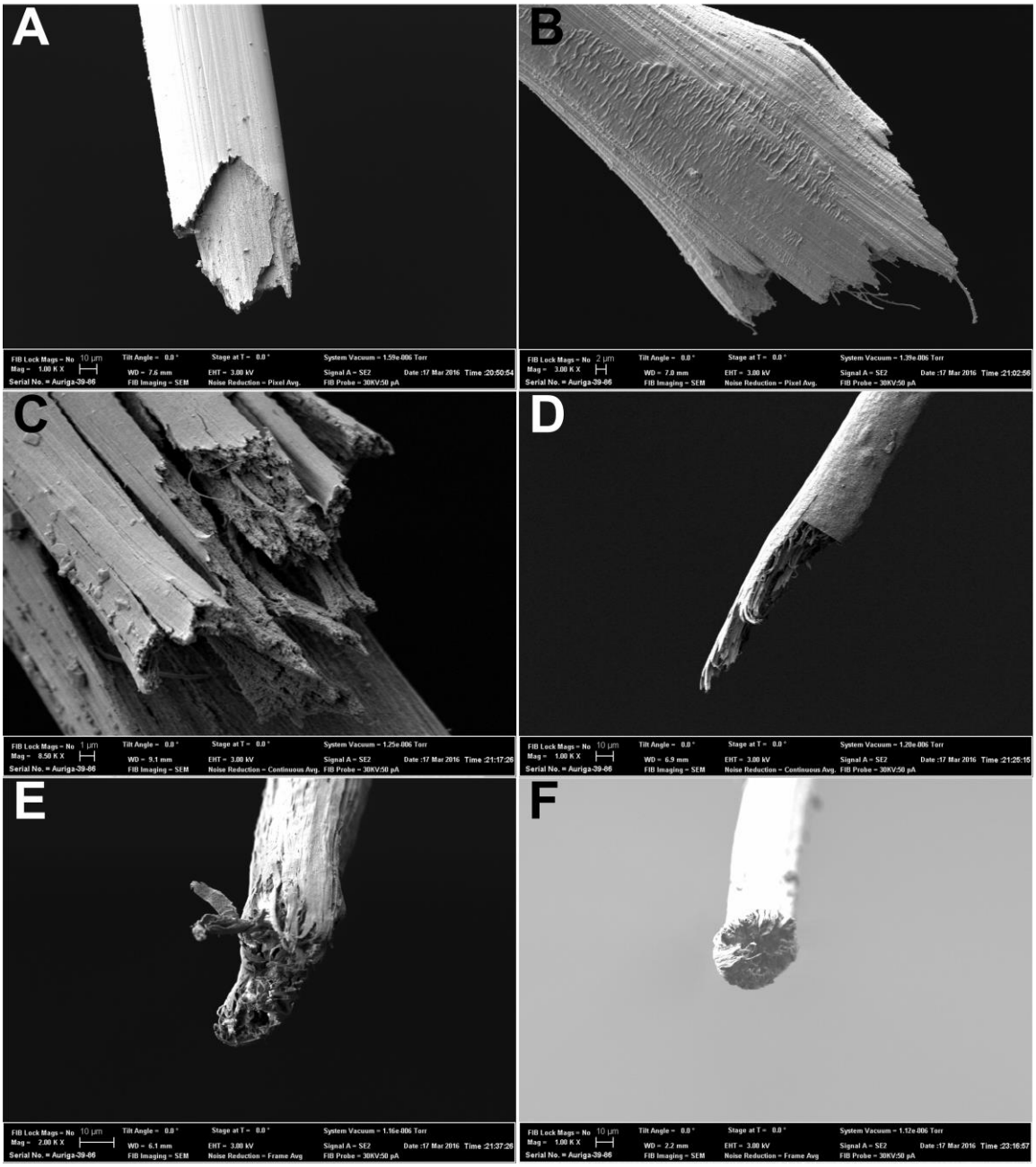
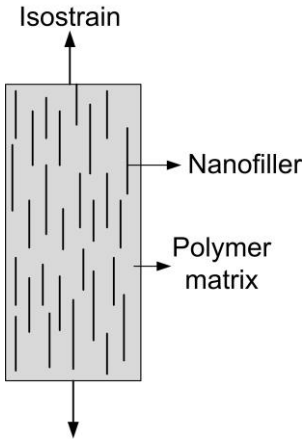


Figure 5.12: SEM images of tensile tested samples showing the failed ends of the filaments. A= P0, B= P1, C= P2, D= P4, E= P5 and F= P3 filament.

From the images it is clear that due to presence of voids and CNT agglomerates, load transfer is inefficient resulting in stress concentration and brittle failure. This type of failure also shows the lack of complete consolidation during wet spinning of the filaments. 'F' shows the failed end of P3 filament, as this was an experimental sample with CNTs and CNFs, the fracture type resembles between brittle and ductile nature. From the SEM/FIB study, presence of void was noticed with relatively consolidated core compared to P4 and P5 filaments. This is the reason for higher strength and modulus of P3 filament compared to that of P4 and P5 filaments.

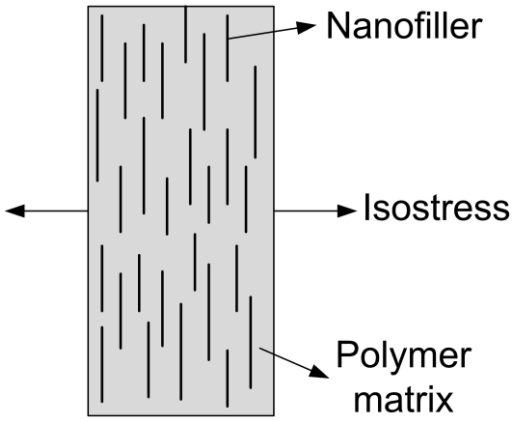
Theoretical calculations of isostress/isostrain conditions of the nanofillers reinforced precursors are as shown in figure 5.13. The isostrain condition and equation 1 is as shown below



$$E_C = E_F \times f + E_M \times (1 - f) \quad \text{eq.1}$$

where, E_C is elastic modulus of composite fiber, E_M is elastic modulus of polymer, and E_F is elastic modulus of nanofillers i.e. CNFs or CNTs. 'f' is volume fraction of nanofiller and (1-f) is volume fraction of the polymer.

The isostress condition and equation 2 is as shown below



$$E_C = \left[\frac{f}{E_F} + \frac{(1-f)}{E_M} \right]^{-1} \qquad \text{eq.2}$$

Calculated isostress/isostrain values are as shown in figure 5.13. Elastic modulus of PAN precursor, P0 = 2.76 GPa, was used as E_M and elastic modulus of CNFs, 240 GPa, as E_F for PAN+CNF filaments. Elastic modulus of CNTs, 1000 GPa, was used for PAN+CNT filaments. The calculated isostrain and isostress elastic modulus are in blue and orange data points, respectively, in the figure 5.13. PAN density of 1.184 g/cm^3, CNF density of 2 g/cm^3 and CNT density of 1.75 g/cm^3 was used for volume percentage calculations. 'A' is the isostress/isostrain calculation for PAN+CNF filaments 'A'' is the magnified plot showing CNF volume fraction percentage in PAN filament. It is evident that the modulus values, grey data points, are within the upper and lower limits of calculated values. 'B' is the isostress/isostrain plot for PAN+CNT filaments and 'B'' is the magnified plot showing the CNT volume fraction percentage in PAN filament. From the data we can notice that the elastic modulus of PAN+CNT filaments, grey data points, is lower than the lower limit of calculated elastic modulus.

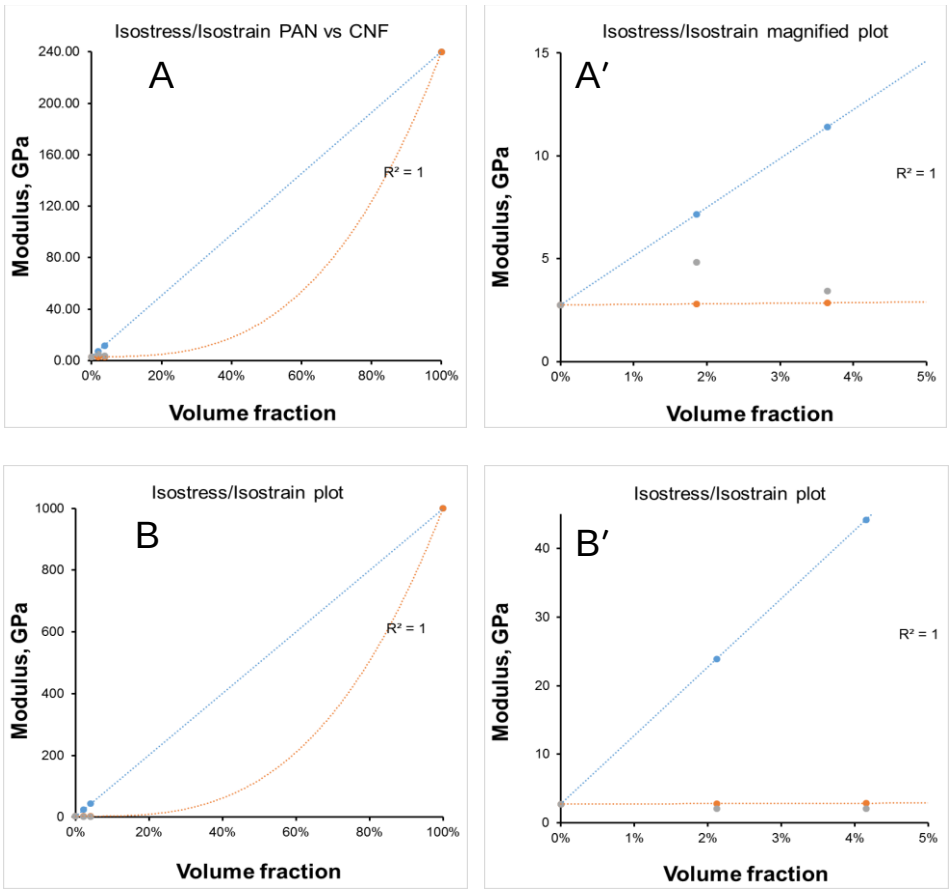


Figure 5.13: Isostrain/isostress calculation of CNFs and CNTs reinforced PAN precursors.

5.5 DMA analysis

Figure 5.14 shows the DMA data of the precursor fibers. The storage or bulk modulus vs temperature is shown in figure 5.14A, and the tan δ vs temperature in 5.14B. It is clear that P1 and P2 filaments have higher modulus than P0 i.e. the PAN filament. The modulus of P1 and P2 filaments are about 6.50 GPa and 4.23 GPa, while that of P0 is 2.03 GPa. The modulus of P1 is more than three times higher and modulus of P2 is more than two times higher than of P0 filament due to CNF reinforcement. Also due to incorporation of CNFs the tan δ shifted from 105 °C for P0 to 118 °C for P1 and P2 filaments. Figure 5.14A also shows that due to inclusion of CNTs in PAN the modulus increased, however the increase in value was not as high as that of CNFs based precursors. Moreover, this increase in modulus in P4 and P5 could not be appreciated because of the fact that the SEM/FIB images revealed large void content, and the tensile properties could not be exploited.

5.6 Tensile properties of hot plate stretched precursors

All the precursor filaments were hot plate drawn and tensile properties were measured. By hot stretching, the orientation of the polymer increased and hence enhanced the strength of the precursors compared to that of the undrawn fiber, as shown in schematic figure 5.15. The tensile data is shown in figure 5.16. The P0′ filaments strength and modulus increased by 3.5 and 2.3 times, respectively, compared to undrawn P0 filament (figure 5.11). Similarly, P1′ filaments strength and modulus increased by 1.5 and 2 times, respectively, compared to undrawn P1 filament. P2′ strength and modulus also increased by 2.1 and 2.4 times compared to P2.

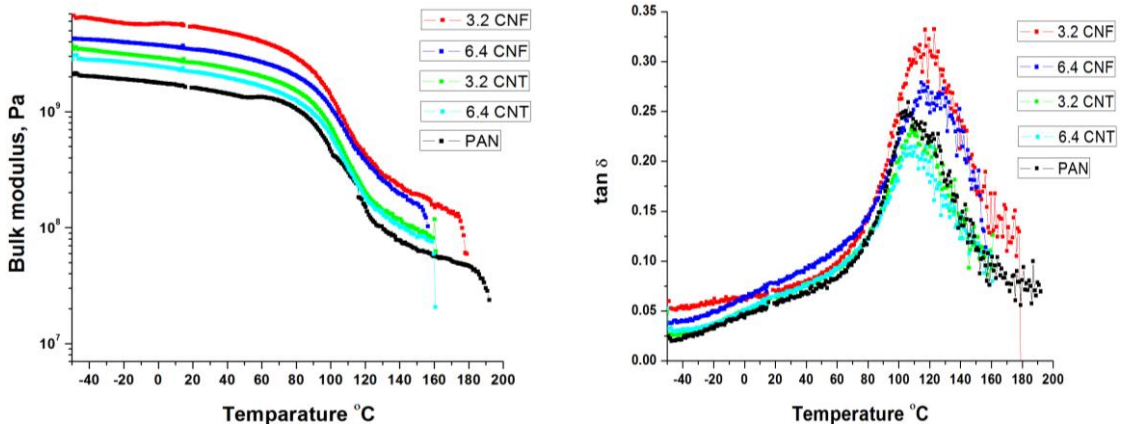


Figure 5.14: 'A' DMA curves of precursors showing bulk modulus vs temperature and 'B' showing the tan δ vs temperature.

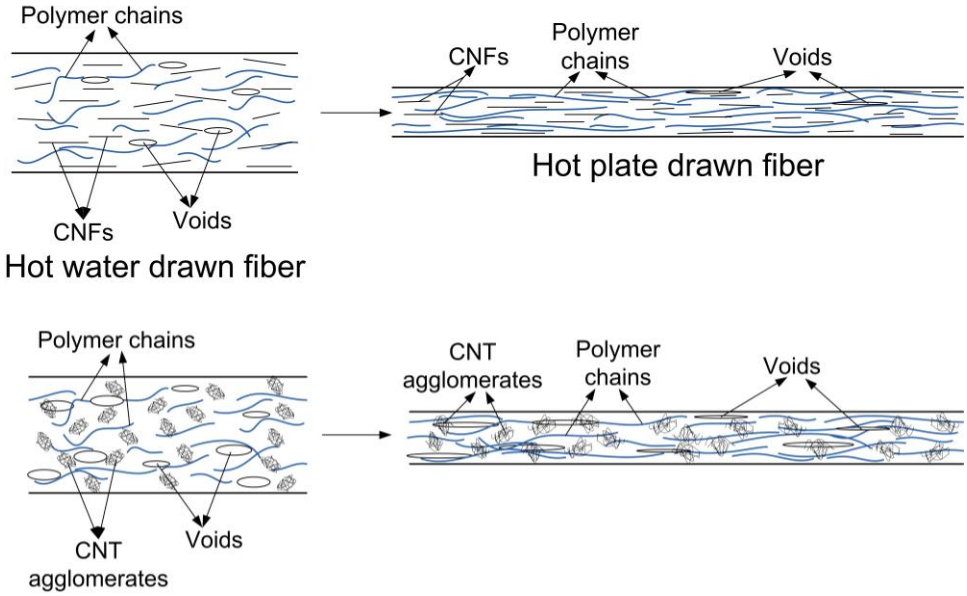


Figure 5.15: Schematic of change in hotplate drawn compared to hot water drawn CNFs and CNTs reinforced precursors.

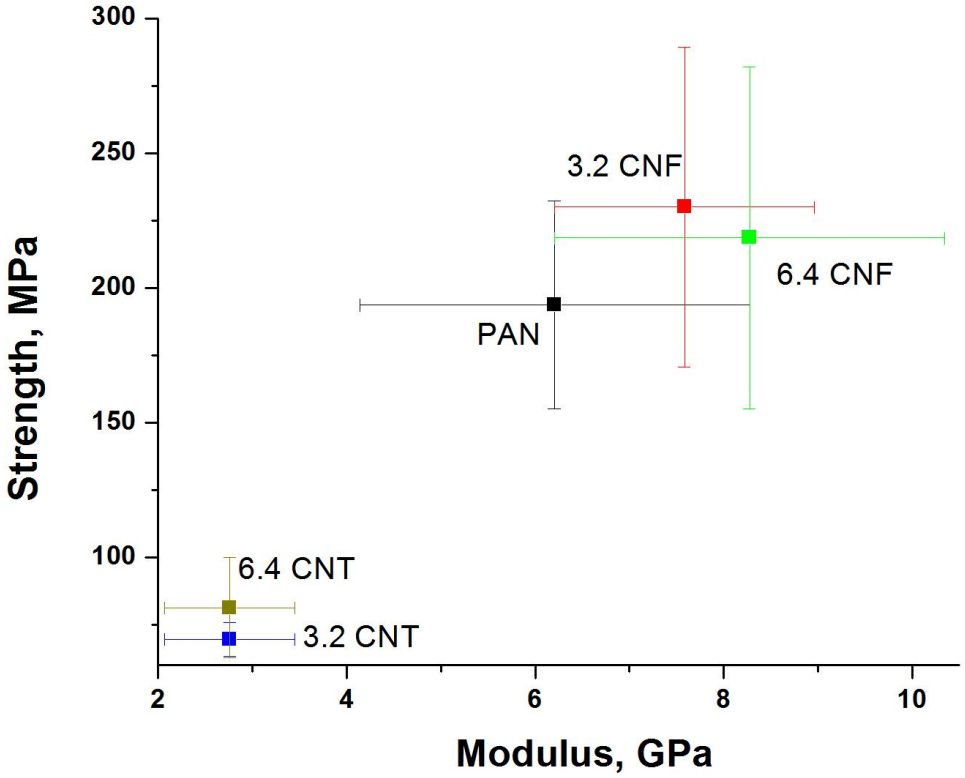


Figure 5.16: Tensile properties data of precursors (P0′ to P5′) stretched on a hot plate.

However, there is no much increase in tensile properties of CNT infiltrated PAN filaments. The strength and modulus of P4′ and P5′ increased by 1.5 times P4 and P5 filaments. However, this change was not significant compared to P1 and P2.

5.7 XRD analysis

X-ray diffraction of the precursors were conducted to study the nature of the peaks compared to commercial PAN fibers. From the figure 5.17, it is evident that the peak positions match that of the commercial PAN peak ($2\theta = 17°$) and the widths of the peaks of precursors are comparable to that of commercial PAN fibers stating that the precursors are not highly amorphous. It is also evident that there is a strong peak of CNFs in 3.2 and 6.4 wt% PAN-g-CNF in PAN filaments. This peak (at 26.56°) represents the (002) plane of graphitic structure and confirms the presence of CNFs in PAN filaments. A weak peak at 26.56° should also be noted representing the P3 filaments (3.2 wt% PAN-g-CNTs + CNFs). As this particular fiber contains both CNTs and CNFs the peak is observed with a very weak intensity. The precursor peaks also indicate that, consolidation of filaments is very close to that of commercial PAN fibers. Finer adjustment to the wet-spinning line, such hot godet rolls multi-stage stretching, winding with optimized tension on the spool could increase the orientation further and match closely to the commercial PAN fibers.

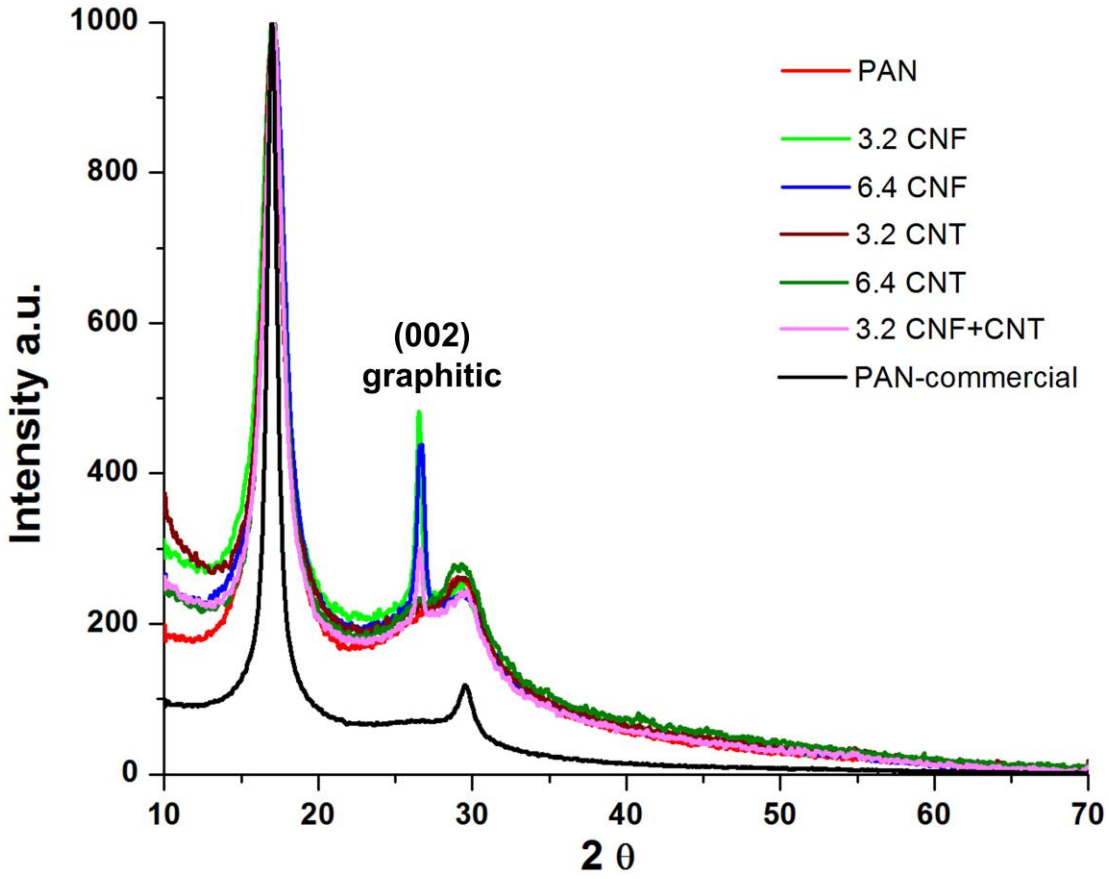


Figure 5.17: Normalized XRD peaks of precursors.

CHAPTER 6

CHARACTERIZATION OF CARBONIZED FILAMENTS

6.1 Microstructure analysis

SEM images of surface topography and FIB milled cross sections of carbonized filaments C0 to C5 are shown in figure 6.1. 'A' and 'A'' are surface and cross section images, respectively, of carbonized C0 filament. From figure 6.1 A′ we can observe that there are few voids in the cross section. B and B′ are surface and cross section images, respectively, of carbonized C1 filament. C and C′ are surface and cross section images, respectively, of carbonized C2 filament. Both B′ and C′ images show few relatively larger voids and small void like circles, which are ends of CNFs. This shows that the CNFs have uniform distribution and are mostly parallel to the filament direction. D and D′ are surface and cross section images, respectively, of carbonized C4 filament. E and E' are surface and cross section images, respectively, of carbonized C5 filament. From 6.1 D and E it is evident that the surface of the CNTs based carbon fibers are not smooth and show the presence of surface voids, and thick and thin places. Cross section images D′ and E′ show that the CNTs are agglomerated and are not uniformly distributed. Presence of large void content is also visible with CNTs agglomerates in the void space. The presence of void can be attributed to rapid coagulation of the filaments during wet spinning and presence of CNT agglomerates has adversely hindered the diffusion of DMF from filament to coagulation bath. Further carbonization of the precursors was not efficient to coalesce the

larger voids which has caused for poor strength and modulus of CNTs infiltrated samples. Moreover the CNTs used in this work are 90% pure and the remaining 10% impurity in each CNT leads to exponential reduction in strength of the CNTs itself.

6.2 Tensile properties

Tensile properties of the carbonized filaments are as shown in figure 6.2. It is evident that as the CNFs dispersed well in the precursors, and as a result of this, the strength and modulus of the carbonized filament C1 and C2 are also higher than that of the C0 filaments. Strength and modulus of C1 filament is almost two and 1.3 times of C0 filament. Presence of CNFs in C1 and C2 not only increased strength but also modulus as the graphitic structure of CNFs is stiffer than CNTs. Similarly, the strength and modulus of C2 is about 1.4 times higher than that of C0 filament. Moreover, due to presence of larger void content and CNT agglomerates (as seen in SEM/FIB images) in C4 and C5, stress concentration on the filaments occur and thus the mechanical properties are lower compared to C0.

SEM images of tensile tested samples of C0 to C5 are shown in figure 6.3. Figure 6.3 'A' is the SEM image of tensile tested C0 filament. As it is observed, the filament has flat fracture; also large surface void is observed. This shows the reason for lower strength of C0 filament. 'B' shows the SEM image of tensile tested sample of C1 filament. Evidence of CNFs protruding out of the filament shows the reinforcement and flat fracture also suggests that CNFs are strongly bonded to the matrix. 'C' shows the SEM image of tensile tested C2 filament.

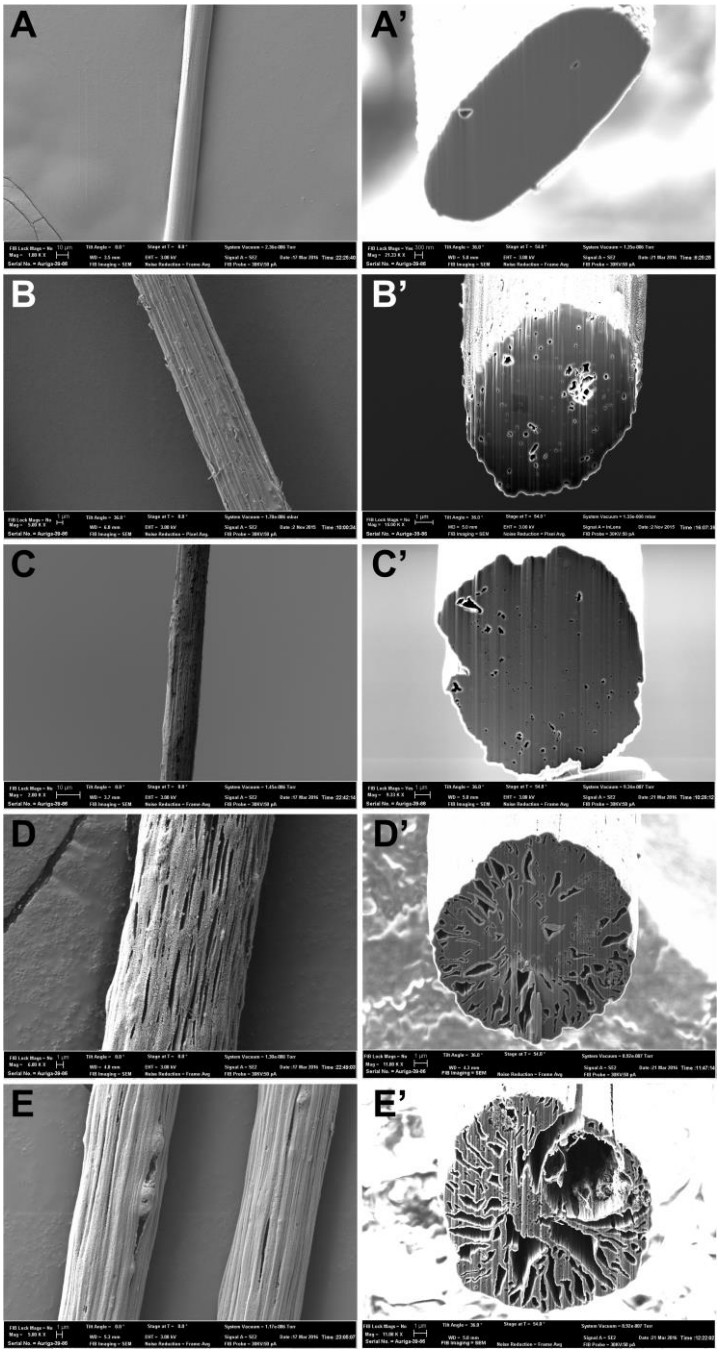


Figure 6.1: SEM images of surface topography and FIB milled cross sections of carbon fibers converted from C0 to C5 precursor filaments.

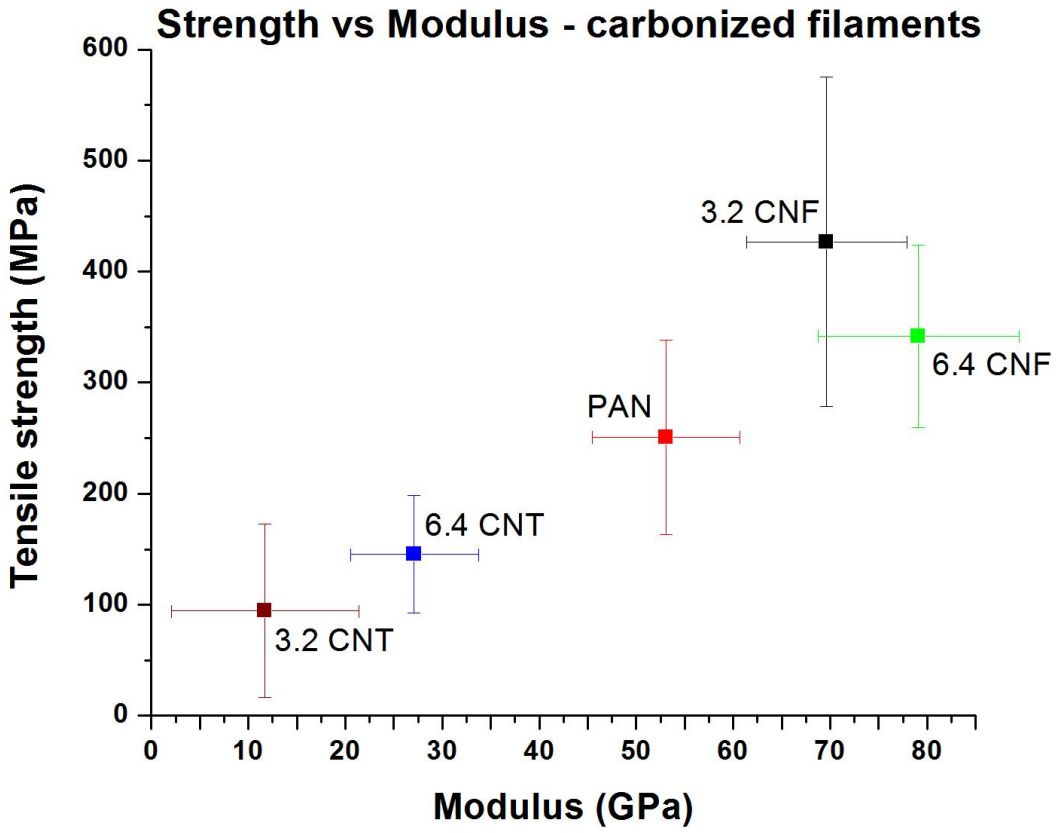


Figure 6.2: Tensile properties of carbonized filaments (C0 to C5)

As we can see the presence of more CNFs protruding out of the tensile tested filament, the stiffness has increased with considerable increase in strength compared to C0 filament. 'D' and 'E' show SEM images of tensile tested sample of C4 and C5 filaments. Due to presence of large voids on the surface and in the core, the strength of the filaments has greatly reduced.

Theoretical calculations of isostress/isostrain conditions of the nanofillers reinforced CFs are as shown in figure 6.4. Equation 1 is for isostrain condition

$$E_C = E_F \times f + E_M \times (1 - f) \qquad \text{eq.1}$$

where, E_C is elastic modulus of composite fiber, E_M is elastic modulus of CF without nanofiller, and E_F is elastic modulus of nanofillers i.e. CNFs or CNTs. 'f' is volume fraction of nanofiller and (1-f) is volume fraction of the polymer.

Equation 2 is for isostress condition

$$E_C = \left[\frac{f}{E_F} + \frac{(1-f)}{E_M} \right]^{-1} \qquad \text{eq.2}$$

Calculated isostress/isostrain values are as shown in figure 6.4. Elastic modulus of PAN based CF, C0 = 53.09 GPa, was used as E_M and elastic modulus of CNFs, 240 GPa, as E_F for CF+CNF filaments. Elastic modulus of CNTs, 1000 GPa, was used for CF+CNT filaments. PAN based CF density of 1.74 g/cm^3, CNF density of 2 g/cm^3 and CNT density of 1.75 g/cm^3 was used for volume percentage calculations. Furthermore, it should be noted that volume percentage of nanofillers is higher than the precursors, as discussed in section 5.4. This is because during CF conversion, more than 30 to 40% weight loss is observed and in this work the weight loss of CF is about 46 %, as per TGA data.

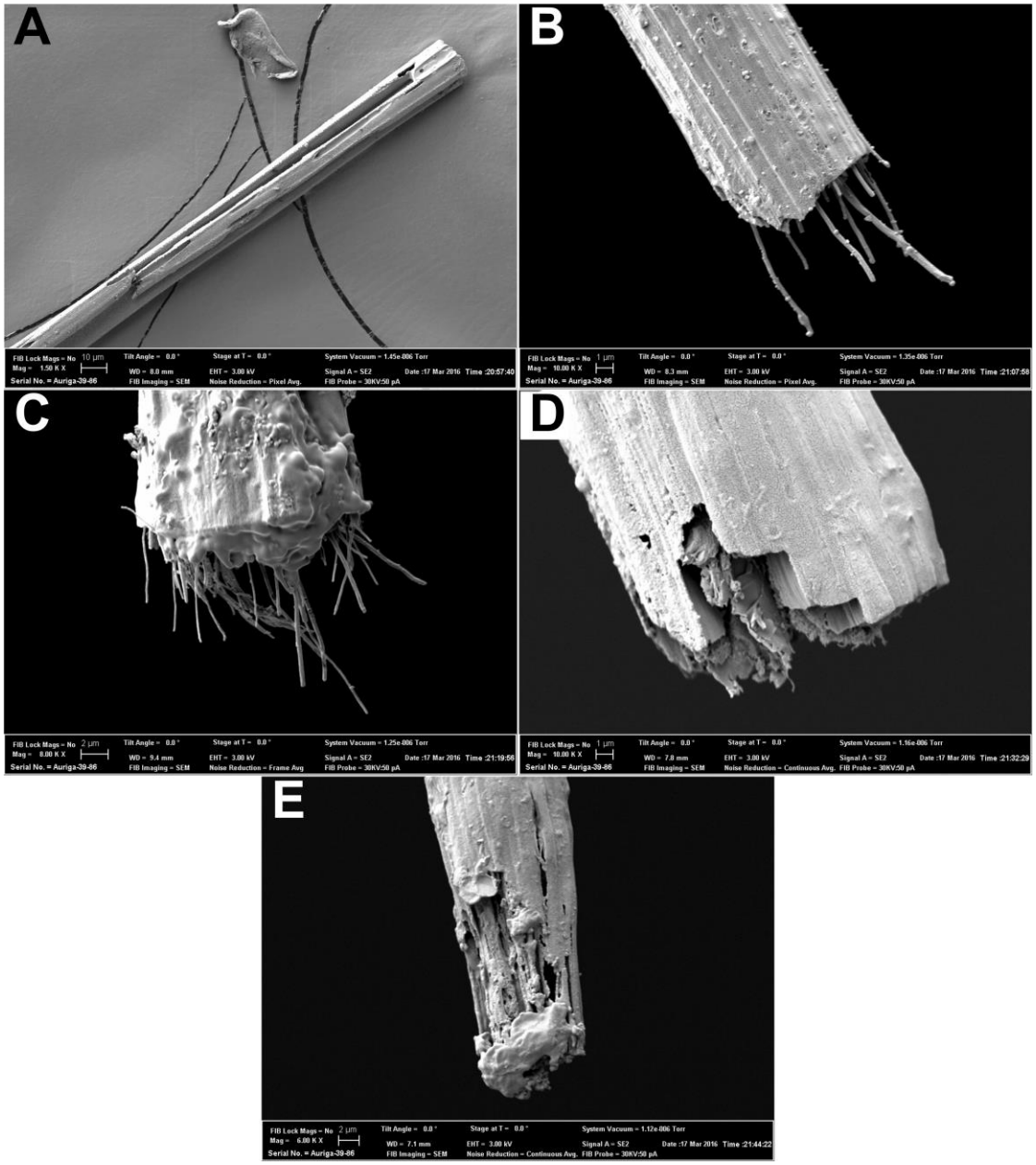


Figure 6.3: SEM images of tensile tested carbonized filaments. ‘A’ is failed end of C0, ‘B’ is failed end of C1, ‘C’ is failed end of C2, ‘D’ is failed end of C4, ‘E’ is failed end of C5.

The calculated isostrain and isostress elastic modulus are in blue and orange data points, respectively, in the figure 6.4. 'A' is the isostress/isostrain calculation for CF+CNF filaments 'A'' is the magnified plot showing CNF volume fraction percentage in CF. It is evident that the modulus values, grey data points, are above the upper limits of calculated values, and this shows that the CF is highly oriented and uniform along the cross section. 'B' is the isostress/isostrain plot for CF+CNT filaments and 'B'' is the magnified plot showing the CNT volume fraction percentage in CF. From the data we can notice that the elastic modulus of CF+CNT filaments, grey data points, is much lower than the lower limit of calculated elastic modulus. This reduction in elastic modulus is because of lack of uniformity along the cross section and longitudinal section. Presence of void, as confirmed from the FIB analysis, has also lowered the elastic modulus drastically.

6.3 XRD analysis

XRD analysis of CF (C0 to C5) compared with commercial CF and CNT yarn is shown in figure 6.5. From the data it is evident that the carbon fibers (C0 to C5) are completely carbonized and the peak at 25.6° which shows the (002) planes. Also, the presence of CNF's, graphitic structure (002) planes, is visible by the presence of a peak at 26.6°. As the concentration of CNFs is higher in C2 the peak intensity is higher than for C1. Furthermore, it can be observed that, weak peaks of (100), (101) planes are visible at 44°. C3 sample shows a weak peak at 25.6° and a stronger peak at 26.6° indicating the presence of both CNFs and CNTs (weak peak at 44°). Presence of void can also be observed comparing the width of the peaks of various samples.

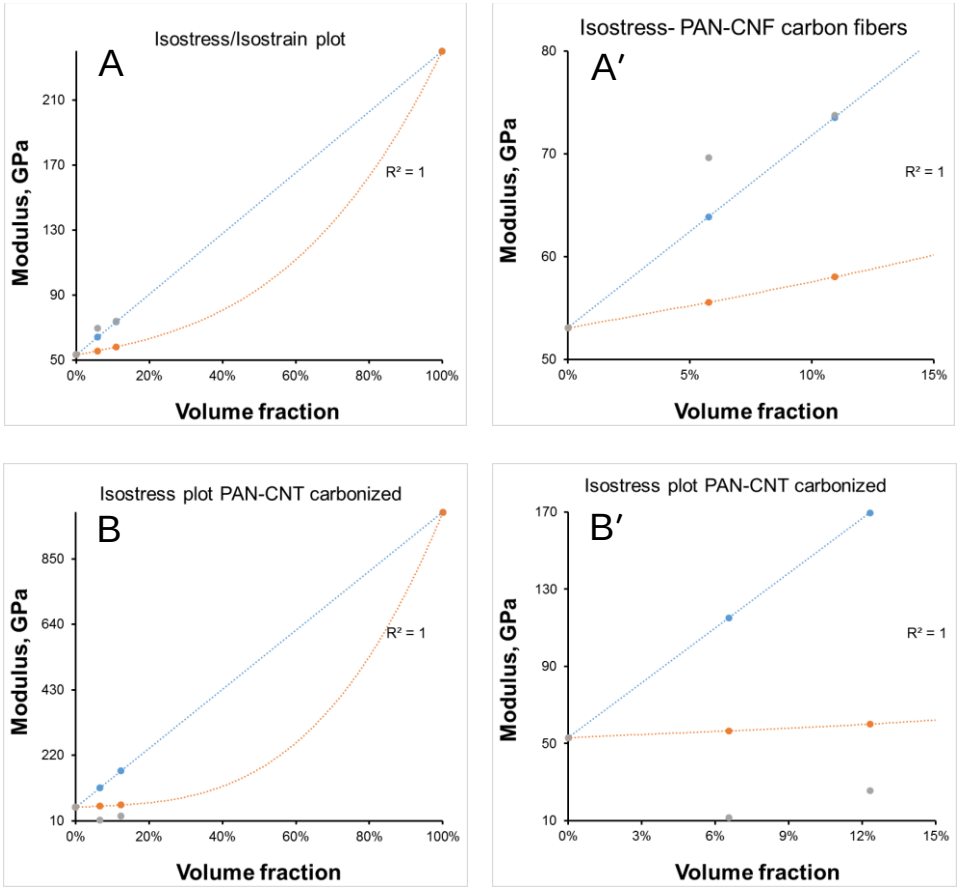


Figure 6.4: Isostrain/isostress calculation of CNFs and CNTs reinforced carbon fibers.

Compared to commercial CF, C0, C3, C4 and C5 have higher amorphous nature while C1 and C2 are comparable to commercial CF or lower. This shows that the consolidation and conversion of the fibers during stabilization and carbonization is complete resulting in negligible to no void formation. Furthermore, it should be noted that as the temperature of the carbonization process increases, the structure is more graphitized and ordered as the carbonization process is subjected to constant load thereby eliminating voids and increasing crystallinity.

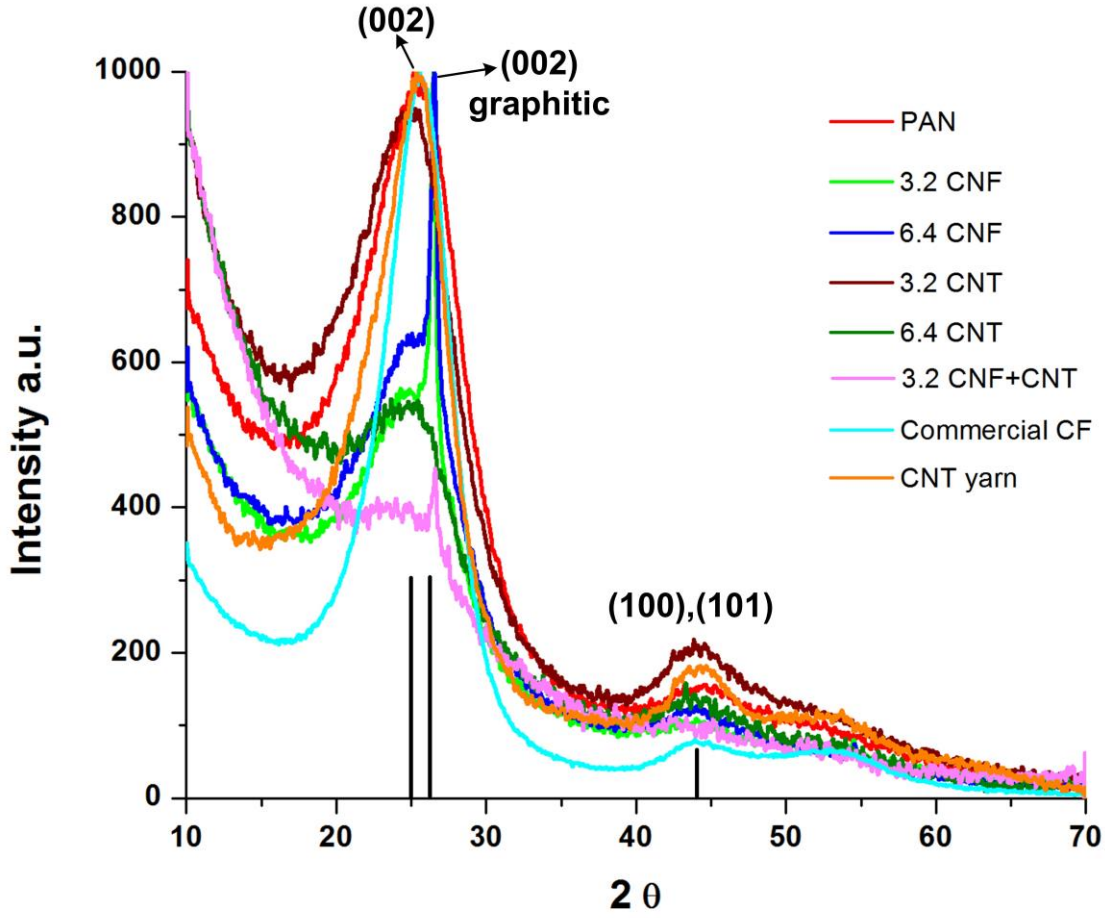


Figure 6.5: XRD data of carbonized filaments

CHAPTER 7

CONCLUSIONS AND FUTURE RECOMMENDATIONS

7.1 Conclusions

In this dissertation, CNT yarns from Nanocomptech (CNTYN) and Generalnano llc (CNTYG) were analyzed for packing, void content and other physical properties and correlated to their mechanical properties. The density of CNT yarn was much lower than that of CNT itself. Furthermore, the analysis for the void content in the CNT yarns showed more than 40 % void content and the density of the yarn was just 0.42 g/cm^3. CNTYG contained more void than CNTYN and hence CNTYN was stronger, as per the mechanical properties evaluation. However, density of CNT itself is 1.75 g/cm^3. This lets one conclude that by increasing the packing of the CNT bundles efficient load transfer between them will enhance the strength of the yarn.

Subsequently solvent densification, 0.1 wt% PAN and 1 wt% PAN densification were carried out separately. The strength and modulus of the solvent densified, 0.1 wt% PAN and 1 wt% PAN infiltrated yarn samples were higher than that of the pristine sample. Further analysis of tensile tested samples using SEM revealed that the CNT bundles were more tightly packed. Furthermore, CNTYN samples appear to be embedded in a polymer matrix, and the TGA on the yarn samples seem to agree with that observation.

Textile grade PAN was used for wet-spinning precursor filaments. PAN-grafted CNTs and CNFs were used as filler materials in textile grade PAN precursor for carbon

fibers preparation. The lower molecular weight PAN was used with the thinking that lower viscosity would allow higher amount of grafted nanotubes/nanofibers in the solution and finally in the fiber. Both CNTs and CNFs were used as nanofillers to enhance the tensile properties of the carbon fibers. CNFs in PAN enhanced the strength and modulus more than two times and 1.4 times compared to PAN based carbon fibers (C0). Strength and modulus of precursors were enhanced due to further orientation of the polymer chains. This was possible because of coalescence of the consolidation of microvoids and load transfer across polymer chains and nanofillers increases and this enhances the strength and modulus.

Carbon fibers with CNFs as fillers had higher strength and modulus than carbon fibers with CNTs. This observation is consistent with earlier findings by other researchers that CNT and CNF. However, the improvement in properties is dependent on the level of interaction between the reinforcing material and the matrix. Unlike in previous studies where available CNT and CNFs were used, in this study PAN-grafted CNTs and CNFs were used. Grafting with PAN certainly helped in achieving better dispersion and thus enhancement in adhesion and subsequently superior mechanical properties. Of the two CNFs show much higher performance improvement compared to CNTs. In this case, the filament obtained was of poor quality due to rudimentary single filament spinning. However with better spinning system and further optimization, it should be possible to enhance the strength and modulus further.

7.2 Recommendations for Future work

- Whereas single hole spinning used was good enough to provide an understanding of the influence of CNT and CNF reinforcement, the properties of the fibers were not same as the one expected in commercial situation. For that a multi-hole spinneret could be used to wet spin PAN with various nanofillers and further carbonization and characterization could be conducted. That will allow the production fibers with diameter and structure that is close to what is used in commercial situation
- As the preliminary studies o stretching of the precursors using a hot plate showed great promise, further studies need to be carried out on hot stretching of precursors, to enhance strength, which is practically possible with multifilament precursors.
- Bonding strength estimation between CNFs and polymer matrix using MEMS device and correlating it to theoretical calculation should be carried out to better understand the bonding characteristics.

REFERENCES

Ando, T. (2000). "Theory of transport in carbon nanotubes." Semiconductor science and technology **15**(6): R13.

Andrews, R., et al. (1999). "Nanotube composite carbon fibers." Applied Physics Letters **75**(9): 1329-1331.

Bajaj, P., et al. (2001). "Thermal behaviour of acrylonitrile copolymers having methacrylic and itaconic acid comonomers." Polymer **42**(4): 1707-1718.

Baker, D. A. and T. G. Rials (2013). "Recent advances in low-cost carbon fiber manufacture from lignin." Journal of Applied Polymer Science.

Behabtu, N., et al. (2013). "Strong, light, multifunctional fibers of carbon nanotubes with ultrahigh conductivity." Science **339**(6116): 182-186.

Buchmeiser, M. R., et al. (2013). "A new carbon precursor: synthesis and carbonization of triethylammonium-based poly (p-phenylenevinylene)(PPV) progenitors." Journal of Materials Chemistry A **1**(42): 13154-13163.

Catta Preta, I. F., et al. (2007). "Thermal behavior of polyacrylonitrile polymers synthesized under different conditions and comonomer compositions." Journal of Thermal Analysis and Calorimetry **87**(3): 657-659.

Chae, H. G., et al. (2009). "Carbon nanotube reinforced small diameter polyacrylonitrile based carbon fiber." Composites Science and Technology **69**(3): 406-413.

Chae, H. G., et al. (2006). "Oriented and exfoliated single wall carbon nanotubes in polyacrylonitrile." Polymer **47**(10): 3494-3504.

Chae, H. G., et al. (2007). "Stabilization and carbonization of gel spun polyacrylonitrile/single wall carbon nanotube composite fibers." Polymer **48**(13): 3781-3789.

Chae, H. G., et al. (2015). "High strength and high modulus carbon fibers." Carbon **93**: 81-87.

Cho, T., et al. (2003). "Structure of carbon fiber obtained from nanotube-reinforced mesophase pitch." Carbon **41**(7): 1419-1424.

Coleman, J. N., et al. (2006). "Small but strong: a review of the mechanical properties of carbon nanotube–polymer composites." Carbon **44**(9): 1624-1652.

Dalton, A. B., et al. (2003). "Super-tough carbon-nanotube fibres." Nature **423**(6941): 703-703.

Dalton, A. B., et al. (2004). "Continuous carbon nanotube composite fibers: properties, potential applications, and problems." Journal of Materials Chemistry **14**(1): 1-3.

Dalton, S., et al. (1999). "Thermal stabilization of polyacrylonitrile fibres." Polymer **40**(20): 5531-5543.

Dauche, F., et al. (1998). "Ribbon-shaped carbon fibers from supercritically extracted mesophase pitches." Carbon **36**(7): 1238-1240.

Deurbergue, A. and A. Oberlin (1991). "Stabilization and carbonization of pan-based carbon fibers as related to mechanical properties." Carbon **29**(4): 621-628.

Devasia, R., et al. (2003). "Cyclization reaction in poly (acrylonitrile/itaconic acid) copolymer: An isothermal differential scanning calorimetry kinetic study." Journal of Applied Polymer Science **88**(4): 915-920.

Diez, N., et al. (2012). "Optimisation of the melt-spinning of anthracene oil-based pitch for isotropic carbon fibre preparation." Fuel Processing Technology **93**(1): 99-104.

Dumanlı, A. G. and A. H. Windle (2012). "Carbon fibres from cellulosic precursors: a review." Journal of Materials Science **47**(10): 4236-4250.

Ericson, L. M., et al. (2004). "Macroscopic, neat, single-walled carbon nanotube fibers." Science **305**(5689): 1447-1450.

Flamant, G., et al. (1999). "Solar processing of materials: opportunities and new frontiers." Solar energy **66**(2): 117-132.

Gao, J., et al. (2005). "Continuous spinning of a single-walled carbon nanotube-nylon composite fiber." Journal of the American Chemical Society **127**(11): 3847-3854.

Ge, H., et al. (2009). "The microstructure of polyacrylonitrile-stabilized fibers." Journal of Applied Polymer Science **113**(4): 2413-2417.

Godshall, D., et al. (2003). "Incorporation of methyl acrylate in acrylonitrile based copolymers: effects on melting behavior." Polymer **44**(15): 4221-4228.

Harris, P. J. (2001). Carbon nanotubes and related structures, Cambridge University Press.

Higginbotham, A. L., et al. (2010). "Lower-defect graphene oxide nanoribbons from multiwalled carbon nanotubes." ACS nano **4**(4): 2059-2069.

Horikiri, S., et al. (1978). Process for production of carbon fiber, Google Patents.

Hou, C., et al. (2006). "Determination of the degradation apparent activation energy of acrylonitrile/acrylic acid copolymers." Journal of Applied Polymer Science **100**(6): 4668-4671.

Hou, Y., et al. (2009). "Thermal-shrinkage investigation of the chemical reaction during the stabilization of polyacrylonitrile fibers." Journal of Applied Polymer Science **114**(6): 3668-3672.

Inagaki, M., et al. (2013). "Aromatic polyimides as carbon precursors." Carbon.

Jung, Y., et al. (2015). "Effect of polymer infiltration on structure and properties of carbon nanotube yarns." Carbon **88**: 60-69.

Kearns, J. C. and R. L. Shambaugh (2002). "Polypropylene fibers reinforced with carbon nanotubes." Journal of Applied Polymer Science **86**(8): 2079-2084.

Kim, J.-w., et al. (2007). "Characteristics of pitch-based carbon fibers containing multi-wall carbon nanotubes." Journal of Industrial and Engineering Chemistry **13**(5): 757-763.

Kosynkin, D. V., et al. (2009). "Longitudinal unzipping of carbon nanotubes to form graphene nanoribbons." Nature **458**(7240): 872-876.

Krutchen, C. M. (1974). MELT EXTRUDABLE POLY ACETYLENE, Google Patents.

Kumar, S., et al. (1993). "Carbon fibre compressive strength and its dependence on structure and morphology." Journal of Materials Science **28**(2): 423-439.

Kumar, S., et al. (2002). "Synthesis, Structure, and Properties of PBO/SWNT Composites&." Macromolecules **35**(24): 9039-9043.

Laplaze, D., et al. (1998). "Carbon nanotubes: the solar approach." Carbon **36**(5): 685-688.

Liu, Y. and S. Kumar (2012). "Recent Progress in Fabrication, Structure, and Properties of Carbon Fibers." Polymer Reviews **52**(3-4): 234-258.

Lv, M.-y., et al. (2009). "Study on the chemical structure and skin-core structure of polyacrylonitrile-based fibers during stabilization." Journal of Polymer Research **16**(5): 513-517.

Maradur, S. P., et al. (2012). "Preparation of carbon fibers from a lignin copolymer with polyacrylonitrile." Synthetic Metals **162**(5): 453-459.

Marcuzzo, J. S., et al. (2013). "Influence of thermal treatment on porosity formation on carbon fiber from textile PAN." Materials Research **16**(1): 137-144.

Meng, J., et al. (2013). "Forming Crystalline Polymer-Nano Interphase Structures for High-Modulus and High-Tensile/Strength Composite Fibers." Macromolecular Materials and Engineering.

Minus, M. L., et al. (2009). "Interfacial Crystallization in Gel-Spun Poly (vinyl alcohol)/Single-Wall Carbon Nanotube Composite Fibers." Macromolecular Chemistry and Physics **210**(21): 1799-1808.

Moniruzzaman, M. and K. I. Winey (2006). "Polymer nanocomposites containing carbon nanotubes." Macromolecules **39**(16): 5194-5205.

Moothi, K., et al. (2012). "Coal as a carbon source for carbon nanotube synthesis." Carbon **50**(8): 2679-2690.

Mora, E., et al. (2002). "A study of pitch-based precursors for general purpose carbon fibres." Carbon **40**(14): 2719-2725.

Naskar, A. K., et al. (2005). "UV assisted stabilization routes for carbon fiber precursors produced from melt-processible polyacrylonitrile terpolymer." Carbon **43**(5): 1065-1072.

O'connell, M. J. (2006). Carbon nanotubes: properties and applications, CRC press.

Ockendon, H. and E. Terrill (1993). "A mathematical model for the wet-spinning process." European Journal of Applied Mathematics **4**(04): 341-360.

Otani, S. (1969). METHOD FOR PRODUCING CARBONIZED I. IGMN FIBER, Google Patents.

Paiva, M., et al. (2003). "UV stabilization route for melt-processible PAN-based carbon fibers." Carbon **41**(7): 1399-1409.

Park, S. H., et al. (2003). "Preparations of pitch-based CF/ACF webs by electrospinning." Carbon **41**(13): 2655-2657.

Park, S. H., et al. (2004). "Preparation of carbonized fiber web from electrospinning of isotropic pitch." Synthetic Metals **143**(2): 175-179.

Qin, X., et al. (2012). "A comparison of the effect of graphitization on microstructures and properties of polyacrylonitrile and mesophase pitch-based carbon fibers." Carbon **50**(12): 4459-4469.

Qin, X., et al. (2012). "Effect of heating and stretching polyacrylonitrile precursor fibers in steam on the properties of stabilized fibers and carbon fibers." Polymer Engineering & Science.

Rahaman, M., et al. (2007). "A review of heat treatment on polyacrylonitrile fiber." Polymer Degradation and Stability **92**(8): 1421-1432.

Razal, J. M., et al. (2007). "Arbitrarily shaped fiber assemblies from spun carbon nanotube gel fibers." Advanced Functional Materials **17**(15): 2918-2924.

Rouse, J. H. (2005). "Polymer-assisted dispersion of single-walled carbon nanotubes in alcohols and applicability toward carbon nanotube/sol-gel composite formation." Langmuir **21**(3): 1055-1061.

Ruan, S., et al. (2006). "Ultra-strong gel-spun UHMWPE fibers reinforced using multiwalled carbon nanotubes." Polymer **47**(5): 1604-1611.

Sawai, D., et al. (1998). "Differential scanning calorimetry evidence for the existence of a first-order thermal transition in ultraoriented at-poly (acrylonitrile)." Macromolecules **31**(6): 2010-2012.

Sawai, D., et al. (2004). "Dynamic mechanical relaxations in poly (acrylonitrile) with different stereoregularities." Macromolecules **37**(8): 2839-2846.

Sawai, D., et al. (1999). "Uniaxial drawing of isotactic poly (acrylonitrile): Development of oriented structure and tensile properties." Macromolecules **32**(17): 5622-5630.

Sears, K., et al. (2010). "Focused ion beam milling of carbon nanotube yarns to study the relationship between structure and strength." Carbon **48**(15): 4450-4456.

Seydibeyoğlu, M. Ö. (2012). "A Novel Partially Biobased PAN-Lignin Blend as a Potential Carbon Fiber Precursor." BioMed Research International **2012**.

Shokuhfar, A., et al. (2006). "Effect of thermal characteristics of commercial and special polyacrylonitrile fibres on the fabrication of carbon fibres." Materials science and technology **22**(10): 1235-1239.

Song, K., et al. (2013). "Structural Polymer-Based Carbon Nanotube Composite Fibers: Understanding the Processing–Structure–Performance Relationship." Materials **6**(6): 2543-2577.

Sreekumar, T. V., et al. (2004). "Polyacrylonitrile single-walled carbon nanotube composite fibers." Advanced Materials **16**(1): 58-61.

Szabó, A., et al. (2010). "Synthesis methods of carbon nanotubes and related materials." Materials **3**(5): 3092-3140.

Tan, L. and A. Wan (2011). "Structural changes of polyacrylonitrile precursor fiber induced by< i> γ</i>-ray irradiation." Materials Letters **65**(19): 3109-3111.

Terrones, M. (2003). "Science and technology of the twenty-first century: synthesis, properties, and applications of carbon nanotubes." Annual review of materials research **33**(1): 419-501.

Vigolo, B., et al. (2000). "Macroscopic fibers and ribbons of oriented carbon nanotubes." Science **290**(5495): 1331-1334.

Wang, Z., et al. (2007). "The extraordinary reinforcing efficiency of single-walled carbon nanotubes in oriented poly (vinyl alcohol) tapes." Nanotechnology **18**(45): 455709.

Watanabe, F., et al. (2000). "Structure of melt-blown mesophase pitch-based carbon fiber." Carbon **38**(5): 741-747.

Wu, G.-P., et al. (2011). "Effect of boric acid on oxidative stabilization of polyacrylonitrile fibers." Fibers and Polymers **12**(7): 979-982.

Wu, G., et al. (2005). "Influence of tension on the oxidative stabilization process of polyacrylonitrile fibers." Journal of Applied Polymer Science **96**(4): 1029-1034.

Xiang, C., et al. (2013). "Graphene Nanoribbons as an Advanced Precursor for Making Carbon Fiber." ACS nano **7**(2): 1628-1637.

Yamane, A., et al. (1997). "Development of high ductility and tensile properties upon two-stage draw of ultrahigh molecular weight poly (acrylonitrile)." Macromolecules **30**(14): 4170-4178.

Yang, K. S., et al. (1999). "Isotropic carbon and graphite fibers from chemically modified coal-tar pitch." Korean Journal of Chemical Engineering **16**(4): 518-524.

Young, K., et al. (2010). "Strong Dependence of Mechanical Properties on Fiber Diameter for Polymer− Nanotube Composite Fibers: Differentiating Defect from Orientation Effects." ACS nano **4**(11): 6989-6997.

Yu, M., et al. (2006). "Evolution of tension during the thermal stabilization of polyacrylonitrile fibers under different parameters." Journal of Applied Polymer Science **102**(6): 5500-5506.

Yu, M., et al. (2010). "Thermal properties of acrylonitrile/itaconic acid polymers in oxidative and nonoxidative atmospheres." Journal of Applied Polymer Science **116**(2): 1207-1212.

Yuan, H., et al. (2011). "Effect of electron beam irradiation on polyacrylonitrile precursor fibers and stabilization process." Journal of Applied Polymer Science **122**(1): 90-96.

Zhang, M., et al. (2004). "Multifunctional carbon nanotube yarns by downsizing an ancient technology." Science **306**(5700): 1358-1361.

Zhang, W., et al. (2004). "New evaluation on the preoxidation extent of different PAN precursors." JOURNAL OF MATERIALS SCIENCE AND TECHNOLOGY-SHENYANG- **20**(4): 369-372.

VITA

Nitilaksha P. Hiremath was born in Karnataka, India. He did his schooling in Hubli, Karnataka, India. He attended Govt. S.K.S.J.T Institute Bangalore, India (2005-2009) from where he graduated with a Bachelor of Textile Technology in Engineering. Nitilaksha came to the United States of America in the fall of 2010 for his Master's degree in Materials Engineering department at Auburn University, Auburn, Alabama. He worked as Graduate Research Assistant for his thesis research, funded by USDA, with Dr. Bryan A. Chin and obtained M.S degree in Materials Engineering in spring of 2013. In spring of 2013 Nitilaksha accepted a Graduate Research Assistantship position at the University of Tennessee at Knoxville, Knoxville, Tennessee and began his Ph.D. program, funded by NASA, in Materials Science and Engineering with Dr. Gajanan S. Bhat from Materials Science and Engineering department. Nitilaksha Hiremath graduated with his Ph.D. degree in December 2016.